CHAPTER 4

Electrochemical studies on self-assembled monolayers (SAMs) of some aromatic thiols and alkoxycyanobiphenyl thiols on gold surface

This chapter deals with our studies on self-assembled monolayers of some aromatic and alkoxycyanobiphenyl thiols on gold surface. We have studied and characterized the monolayer formation of 2-naphthalenethiol, thiophenol (TP), o-aminothiophenol (o-ATP), p-aminothiophenol (p-ATP) and alkoxycyanobiphenyl thiols with different alkyl chain lengths on Au surface using organic solvents as an adsorbing medium. The barrier properties and structural arrangements of these monolayers were evaluated and characterized using electrochemical, spectroscopic and microscopic techniques. Cyclic voltammetry and electrochemical impedance spectroscopy were extensively used for the study of electron transfer reactions on these SAM modified surface. It is found that the self-assembled monolayers of aromatic thiols on Au surface generally exhibit poor electrochemical blocking ability towards the redox reactions. In this work, we have tried to improve the blocking ability of these aromatic SAMs on Au surface using a variety of methods such as potential cycling, annealing and mixed SAM formation. We have used potassium ferro/ferri cyanide $\{[Fe(CN)_6]^{3-|4-}\}$, hexaammineruthenium(III) chloride $\{[Ru(NH_3)_6]^{2+|3+}\}$ complexes as redox probe molecules to evaluate the barrier property of these aromatic monolayers on Au surface. We have studied and characterized the monolayers of these thiol molecules on Au surface using organic solvents as an adsorbing medium in order to compare their

electrochemical blocking ability and structural arrangement with the corresponding monolayers prepared using the hexagonal liquid crystalline phase as an adsorbing medium that has been discussed in the next chapter.

This chapter has been divided into three parts. The first part deals with the monolayer formation and characterization of 2-naphthalenethiol on Au surface that has been studied and reported for the first time in literature. The second part contains the study of SAM formation of TP, o-ATP and p-ATP on polycrystalline Au surface. The effects of pH and mixed SAM formation on the blocking ability of these monolayers have been investigated and discussed. The third and final part deals with the monolayer formation and characterization of alkoxycyanobiphenyl thiols with different alkyl chain lengths on Au surface. The important feature of these thiol molecules is that it contains both the aliphatic and aromatic groups in its structure.

I. SAM OF 2-NAPHTHALENETHIOL ON GOLD SURFACE

4.1. Introduction

Self-assembled monolayer (SAM) refers to a single layer of molecules on a substrate, which are adsorbed spontaneously by chemisorption and exhibit a high degree of orientation, molecular ordering and packing density [1,2]. They have received a great deal of attention in recent times due to their potential application in a variety of fields such as sensors [3-6], photolithography [7-9], nonlinear optical materials [10], high-density memory storage devices [11] and corrosion protection [12,13]. Even though adsorption of several functional groups on various metal and non-metallic surfaces have been reported in literature, it is the thiols and disulfides on gold that have been extensively studied in recent times [14]. The various aspects of monolayer formation, structure, packing, orientation, wetting properties and stability have

been examined using different techniques like Fourier transform infrared spectroscopy (FTIR), contact angle measurements, X-ray photoelectron spectroscopy (XPS), ellipsometry and scanning probe microscopy (SPM). Although a complete characterization of SAMs depends on the above-mentioned techniques, the electrochemical techniques namely cyclic voltammetry (CV) and electrochemical impedance spectroscopy (EIS) can be used effectively to understand the packing density, surface coverage and distribution of pinholes and defects in the formation of the monolayer [14].

We find from literature that there are much less reports on aromatic thiol monolayers in contrast to that of long chain aliphatic thiols. Aromatic thiol monolayers represent interesting systems due to the highly delocalized π-electron density and structural rigidity of the phenyl ring. There have been some studies on thiophenol and functionalized thiophenol SAMs on gold [15-19]. Vijayamohanan et al. [20-25] characterized the monolayer formation of naphthalene disulfide and Naphtho[1,8-cd]-1,2-dithiol on Au and Ag using electrochemical techniques, STM, XPS and surface enhanced Raman scattering (SERS). Apart from naphthalene disulphide, 1,4-dimethoxynaphthalene norbornylogous compounds were also reported and it was found that the electron transfer rate is enhanced compared to their alkane analogues due to the rigidity of norbornylogous bridges [26]. Chang et al. reported (6-alkoxynaphth-2-yl)methanethiol SAM on Au and Ag by characterizing them using contact angle measurements, ellipsometry and reflection absorption IR spectroscopy and found that the naphthalene ring forms a herringbone structure with a tilted configuration [27]. Whitesides et al. investigated the metal-insulator-metal junction based on SAM of 2-naphthalenethiol on Au and Ag by measuring the breakdown voltage and found that the SAM on Au junction is mechanically stable but immediately breaks down on application of potential [28]. To the best

of our knowledge, there is no report in literature on the monolayer formation and characterization of 2-naphthalenethiol on gold except by Randall and Joseph [29]. These authors reported the formation of SAM of 2-naphthalenethiol and bis(2-naphthyl) disulfide onto bulk gold using liquid chromatography and diode array spectroscopy and showed that the naphthalene ring is tilted to the Au surface normal. There is, however, no report on the electrochemical characterization, determination of surface coverage based on pinhole defect analysis, study on kinetics of SAM formation and structural arrangement of SAM of 2-naphthalenethiol on Au.

In this chapter, we discuss the results of our study on the self-assembled monolayer of 2-naphthalenethiol on Au and its characterization using electrochemical, spectroscopic (FTIR) and microscopic (STM) techniques. We have used electrochemical techniques such as cyclic voltammetry (CV) and electrochemical impedance spectroscopy (EIS) to evaluate the barrier properties of the monolayer based on its structural ordering and packing. We have also studied the electron transfer process of two important redox systems viz., $[Fe(CN)_6]^{3-|4-}$ and $[Ru(NH_3)_6]^{2+|3+}$ on the 2-napthalenethiol monolayer modified Au electrode. In addition, EIS measurement is used for the determination of surface coverage of the monolayer and pinholes and defects analysis. The kinetics of adsorption of the monolayer on Au is also investigated using impedance measurements. Grazing angle FTIR spectroscopy, STM and interfacial capacitance studies are used to determine the orientation and structural arrangement of SAM on Au surface. The effects of potential cycling and annealing processes on the barrier property and structural arrangement of the monolayer have also been investigated.

4.2. Experimental section

4.2.1. Chemicals

All the chemical reagents used in this study were analar (AR) grade reagents. 2-naphthalenethiol (Aldrich), ethanol 99.95% (Merck), lithium perchlorate (Acros Organics), potassium ferrocyanide (Loba), potassium ferricyanide (Qualigens), sodium fluoride (Qualigens), perchloric acid (Qualigens) and hexaammineruthenium(III) chloride (Alfa Aesar) were used in this study as received. Millipore water having a resistivity of 18 MΩ cm was used to prepare all the aqueous solutions.

4.2.2. Electrodes and cells

Evaporated gold (~100 nm thickness) on glass with chromium underlayers (2-5nm thickness) was used as the substrate for SAM formation and its characterization. The substrate was heated to 350^0C during gold evaporation under a vacuum pressure of 2 X 10^{-5} mbar, a process that normally yields a substrate with predominantly Au (111) orientation. The evaporated gold samples were used as strips for electrochemical, FTIR and STM studies. We have also carried out the electrochemical experiments with a gold wire as a working electrode, which was constructed by a proper sealing of 99.99% pure gold wire (Arora Mathey) of 0.5mm diameter with soda lime glass having thermal expansion coefficient close to that of gold. The electrode has a geometric area of 0.002 cm^2. This small area-working electrode has a highly reproducible true surface area (as measured by potential cycling in 0.1M perchloric acid) even after repeated usage. A conventional three-electrode electrochemical cell was used for the studies involving electrochemical techniques. A platinum foil of large surface area was used as the counter electrode and a saturated calomel electrode (SCE) as the reference electrode.

The cell was cleaned thoroughly before each experiment and kept in a hot air oven at 100^0C for at least 1 hour before the start of the experiment.

4.2.3. Electrode pre-treatment and thiol adsorption

Immediately before use, the gold wire electrode was polished with emery papers of grade 800 and 1500 respectively followed by polishing in aqueous slurries of progressively finer alumina (1.0, 0.3 and 0.05 μm sizes) and then ultrasonicated to remove alumina particles. Then it was cleaned in a "piranha" solution (a mixture of 30% H_2O_2 and Conc.H_2SO_4 in 1:3 ratio; *Caution! Piranha solution is very reactive with organic compounds, storing in a closed container and exposure to direct contact should be avoided*). Finally it was rinsed in distilled water thoroughly followed by rinsing in millipore water before SAM formation. In the case of evaporated Au, the strips were used for SAM formation and it was pretreated with "piranha" solution. The monolayers were prepared by keeping the gold electrode in 20mM 2-naphthalenethiol in ethanol for about 1hour. After the adsorption of thiol, the electrode was rinsed with ethanol, distilled water and finally with millipore water. For the grazing angle FTIR spectroscopy and STM analysis, the evaporated Au samples were used as strips for thiol adsorption.

4.2.4. Electrochemical characterization

Cyclic voltammetry and electrochemical impedance spectroscopy were used for the electrochemical characterization of SAM-modified electrodes. The barrier property of the monolayer has been evaluated by studying the electron transfer reaction using two different redox probes namely potassium ferrocyanide (negative redox probe) and hexaammineruthenium(III) chloride (positive redox probe). Cyclic voltammetry was performed in two different

solutions viz., 10mM potassium ferrocyanide with 1M sodium fluoride as a supporting electrolyte at a potential range of –0.1V to 0.5V vs. SCE and 1mM hexaammineruthenium(III) chloride with 0.1M lithium perchlorate as the supporting electrolyte at a potential range of –0.4V to 0.1V vs. SCE. We have used a potential sweep rate of 50 mV/s for all the cyclic voltammetric measurements. The impedance measurements were carried out using an ac of 10mV amplitude signal at a formal potential of the redox couple, in solution containing always equal concentrations of both the oxidized and reduced forms of the redox couple namely, 10mM potassium ferrocyanide and 10mM potassium ferricyanide in 1M NaF. A wide frequency range of 100kHz to 0.1Hz was used for the impedance studies. The gold oxide stripping analysis was conducted in 0.1M perchloric acid in the potential range of 0.2V to 1.4V vs. SCE. Adsorption kinetics studies of monolayer formation were carried out in 10μM 2-naphthalenethiol + 0.1M $LiClO_4$ in ethanol solution at different potentials using the evaporated Au electrodes as strips by measuring the real and imaginary components of impedance. All the experiments were performed at room temperature.

4.2.5. Instrumentation

Cyclic voltammetry was carried out using an EG&G potentiostat (model 263A) interfaced to a personal computer (PC) through a GPIB card (National Instruments). The potential ranges and scan rates used for the studies are shown in the respective diagrams. For electrochemical impedance spectroscopic studies, the potentiostat was used along with an EG&G 5210 lock in amplifier controlled by Power Sine software. For adsorption kinetics studies of monolayer formation an EG&G potentiostat (model 263A) along with an EG&G 5210 lock in amplifier interfaced to a PC was used. The real and

imaginary components of impedance were acquired at a sampling rate of 100ms for initial 20s and at 1s for the remaining time of monolayer adsorption. The data acquisition was carried out using PCL 203A (Dyanalog) data acquisition card interfaced with LabTech notebook software.

A home built scanning tunneling microscope (STM) in high-resolution mode described elsewhere [30] was used to probe the SAM modified gold surface. STM images were obtained at room temperature in air and the instrument was operated in constant current mode with a tunneling current of 1nA at a sample bias voltage of +100mV. Prior to these experiments, the instrument was calibrated with highly oriented pyrolytic graphite (HOPG) (ZYA grade, Advanced Ceramic). An electrochemically etched tungsten tip was used as the probe. The images shown here were plane corrected and Fourier filtered using scanning probe image processor (SPIP) software (Image Metrology, Denmark). To ensure that the images shown were representative of the monolayer morphology, multiple images were taken at different locations and scan ranges.

The FTIR spectra were obtained using a FTIR 8400 model (SHIMADZU) with a fixed 85^0 grazing angle attachment (FT-85; Thermo Spectra-Tech).

4.3. Results and discussion

4.3.1. Electrochemical characterization

Cyclic voltammetry and electrochemical impedance spectroscopy have been used for the electrochemical characterization of the monolayer of 2-naphthalenethiol on Au surface. Figure 1 shows the cyclic voltammograms of bare gold electrode (Fig. 1(a)) and 2-naphthalenethiol modified gold electrode (Fig. 1(b)) in 10mM potassium ferrocyanide with 1M NaF as the supporting

electrolyte at a potential scan rate of 50 mV/s. It can be seen that the bare gold electrode shows a reversible peak for the redox couple indicating that the reaction is diffusion controlled. In contrast, for the SAM modified electrode, the CV exhibits an irreversible behaviour with a large peak separation and significant peak currents indicating that the electron transfer reaction occurs by an irreversible process. Such a behaviour is typical of a monolayer with rather poor blocking properties to the redox species.

Figure 2 shows the impedance plots of the bare gold electrode and SAM modified electrode in equal concentrations of potassium ferro/ferri cyanide with 1M NaF as the supporting electrolyte. Figure 2 (a) shows a straight line at low frequency and a very small semicircle at high frequency region indicating that the process is essentially diffusion-controlled for the redox couple on a bare gold electrode. The impedance plot of SAM modified electrode in Figure 2 (b) shows the behaviour of a blocking monolayer with a well-defined semicircle at higher frequencies.

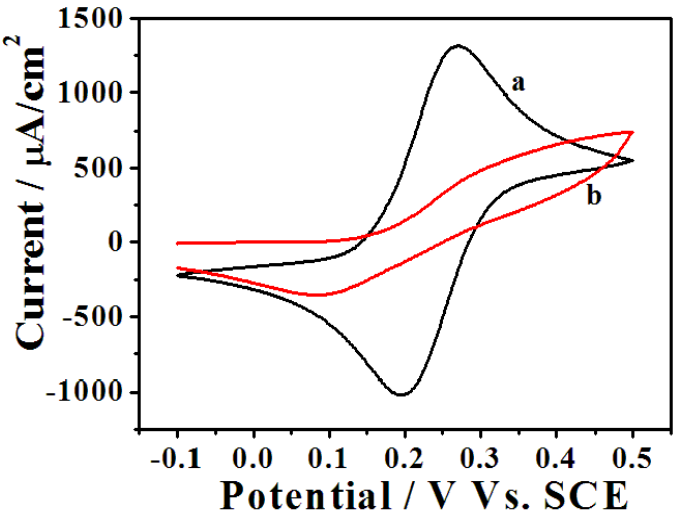

Figure 1: Cyclic voltammograms of (a) bare Au electrode and (b) SAM of 2-naphtalenethiol modified Au electrode in 10mM potassium ferrocyanide with 1M NaF as a supporting electrolyte at a potential scan rate of 50 mV/s.

These impedance values are fitted to a standard Randle's equivalent circuit model having parallel R_{ct} and CPE (constant phase element) components with a series uncompensated solution resistance R_u. From the fitting, a charge transfer resistance (R_{ct}) of 0.55 Ω cm^2 is measured for the bare gold electrode while the monolayer-modified electrode shows a higher R_{ct} value of 190 Ω cm^2. This value is lower compared to the R_{ct} value of 568 Ω cm^2 reported for the SAM of naphthalene disulphide on Au by Vijayamohanan et al. [25].

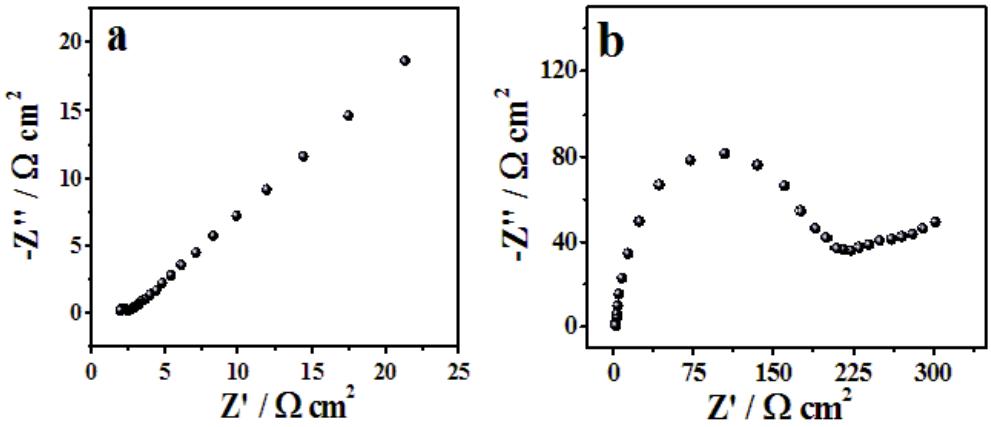

Figure 2: Impedance plots in 10mM potassium ferrocyanide and 10mM potassium ferricyanide with 1M NaF as the supporting electrolyte for (a) bare Au electrode and (b) monolayer of 2-naphthalenethiol coated Au electrode.

We have tried to improve the blocking behaviour of the monolayer-modified electrode by two different processes, namely, by subjecting the freshly formed SAM to (i) potential cycling in a pure supporting electrolyte and (ii) annealing at $72^0 \pm 2^0$C.

4.3.2.Effect of potential cycling and annealing

Immediately after the monolayer formation, the electrode is potential cycled between 0.0 V to 0.6 V vs. SCE in 1M NaF aqueous solution without any redox species and the same electrode is used for the cyclic voltammetry and impedance spectroscopic studies to determine the barrier property of the monolayer. In the case of annealing, after the thiol adsorption, the gold electrode is taken out, washed completely and immediately kept in a hot air oven for about half an hour at $72^0 \pm 2^0$C. It was then allowed to cool down to room temperature and used for the analysis.

Figure 3 shows, respectively, the CVs of the monolayer-modified electrode, potential cycled and annealed (after the SAM formation) electrodes in 10mM potassium ferrocyanide with 1M NaF as the supporting electrolyte and at a potential scan rate of 50 mV/s. For comparison, the cyclic voltammogram of bare gold electrode for the same redox reaction is also shown in the inset of Figure 3. Figure 3(a) shows an irreversible peak formation for the SAM modified electrode. In contrast, the potential cycled electrode shows a better blocking behaviour for the redox reaction (Fig. 3(b)). However the barrier property of the SAM modified electrode has dramatically improved after annealing as can be seen from the figure 3(c). It is evident form the CVs that the electron transfer reaction through the monolayer film is almost totally inhibited, a process that can only be attributed to a more compact organization and structural modification of the monolayer after annealing.

Figures 4(a) and (b) show respectively, the impedance plots of potential cycled and annealed electrodes (after SAM formation), in equal concentrations of potassium ferro/ferri cyanide with NaF as the supporting electrolyte. The impedance values are fitted to standard Randle's equivalent circuit comprising of faradaic impedance Z_f, which is parallel to a constant

phase element (CPE) represented by Q and in series with the uncompensated solution resistance R_u. The faradaic impedance Z_f is a series combination of charge transfer resistance R_{ct} and the Warburg impedance W.

Table 1 shows the values obtained from the equivalent circuit fitting of impedance values for various samples. It can be seen from the table that the R_{ct} values, as expected are higher for the monolayer-modified electrodes when compared to that of bare gold electrode. The SAM modified electrode after potential cycling in 1M NaF shows a very little increase in the R_{ct} value when compared to the fresh monolayer coated electrode, which implies that the charge transfer process is inhibited only marginally by the potential cycling process. This is in contrast to the CV behaviour as seen from figure 3(b) for the electrode, which is potential cycled, the shape of which suggests a more blocking behaviour than the freshly formed SAM. This behaviour implies a possibility of some structural re-organization of the monolayer due to potential cycling without significantly affecting the ionic permeability to the redox species, as revealed by the R_{ct} values. Such behaviour was also reported earlier in the case of aliphatic thiol monolayers [31-34]. The fact that the R_{ct} value is very high (3854 Ω cm^2) for the annealed SAM suggests that the barrier property of the monolayer to the electron transfer reaction has improved remarkably and it is almost completely under charge transfer control. The impedance diagram of the redox reaction on the annealed SAM (Fig. 4(b)) shows a large semicircle in the entire range of frequencies. This is fitted to a parallel combination of Q (CPE) and charge transfer resistance, R_{ct} with a series uncompensated solution resistance R_u. The R_{ct} value of 3854 Ω cm^2 reported here for the SAM of 2-naphthalenethiol on Au is very much higher when compared to the literature values of 568 Ω cm^2, 1100 Ω cm^2 and 1300 Ω cm^2 for the respective SAMs of

naphthalene disulphide (NDS), diphenyldiselenide (DDSe) and diphenyldisulphide (DDS) on gold reported by Vijayamohanan et al. [22,24,25], which implies the compact and highly dense formation of SAM of 2-naphthalenethiol on Au surface.

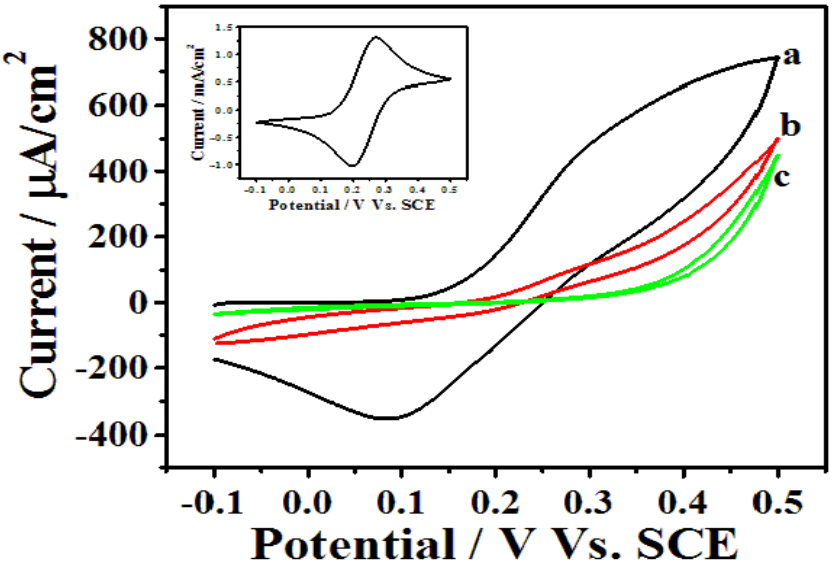

Figure 3: Cyclic voltammograms in 10mM potassium ferrocyanide with 1M NaF as supporting electrolyte at a potential scan rate of 50 mV/s for, (a) SAM of 2-naphthalenethiol modified Au electrode, (b) potential cycled electrode after the SAM formation of 2-naphthalenethiol on Au, and (c) annealed electrode after the SAM formation of 2-naphthalenethiol on Au surface. Inset shows the cyclic voltammogram of bare Au electrode in the same solution for comparison.

Table-1

R_{ct} values obtained from the equivalent circuit fitting analysis of impedance data for various electrodes.

Sample	R_{ct} (Ω cm^2) $[Fe(CN)_6]^{3-\|4-}$	R_{ct} (Ω cm^2) $[Ru(NH_3)_6]^{2+\|3+}$
Bare Au	**0.55**	**1.26**
SAM of 2-NT on Au	**190**	**5.00**
Potential cycled SAM	**221**	**11.59**
Annealed SAM	**3854**	**34.75**

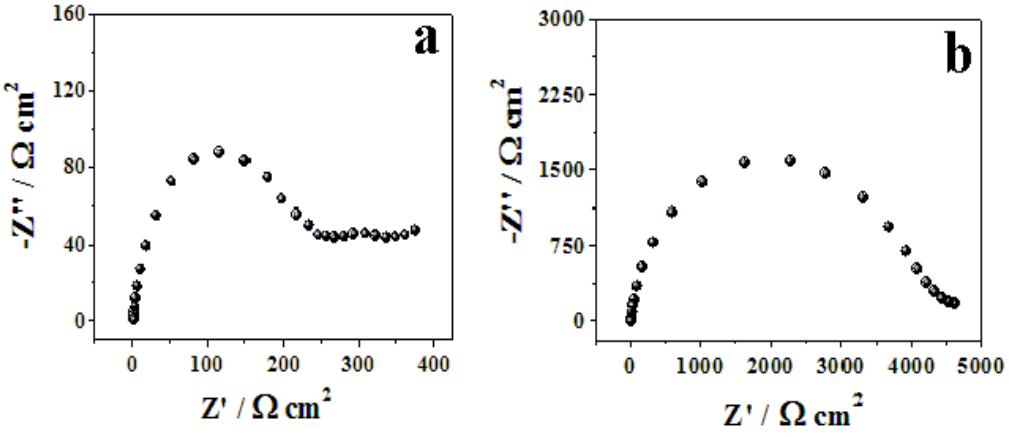

Figure 4: Impedance plots in an aqueous solution of 10mM potassium ferrocyanide and 10mM potassium ferricyanide with 1M NaF as the supporting electrolyte for, (a) potential cycled electrode after the monolayer formation, and (b) annealed electrode after the monolayer formation.

From the impedance diagram (Fig. 4), it can be seen that there is a low frequency component in the case of the SAM modified electrodes (including for the potential cycled and annealed samples), which can arise due to slow ionic diffusion through the pinholes and defects present in the SAM. This low frequency diffusion region is significantly less in the case of annealed sample. For the equivalent circuit fitting analysis of impedance values, we have considered only the semicircle component and fitted the data from 100 KHz to 1Hz. The measured R_{ct} values are shown in the Table 1.

We have also used hexaammineruthenium(III) chloride as a redox probe to determine the barrier property of the monolayer of 2-naphthalenethiol on Au surface. Figures 5(a-c) show the CVs obtained for the bare gold electrode, SAM coated and annealed electrodes respectively. It can be seen from the figure that the ruthenium redox reaction is not blocked even in the case of annealed SAM electrode, which is very much in contrast to the behaviour of the potassium ferrocyanide redox system. It can also be seen that the monolayer-coated electrode shows nearly reversible peaks for the ruthenium redox reaction showing facile nature of the electron transfer process with the reaction under diffusion control.

Figure 6 shows the impedance plots of the bare gold and SAM modified electrodes (including the potential cycled and annealed electrodes) in 1mM hexaammineruthenium(III) chloride with 0.1M $LiClO_4$ as the supporting electrolyte at the formal potential. The equivalent circuit fitting analysis of the impedance plots shows that there is a small increase in the R_{ct} values for the SAM modified electrodes when compared to the bare gold electrode. The high frequency part of the impedance data shows a small semicircle as can be seen from the inset of the respective diagrams. The impedance analysis also indicates that there is a small increase in R_{ct} value with the potential cycling and

annealing processes. This implies that the electron transfer process is not significantly inhibited in the case of ruthenium redox reaction. Since the electron transfer reaction is almost fully inhibited in the case of ferrocyanide ions, which has a comparable ionic size (0.64nm for the ruthenium hexamine complex vs. 0.60nm for the potassium ferrocyanide complex [19]), it is difficult to conclude that ruthenium ions can have access to the electrode surface through the pinholes and defects present in the monolayer and ferrocyanide cannot.

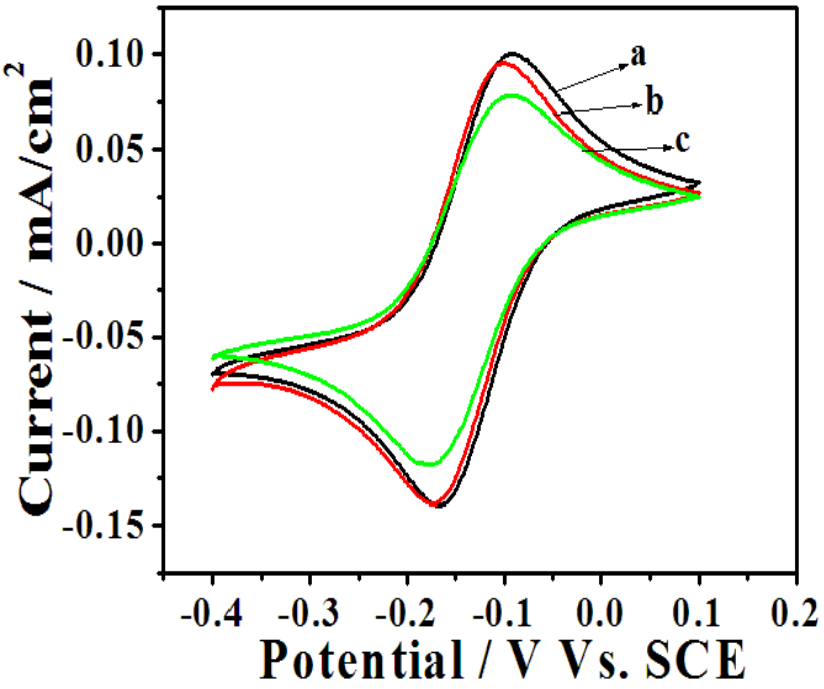

Figure 5: Cyclic voltammograms in 1mM hexaammineruthenium(III) chloride with 0.1M $LiClO_4$ as supporting electrolyte at a potential scan rate of 50 mV/s for, (a) bare Au electrode, (b) SAM of 2-naphthalenethiol modified Au electrode and (c) annealed electrode after the SAM formation.

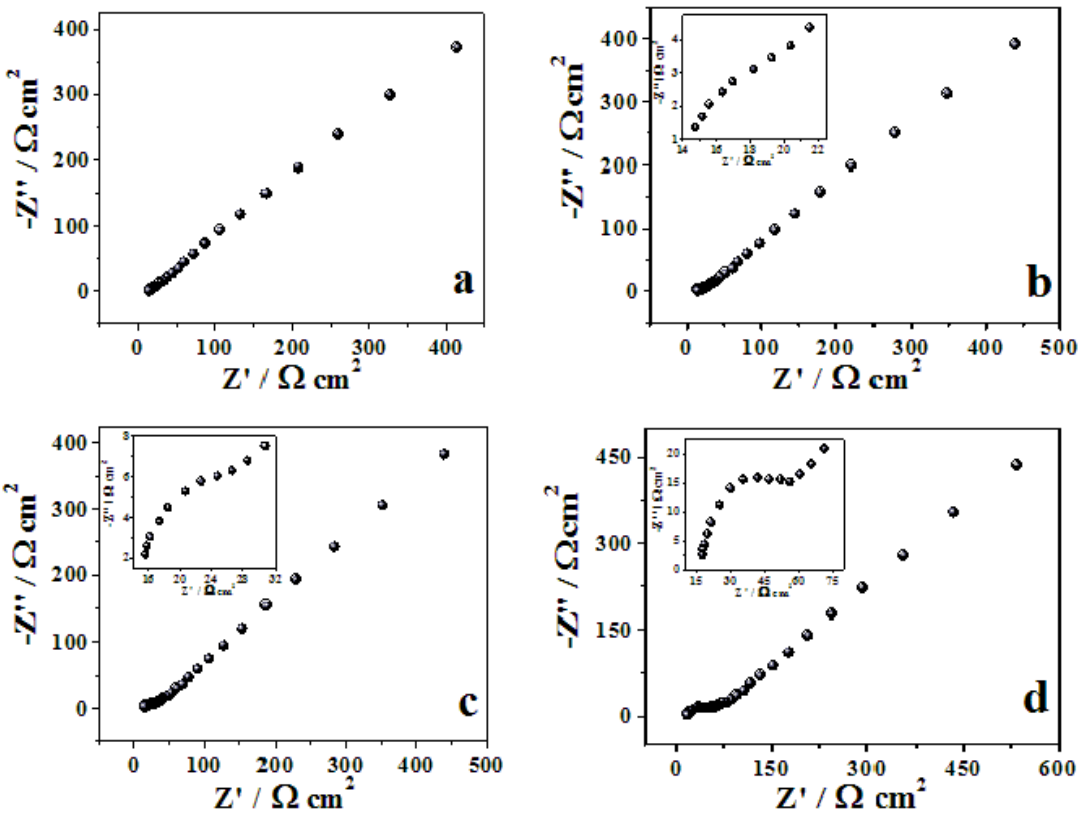

Figure 6: Impedance plots in 1mM hexaammineruthenium(III) chloride with 0.1M $LiClO_4$ as the supporting electrolyte for, (a) bare Au electrode, (b), SAM of 2-naphthalenethiol coated Au electrode, (c) potential cycled electrode after the monolayer formation and (d) annealed electrode after the monolayer formation. Inset shows the zoomed impedance plots of the above-mentioned electrodes at high frequency region, indicating the marginal increase in the R_{ct} values of the respective electrodes.

In general, the electron transfer reaction on the SAM modified gold electrodes can occur either through pinholes and defects present in the monolayer or by tunneling process. In the case of aromatic thiols the electron transfer can be further facilitated by the delocalized π-electrons present in the molecule due to extended conjugation. It is well known that the long chain aliphatic thiols form a well-packed, highly dense monolayer, free of measurable pinholes and act as a barrier to the electron transfer reaction and ion penetration. If the electron transfer occurs through the pinholes and defects present in the monolayer, then the response of cyclic voltammogram will depend upon the distribution of pinholes and defects present in the structure of the monolayer. A linear diffusion process is expected when the pinholes are close enough for the diffusion layers to be overlapping with each other facilitating the electron transfer reaction. If the pinholes and defects are more widely spaced and evenly distributed, then there is no overlap of the diffusion layer and the pores constitute an array of microelectrodes leading to a radial diffusion. In the case of SAM of 2-naphthalenethiol on Au, the response obtained in the cyclic voltammogram of $[Fe(CN)_6]^{3-|4-}$ redox couple (Fig. 1(b)) shows that the linear diffusion is dominant and the electron transfer occurs through the gaps available in the monolayer. The potential cycling effect leads to an effective packing of the monolayer with much less pinholes and defects (Fig. 3(b)). After annealing, the radial diffusion process dominates and the electrode behaves like a microelectrode array with an excellent blocking of the redox reaction (Fig. 3(c)).

We have carried out several of experiments intended to evaluate the integrity of the monolayer and to rule out the possibility of any reaction product blocking the $[Fe(CN)_6]^{3-|4-}$ redox reaction. One of the experiments involved first carrying out CV studies in the potential range from –0.4V to 0.1V vs. SCE

corresponding to that of $[Ru(NH_3)_6]^{2+|3+}$ redox reaction where a reversible CV is obtained (Fig. 7(a)). This is followed by scanning the same electrode in the potential region from –0.1V to 0.5V vs. SCE corresponding to $[Fe(CN)_6]^{3-|4-}$ redox reaction. Here the CV (Fig. 7(b)) shows a fully blocking behaviour. Further scanning at the potential range of $[Ru(NH_3)_6]^{2+|3+}$ redox reaction again exhibits a reversible CV (Fig. 7(c)). From these experiments we show that the monolayer is neither desorbed nor undergo any structural transformation within these potential ranges. It is very clear from the above series of experiments that the monolayer of 2-naphthalenethiol on Au is selective to ruthenium redox reaction and blocks potassium ferrocyanide reaction. These studies also prove that 2-naphthalenethiol does not undergo any redox reaction within the potential range of our study. Figure 7 shows the CV responses for the above-mentioned series of experiments.

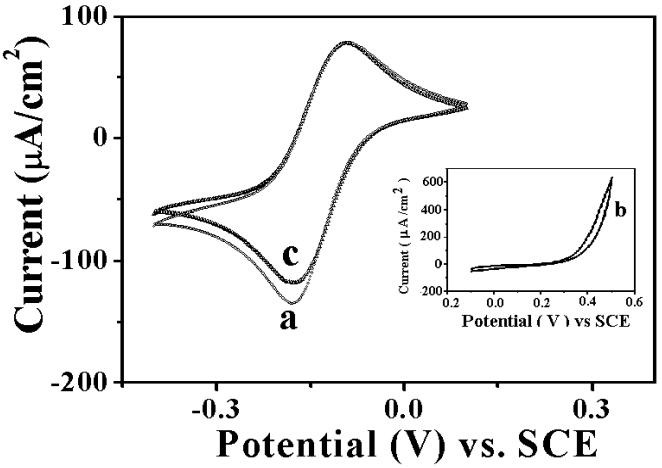

Figure 7: Cyclic voltammograms of SAM of 2-naphthalenethiol on Au coated electrodes at a potential scan rate of 50mV/s in, (a) 1mM hexaammineruthenium(III) chloride with 0.1M $LiClO_4$ as the supporting electrolyte. (b) 10mM potassium ferrocyanide with 1M NaF as the supporting electrolyte after the above scan. (c) Again in 1mM hexaammineruthenium(III) chloride with 0.1M $LiClO_4$ as the supporting electrolyte after the above scan.

We have also studied the potential dependence of interfacial capacitance of the monolayer of 2-naphthalenethiol on Au surface. Figure 8 shows a plot of change of interfacial capacitance of the monolayer-coated electrode with the potential. These studies clearly indicate that the monolayer is stable and intact on the electrode surface at the potential ranges used for the study of electron transfer processes of both potassium ferro/ferri cyanide and hexaammineruthenium(III) chloride redox couples. The measured capacitance values in 1M NaF aqueous solution also do not show any large changes within in the potential range of -0.6V to +0.8V vs. SCE except at extreme ranges used for the analysis. This means that the 2-naphthalenethiol does not desorb or undergo any redox reaction on the electrode surface at this potential range. It is also clear from these studies that the potential dependent structural change of monolayer has not occurred at the potential range of the $[Ru(NH_3)_6]^{2+|3+}$ redox reaction which would have been reflected in abnormal increase in the capacitance value. This also rules out the possibility of hexaammineruthenium(III) species penetrating through the film and undergoing the redox reaction.

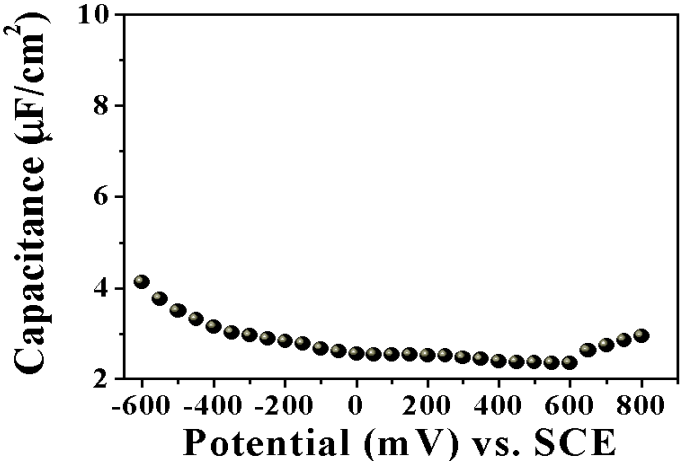

Figure 8: A plot of change of interfacial capacitance of SAM of 2-naphthalenethiol on Au coated electrode with potential.

The fact that the annealed monolayer completely blocks the electron transfer reaction in the case of ferrocyanide system and allows the ruthenium redox reaction shows that the SAM, far from acting as an effective barrier, actually facilitates the electron transfer reaction of ruthenium complex. It is well known that the hexaammineruthenium(III) chloride undergoes outer sphere electron transfer reaction in which the redox species approaches the SAM modified electrode surface and exchanges electron with the metal at a minimal distance with the hydration shell remaining intact [35]. This is in contrast to that of redox reaction of potassium ferro/ferri cyanide system, which involves the formation of reaction intermediates getting adsorbed on the electrode surface. In this case, the electron transfer is accompanied by a change in the structure of the coordination shell thereby involving bond rearrangements [36]. We feel that such a process is inhibited due to inaccessibility of the electrode surface to the redox species. The electron transfer process in the case of hexaammineruthenium(III) chloride reaction can take place by tunneling provided the process is facilitated by a suitable mediator. The tunneling process via the alkyl chain is well known in the case of alkanethiols [37-40] and oligophenylenevinylene bridges between a gold electrode and a tethered redox species in contact with an aqueous electrolyte [41]. However the electron transfer by tunneling will exhibit distance dependence and when the redox species is separated by several Å from the surface, the process should slow down and follow charge transfer kinetics. For a distant dependent electron transfer for a donor-bridge-acceptor system, the current (I) is exponentially related to the distance separating the centers of donor-acceptor (R) by the relationship $I \propto e^{-\beta R}$ where β is the inverse decay length which is a structure related attenuation factor for the SAM. While this factor is around $0.8 Å^{-1}$ for alkanethiols [40], it is generally low ($0.1\text{-}0.6 Å^{-1}$) for oligophenylene thiols [42]

and other conjugated oligomers [43], which is attributed to delocalization of donor and acceptor states on the bridge.

The fact that the reaction is not inhibited to a significant extent with diffusion control at lower frequencies points to a tunneling process where the π-electrons in the naphthalene ring facilitates the electron transfer between the ruthenium complex and the gold electrode. It has been earlier reported that in the case of both aromatic and hetero aromatic thiols, the electron transfer reaction is facilitated by the presence of highly delocalized π-electrons in the aromatic ring and also by the extended conjugation of the molecules [44-46]. This property of the aromatic SAM is extensively used for sensor and catalysis applications [47-49]. The aromatic SAM can also be used as a molecular bridge to study the effect of different interaction forces, ionic and hydrogen bonding in the long-range electron transfer reaction. The observed results were attributed to the tunneling process due to the presence of delocalized π-electrons in the aromatic ring, which acts as a bridge between the electrode surface and the redox probe [50-52]. In our case, the facile nature of electron transfer reaction of the ruthenium complex at the SAM-solution interface suggests a tunneling process, where the naphthalene ring with the delocalized π-electrons acts as a bridge between the monolayer-modified electrode and ruthenium complex.

4.3.3. Study of kinetics of adsorption of 2-naphthalenethiol on Au

While the kinetics of adsorption of alkanethiol SAMs on gold has been well studied [53-57], there are very few reports in literature on the kinetics of SAM formation of aromatic thiols. A study of the adsorption kinetics provides information on the monolayer evolution and structural organization with time. In the case of alkanethiol, the kinetics of monolayer formation is fairly clear.

The adsorption process generally follows the Langmuir kinetics at higher concentrations and diffusion controlled Langmuir model at lower concentrations of aliphatic thiols [53-57].

In the present work, we have studied the adsorption kinetics of 2-naphthalenethiol on gold using electrochemical impedance spectroscopy. In electrochemical systems, one of the earliest methods used for the study of adsorption kinetics is the measurement of interfacial capacitance [58]. It is well known that the capacitance of the electrical double layer precisely describes the adsorption properties and is being used widely in the study of self-assembled monolayer [59]. The monolayer forms a dielectric barrier between the metal and the electrolyte. The interfacial capacitance of a Metal-SAM-electrolyte interface consists of a series combination of the capacitance of SAM and capacitance of the diffuse layer. The overall capacitance is dominated by the smaller of the two, namely, the capacitance of SAM [1,2].

The adsorption kinetics of 2-naphthalenethiol monolayer on Au has been followed by measuring the impedance as a function of time using 10μM solution of 2-naphthalenethiol and 0.1M $LiClO_4$ in ethanol. The kinetics of SAM formation was carried out at two different potentials viz., 0V and 0.175V vs. SCE. From the imaginary component of impedance at the high frequency pseudo plateau region, the capacitance of the monolayer was measured as a function of time [56,57]. The surface coverage (θ) was obtained using the formula,

$$\theta = (C_0 - C_i) / (C_0 - C_f) \qquad (1)$$

where C_0 is the bare gold capacitance, C_i is the capacitance at any time t and C_f is the capacitance of the fully covered monolayer. Figures 9(a) and (b) show the plots of surface coverage with time for two different potential values. There are

two distinct time constants that can be seen from the θ-t plots. During the first fast step (from 0s to about 150s) almost 80-85% of coverage is completed and the second slower step (150s-1000s) extends to the almost complete coverage of the monolayer. We have fitted the data up to 1000s. However it can be seen from the figures that the complete coverage occurs beyond 3000s. We have observed some fluctuations in the surface coverage values beyond 2000s as can be seen from the Fig. 9. However such a behaviour had not been reported in the case of adsorption of alkanethiols on Au [53-57]. These fluctuations signify the rearrangement of molecules on the surface during the monolayer formation. We have calculated rate constants for the adsorption kinetics based on Langmuir and Diffusion controlled Langmuir (DCL) adsorption isotherms, which are represented as follows,

$$\theta(t) = [1- \exp (- k_m t)] \quad (2)$$

$$\theta(t) = [1- \exp (-k_m \sqrt{t})] \quad (3)$$

where θ(t) is the surface coverage at any instant time t and k_m is the rate constant of adsorption.

The insets of figures 9(a) and (b) show the plots of (1-θ) vs. time for the duration of the first time constant for the respective potentials. We obtained an excellent fit for these plots using Langmuir adsorption isotherm. We find that the rate constant values obtained from the first time constant, k_m for 2-naphthalenethiol adsorption varies with the applied potential viz., $0.0588s^{-1}$ and $0.0379s^{-1}$ for 0V and 0.175V vs. SCE respectively. The initial rate of adsorption is distinctly faster at 0V vs. SCE. However the full coverage is reached only beyond 2500s. In the case of 0.175V vs. SCE though the initial rate of adsorption is slower, the full coverage is reached at the end of 1000s. We have used concentration independent rate constant k_a in order to compare with the

rate of adsorption of alkanethiols as reported in literature [53-57]. We find that k_a value obtained for 2-naphthalenethiol at 0.175V vs. SCE is close to that of alkanethiol value of about 2800 $M^{-1}s^{-1}$ [56]. However the rate of adsorption k_a of 5880 $M^{-1}s^{-1}$ at 0V vs. SCE is very much higher.

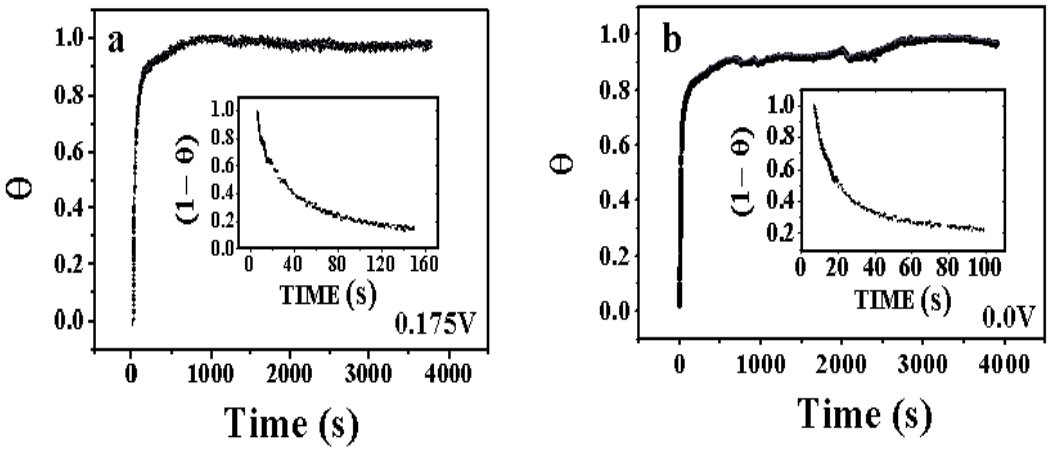

Figure 9: Surface coverage (θ) vs. time plots for 10μM 2-naphthalenethiol + 0.1M $LiClO_4$ in ethanol at potentials of (a) 0.175V and (b) 0V vs. SCE. The insets show the respective plots of (1-θ) vs. time during the initial duration of the adsorption corresponding to the first time constant.

The interfacial capacitance value of SAM modified electrode was determined to be 2.76 ± 0.13μF/cm^2, which is somewhat higher than the theoretical value of the capacitance for the SAM of 2-naphthalenethiol on Au obtained using the following expression,

$$C = \varepsilon \varepsilon_0 A / d \qquad (4)$$

where C is the capacitance, ε is the dielectric constant, ε_0 is the permitivity of vacuum and d is the thickness of the monolayer. From the measured capacitance value, using the above equation we have calculated the thickness of the monolayer to be 8.02Å. Since the molecular length of 2-naphthalenethiol is

9.3Å, the lower value of the monolayer thickness obtained implies that the molecules are tilted from the surface normal. From the molecular length of 9.3Å for 2-naphthalenethiol and a monolayer thickness of 8.02Å, we have determined the tilt of the molecule to be about 30^0 from the Au surface normal.

4.3.4. Pore size analysis of the 2-naphthalenethiol SAM on Au

Electrochemical impedance spectroscopic studies on the SAM modified electrodes can provide valuable information on the distribution of pinholes and defects in the monolayer. Finklea et al. [60] developed a model for the impedance response of a monolayer-modified electrode, which behaves as an array of microelectrodes. Fawcett and coworkers have extensively studied the monolayer integrity by pore size analysis using electrochemical impedance data [61-63]. Based on the work of Matsuda [64] and Amatore [65], a model has been developed to fit the faradaic impedance data obtained for the electron transfer reactions at the SAM modified electrode, to understand the distribution of pinholes in the monolayer. The impedance expressions have been derived by assuming that the total pinhole area fraction, $(1-\theta)$ is less than 0.1, where θ is the surface coverage of the monolayer. Both the real and imaginary parts of the faradaic impedance values are plotted as a function of $\omega^{-1/2}$. There are two limiting cases for this theory to be applied. At higher frequencies the diffusion profiles of each individual microelectrode constituent of the array is separated in contrast to the situation at lower frequencies where there is an overlap.

In the case of SAM of 2-naphthalenethiol on Au, the presence of pinholes and defects are analyzed using the above-mentioned model. Figures 10 (a-e) show the real and imaginary parts of the faradaic impedance of different

SAM modified systems plotted as a function of $\omega^{-1/2}$. For comparison the plot of bare gold electrode is also shown in figure 10(a). Figures 10 (b) and (c) show the plots of real component of faradaic impedance Z'_f vs. $\omega^{-1/2}$ for the monolayer-coated electrode and annealed SAM electrodes respectively. Figures 10(d) and (e) show the plots of imaginary component of the faradaic impedance Z''_f vs. $\omega^{-1/2}$ for the respective above-mentioned electrodes. The faradaic impedance plots show the features similar to that of an array of microelectrodes. There are two linear domains at high and low frequencies for the Z'_f vs. $\omega^{-1/2}$ plot and a peak formation in the Z''_f vs. $\omega^{-1/2}$ plot corresponding to the frequency of transition between the two linear domains. According to the model proposed, this frequency separates the two time dependent diffusion profiles for the microelectrodes.

The surface coverage of the monolayer can be obtained from the slope of the Z'_f vs. $\omega^{-1/2}$ plot at a higher frequency region and it is given by,

$$m = \sigma + \sigma / (1 - \theta) \qquad (5)$$

where m is the slope, θ the surface coverage of the monolayer and σ the Warburg coefficient, which can be obtained from the unmodified bare gold electrode.

From the analysis of Fig. 10(b) and (c), a surface coverage value of 99% is obtained for the monolayer-modified electrode, which increases to a value of 99.5% after the annealing effect. It is proposed that the thermal annealing process eliminates any trapped solvent molecules (ethanol) during the adsorption process and helps in the formation of a highly dense, well-packed and compact monolayer.

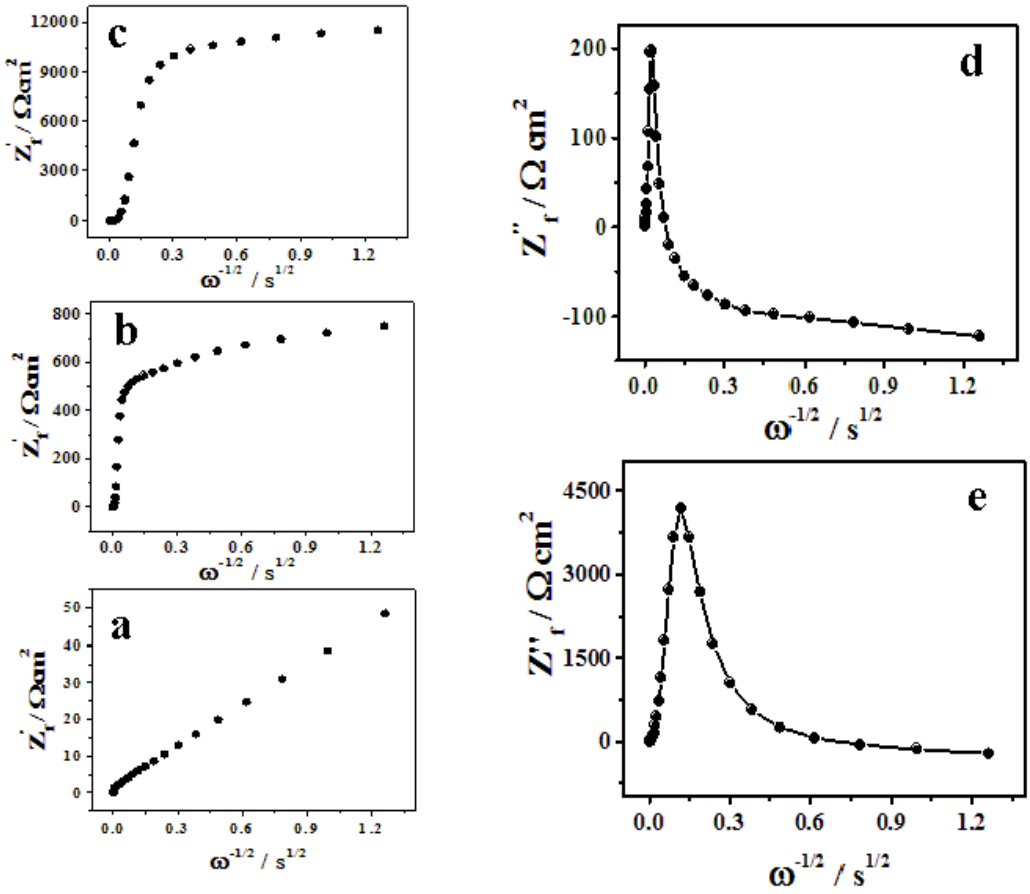

Figure 10: Plots of real part of the faradaic impedance (Z'_f) vs. $\omega^{-1/2}$ for, (a) bare Au electrode, (b) SAM of 2-naphthalenethiol coated Au electrode, and (c) annealed electrode after the SAM formation. Plots of imaginary part of the faradaic impedance (Z''_f) as a function of $\omega^{-1/2}$ for, (d) SAM of 2-naphthalenethiol modified Au electrode and (e) annealed electrode after the monolayer formation.

4.3.5. Gold oxide stripping analysis

The cyclic voltammogram of the gold electrode in 0.1M $HClO_4$ shows the usual features due to gold oxide formation during the positive potential scanning and oxide stripping upon reversing the scan direction. The quantity of electric charge passed during its removal of oxide is proportional to the effective electrode area. By comparing the charge of a SAM modified electrode with the respective charge of the bare gold electrode, the surface coverage of the monolayer can be measured qualitatively.

Figure 11 shows the cyclic voltammograms of gold oxidation in 0.1M $HClO_4$. Figure 11(a) shows the gold oxide formation and stripping peaks for a bare gold electrode. Figures 11(b) and (c) show the CVs for the SAM of 2-naphthalenethiol on Au before and after thermal annealing respectively. Compared to bare gold electrode, the measured charge on the monolayer-modified electrodes is significantly less as expected. It can be seen that the charge values measured for these two electrodes before and after annealing, from the cathodic stripping peaks are almost the same (350 nC/cm^2). The area fraction of the coverage is calculated to be 0.95 from the formula $(1-Q_{SAM} / Q_{Au})$ where the Q_{SAM} is the charge measured for the monolayer-covered electrode and Q_{Au} for the bare gold electrode. This coverage fraction is much smaller than the value obtained from the impedance plot viz., 0.99 – 0.995. This difference in the values can be attributed to the fact that smaller OH^- ions have easier access to the electrode surface compared to the bulkier ferrocyanide ions, which are used as coverage probes in these two methods.

However, after 3 to 4 cycles in 0.1M $HClO_4$, the voltammogram is almost similar to that of the bare gold electrode indicating the complete removal of the monolayer. The desorption of the monolayer is confirmed by the fact that

the potassium ferrocyanide electron transfer reaction produces reversible peaks on the electrode which was subjected to the oxide stripping experiment. This indicates that the monolayer is not electrochemically stable when cycled to very high positive potentials.

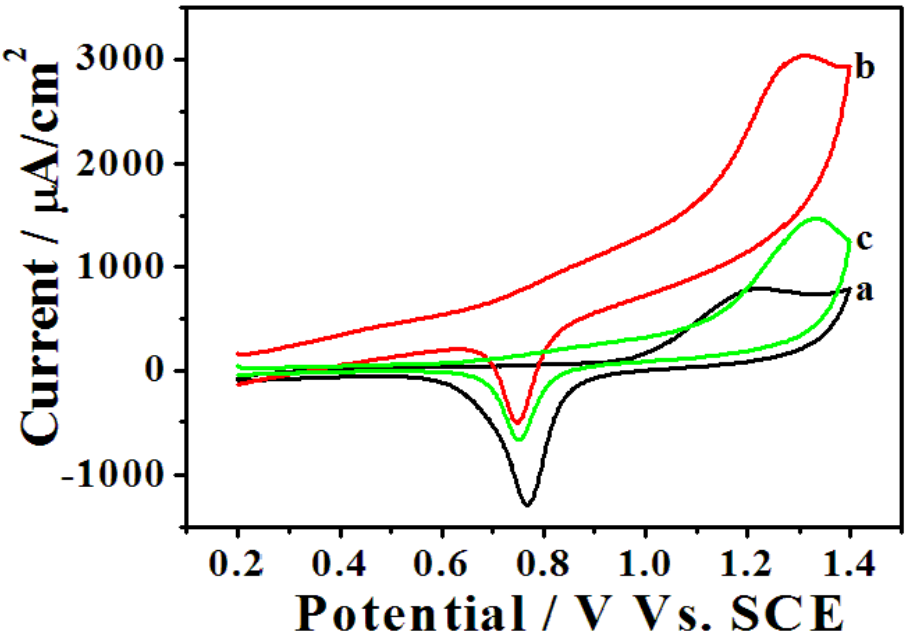

Figure 11: Cyclic voltammograms of gold oxide stripping analysis in 0.1M $HClO_4$ for, (a) bare Au electrode, (b) SAM of 2-naphthalenethiol modified Au electrode and (c) annealed SAM after the monolayer formation.

4.3.6. Grazing angle FTIR spectroscopy

We have carried out grazing angle FTIR spectroscopy on SAM of 2-naphthalenethiol on Au to characterize its orientation. Figures 12(a) and (b) show the FTIR spectrum of monolayer modified Au surface before and after the annealing effect respectively. The bulk spectrum of 2-naphthalenethiol is also shown in the figure 12(c). The multiple peaks between 1600 to 1700 cm^{-1} are

due to the aromatic ring C-C stretching mode. The peaks at 916 and 853 cm^{-1} are due to the out of plane bending modes of aromatic C-H group. The presence of peaks due to aromatic ring C-C stretching mode and out of plane bending of aromatic C-H group implies that the naphthalene ring is not lying parallel to the Au surface. However we do not see any peak at 3050 cm^{-1} due to the stretching mode of aromatic ring C-H group as it is obscured by the rapid fall of detector sensitivity in that region.

The striking feature of the two spectra is the positive shift in the wavenumber for the aromatic ring C-C stretching mode after annealing. There is a positive peak shift by ~4-5 cm^{-1} which can be attributed to the formation of a highly ordered and compact monolayer after annealing process. The annealing effect improves the packing density of the monolayer by making the aromatic ring moiety to be tilted slightly, thereby increasing the van der Waals interaction among the aromatic rings. These results show that the effect of annealing leads to the formation of a well packed highly oriented monolayer of 2-naphthalenethiol on Au surface.

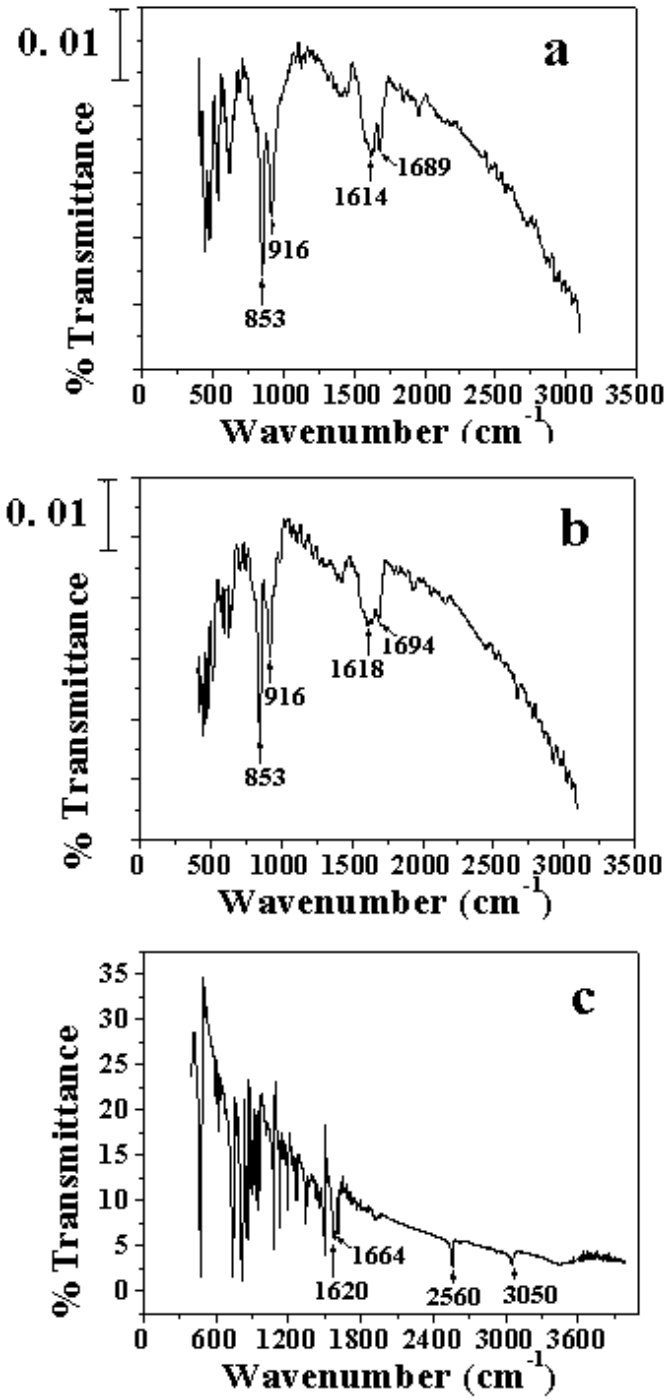

Figure 12: Grazing angle FTIR spectra of (a) monolayer of 2-naphthalenethiol coated Au electrode, (b) annealed electrode after the monolayer formation and (c) bulk 2-naphthalenethiol in KBr.

4.3.7. Scanning tunneling microscopy (STM)

STM studies have been used to characterize the structure of the monolayer at molecular level and also to understand nature of the adsorbed film. Figure 13(a) shows the constant current STM image of bare gold surface, which was used for forming the monolayer film at 6nm x 6nm range. Though the atomic features could not be resolved, the surface has a predominantly Au (111) orientation as determined by X-ray diffraction studies. Figure 13(b) shows the Fourier filtered constant height images of 2-naphthalenethiol monolayer adsorbed on the evaporated gold surface at 6nm x 6nm range. The chemisorbed S-S bond distance is determined to be 5Å in the adjacent columns of the image (Fig. 13(c)). The vertical bright spots correspond to the individual molecules of 2-naphthalenethiol adsorbed on Au surface. These molecules, which are arranged in diagonal rows, are separated by a distance of 8.4Å. It can be seen that the area per molecule corresponds to 42Å^2 (8.4Å x 5Å). This value almost exactly corresponds to the observed value of 41.4Å^2 per naphthalene molecule on a smooth polycrystalline Au surface [29]. Again, from the STM image (Fig. 13), the monolayer coverage on the gold surface is calculated to be about $4x10^{-10}$ mol per true surface area (roughness factor of gold surface used for STM measurements is 1.6). A closer look on the image shows that the high electron density region in the individual molecular space spreads to about 6Å, a rather large value for the naphthalene ring in upright orientation. This means that the molecule is canted with respect to the Au surface normal, which is in agreement with the earlier results of Kolega and Schlenoff [29]. This structural orientation of naphthalene ring on Au surface obtained for the monolayer using STM is again in conformity with our earlier results of both the electron transfer reaction of ruthenium complex (based on CV and EIS) and grazing angle FTIR spectroscopy. The possible structure of 2-naphthalenethiol orientations on gold

is modeled based on the features of the molecular arrangement shown in figure 13(c). The schematic structure with respect to underlying gold surface is shown in figure 13(d) along with the dimensions. It can be seen that the surface structure can be described as $\sqrt{3}$ x 3 R 30^0 overlayer structure of 2-naphthalenethiol on gold.

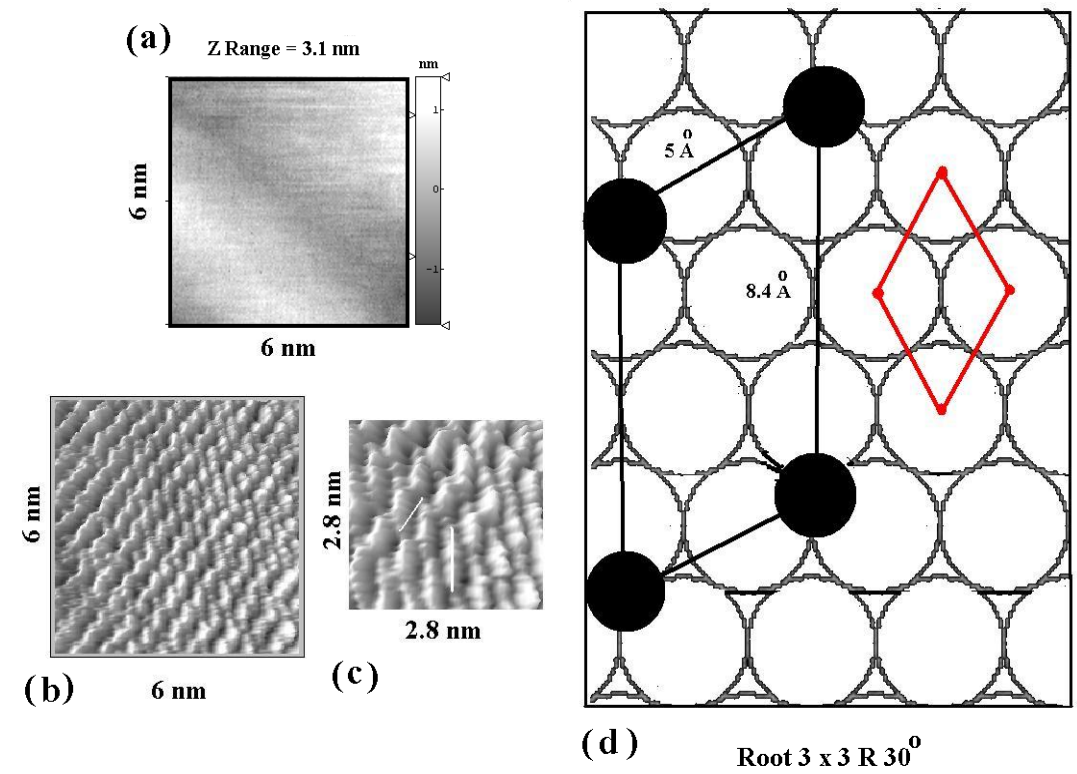

Figure 13: (a) STM image of bare Au surface at 6nm x 6nm range. (b) Constant height STM image of 2-naphthalenethiol adsorbed on Au surface at 6nm x 6nm scan range showing individual molecules. (c) Zoomed image of 2.8nm x 2.8nm. The slanted white line of 5Å corresponds to the distance between sulphur atoms of adjacent columns of 2-naphthalenethiol molecules and vertical line of 8.4Å corresponds to the distance between the two sulphur atoms of adjacent rows of 2-naphthalenethiol molecules. (d) Model of adsorption of 2-naphthalenethiol on Au surface and its structural orientation of $\sqrt{3}$ X 3 R30^0 overlayer. The arrangement of Au substrate atoms is shown in diamond shape on the right.

II. SAMs OF THIOPHENOL AND AMINOTHIOPHENOLS ON Au

4.4. Introduction

We have carried out studies on the monolayer formation and its characterization of some aromatic thiols namely thiophenol (TP), o-aminothiophenol (o-ATP) and p-aminothiophenol (p-ATP) on polycrystalline Au surface. We have evaluated the barrier property and blocking ability of these aromatic monolayers on Au surface by studying the electron transfer reactions of redox probe molecules on the SAM modified surfaces using electrochemical techniques such as cyclic voltammetry and electrochemical impedance spectroscopy. We have also studied the effect of pH on the blocking ability of the monolayers of aminothiophenols on Au surface. It is found that the monolayers of these aromatic thiols on Au surface exhibit a poor blocking ability towards the redox reactions. We have tried to improve the barrier property of these aromatic monolayers on Au surface by potential cycling and mixed SAM formation using aliphatic thiols of comparable chain length.

We find from literature that there are a large number of reports on the SAM of n-alkanethiols on gold surface [66-70], which is the most widely studied system due to the flexibility offered by the long aliphatic chains, the inertness of gold substrate and the ease of preparation method by a simple immersion process [14]. Usually, the SAMs of aliphatic thiols are obtained by immersing the metal into a dilute organic solution containing the thiol molecules whose concentration varies from typically μM to mM in solvents such as ethanol and acetonitrile. The SAMs of long-chain n-alkanethiols, which exhibit a high degree of organization and long range ordering have been used as model systems to study the electron transfer mechanism [71-75] and ω-functionalized aliphatic thiols have been extensively used for modifying the surface properties. The blocking ability of the monolayer is usually evaluated

by studying the electron transfer reactions of the redox probes like potassium ferro/ferri cyanide and hexaammineruthenium(III) chloride on SAM modified surfaces using electrochemical techniques namely cyclic voltammetry and electrochemical impedance spectroscopy [61-63,76].

In contrast to the well-studied long chain aliphatic thiols used for SAM formation, there is relatively a little attention that has been paid to the aromatic thiols. In recent times, the research work on the SAM of aromatic thiols on Au surface has attracted renewed interest due to their potential applications in molecular electronics especially in the study of molecular wires and coulomb blockade [77-81]. Aromatic thiol monolayers represent an interesting system owing to the presence of delocalized π-electrons in the aromatic phenyl ring, which results in increased electrical conductivity and the rigidity of aromatic phenyl ring, which reduces the molecular flexibility. SAMs based on aromatic thiols offer an opportunity to enhance the electrical coupling between the electronic states of the electrode and the redox species in the solution. In addition, it would be of great interest to study the electrode kinetics of SAM modified electrodes using aromatic thiols. It is well known that the monolayers of long chain aliphatic thiols offer a high resistance and slow down the electrode kinetics significantly. On the other hand, the SAM of aromatic thiols are expected to show a lower barrier to the electrode kinetics due to the presence of high density of delocalized π-electrons in the phenyl ring. The pioneering experiments on the adsorption of purely aromatic thiols were carried out by Hubbard et al. [82], who studied the monolayer formation of thiophenol, benzyl mercaptan and few other aromatic molecules on platinum [Pt (111)] and silver [Ag (111)] using Auger electron spectroscopy (AES) and Electron energy loss spectroscopy (EELS). These studies shown that the monolayers formed on Pt (111) surface did not possess the long range ordering unlike that of Ag (111),

where they exhibit a long range order. Later, using vibrational spectroscopic studies it has been shown that the aromatic molecules attach to the Au surface through the thiolate bond formation and the results were helpful to determine the orientation of molecules on the surface [83].

There are a few reports in literature on the SAM of thiophenol (TP) and aminothiophenols (ATPs) on Au surface. Rubinstein et al. were the first to investigate the formation of SAM based on aromatic thiols using electrochemical techniques [84]. These authors studied the formation of SAMs of thiophenol, biphenyl mercaptan and terphenyl mercaptan on gold surface and found that the ordering, packing efficiency, stability and blocking ability of the monolayers increased from thiophenol (TP) to terphenyl mercaptan [84]. There are however a very few reports in literature on the electrochemistry of SAM of p-aminothiophenol (p-ATP) on gold surface. Crooks et al. reported the formation of SAM of p-aminothiophenol on Au surface and found that the electron transfer reactions on the SAM modified surfaces were affected by the pH of the medium [85]. The interesting aspect of this work is that the redox reaction of hexaammineruthenium(III) chloride is facilitated even in acidic medium and no mechanism for this unusual behaviour of SAM has been proposed. Shannon et al. [86] reported the electrochemistry of mixed monolayers of p-aminothiophenol (p-ATP) and thiophenol (TP) on Au surface and proposed an ECE mechanism for the oxidation of SAM in acidic medium resulting in the formation of dimer species, which has been proved by spectroscopic techniques. Lukkari et al. reported the formation of SAM of p-aminothiophenol on gold [87] and found that the potential for the surface reaction of oxide stripping is shifted in the case of SAM modified electrodes in acidic medium. These authors also proposed an ECE mechanism for the formation of quinone derivative during dimerization reaction and the different

species formed during the oxidation reaction have been confirmed by XPS, electro-reflectance spectroscopy and electrochemical techniques. A thorough investigation on the electrochemistry and structure of the SAMs of isomers of aminothiophenols on gold surface has been reported by Batz et al. [88]. These authors found that the packing density of SAM varies in the order p-ATP>m-ATP>o-ATP>TP and results in benzoquinone form during oxidation in acidic medium, which has been confirmed by XPS. Mohri et al. [89,90] reported the kinetic study on the monolayer formation of p-ATP on gold surface and also the desorption of p-ATP bound to a gold surface using UV-absorption spectroscopy and XPS.

While studies on the SAMs of thiophenol (TP) and aminothiophenols (ATPs) on Au surface are available in literature [82-90], there is however, no reported works on mixed SAMs using aliphatic thiols. The aliphatic thiols with their small Van der Waals radii can easily pack the vacant regions occurring due to pinholes and defects in the monolayer. This can provide effective barrier to the access of redox species to the electrode surface. In this work we have also tried to improve the blocking ability of TP and ATPs monolayers using two different approaches namely, (i) the effect of potential cycling and (ii) formation of mixed SAM using 1-Octanethiol and 1,6-Hexanedithiol. These alkanethiols have comparable chain lengths with the thiophenol and aminothiophenols. The effect of potential cycling on the structural aspects of the monolayers on various surfaces had earlier been discussed and reported in literature by other groups [31-33,91,92]. Anderson and Gatin studied the self-assembled monolayer (SAM) of octanethiol on gold using polarization modulation Fourier transform infrared reflection absorption spectroscopy (PM-FTIRRAS) and found that the applied potential induces the structural changes on the monolayer resulting in the formation of a compact and more organized

monolayer [33]. Whitesides et al. studied the wetting of SAMs of alkanethiolates on gold surface by applied electrical potentials using contact angle measurements and found that it is possible to prepare patterned SAMs in which certain regions can be transformed from hydrophobic to hydrophilic nature by changing the electrode potential [91]. Boubour and Lennox reported the stability of ω-functionalized SAMs as a function of applied potential [32] and the potential induced defects in n-alkanethiol monolayers [31] by studying the ionic permeability using electrochemical impedance spectroscopy. There are several reports in literature on the study of electron transfer reactions through mixed monolayers [93-96]. The replacement of one thiol by another thiol moiety was also reported. Even though there are quite a few reports on the electrochemical aspects of SAM of TP and ATPs, we find from literature that the electron transfer reactions of redox couples, the effect of pH and a clear understanding of pinholes and defects, determination of surface coverage on the SAM modified surfaces have not been clearly resolved and reported. We have also used a mixed aromatic-aliphatic thiol monolayer in order to improve the blocking ability of the SAM, essentially by filling up the pinholes and defects present within the monolayer.

In this section, we discuss the results of our study on the electrochemistry of self-assembled monolayers of thiophenol (TP), o-aminothiophenol (o-ATP) and p-aminothiophenol (p-ATP) on gold surface. We have also described the effect of potential cycling and mixed SAM formation on the blocking property of these monolayers on Au surface. Electrochemical techniques such as cyclic voltammetry (CV), electrochemical impedance spectroscopy (EIS) and gold oxide stripping analysis were employed to evaluate the barrier properties of the monolayer. We have used two important redox systems namely $[Fe(CN)_6]^{3-|4-}$ and $[Ru(NH_3)_6]^{2+|3+}$ to study the redox reactions

on the SAM modified electrodes. The effect of pH on the blocking ability of these monolayers has also been investigated using CV and EIS by studying the electron transfer reactions of the redox probes on the SAM modified surfaces under the acidic and basic conditions. Impedance spectroscopy data were used to determine the charge transfer resistance (R_{ct}) value, which is the measure of blocking ability of the monolayer towards the diffusion of redox species. In addition, EIS data are used for the determination of surface coverage and pinholes and defects analysis.

4.5. Experimental section

4.5.1. Chemicals

All the chemical reagents used in this study were analytical grade (AR) reagents. Thiophenol (Aldrich), o-Aminothiophenol (Aldrich), p-Aminothiophenol (Aldrich), 1-Octanethiol (Aldrich), 1,6-Hexanedithiol (Aldrich), ethanol (99.95%; Merck), potassium ferrocyanide (Loba), potassium ferricyanide (Qualigens), hexaammineruthenium(III) chloride (Alfa Aesar), sodium fluoride (Qualigens), lithium perchlorate (Acros Organics) and perchloric acid (Qualigens) were used in this study as received. Millipore water having a resistivity of 18 MΩ cm was used to prepare the aqueous solutions.

4.5.2. Fabrication of electrodes and electrochemical cell

We have carried out the monolayer adsorption, preparation of mixed SAM and its electrochemical characterization using a gold wire electrode. Gold sample of purity 99.99% was obtained from Arora Mathey, India. The gold wire electrode was fabricated by proper sealing of a 99.99% pure gold wire of 0.5mm diameter with soda lime glass having a thermal expansion coefficient close to that of gold. The electrical contact has been provided through a copper

wire. This planar disc electrode has a geometric area of 0.002 cm^2. This small area-working electrode has a highly reproducible true surface area even after repeated usage, which has been confirmed by the measurement of roughness factor of the gold wire electrode by potential cycling in 0.1M perchloric acid. A conventional three-electrode electrochemical cell was used for the experimental studies involving the characterization of SAM modified electrodes using electrochemical techniques. A platinum foil of large surface area was used as a counter electrode and a saturated calomel electrode (SCE) was used as a reference electrode while the SAM modified electrodes were used as the working electrode. The cell was cleaned thoroughly before each experiment and kept in a hot-air oven at 100^0C for at least 1 hour before the start of the experiment.

4.5.3. Electrode pre-treatment and preparation of aromatic SAMs and mixed SAMs on gold surface

Immediately before use, the gold wire electrode was polished with emery papers of grade 800 and 1500 respectively, followed by polishing in aqueous slurries of progressively finer alumina of sizes ranging from 1.0μm, 0.3μm to 0.05 μm on a microcloth. After this, the electrode was ultrasonicated in millipore water to remove alumina particles. Then it was cleaned in a "piranha" solution, which is a mixture of 30% H_2O_2 and concentrated H_2SO_4 in 1:3 ratio. Finally, the polished gold wire electrode was thoroughly cleaned and rinsed in distilled water, followed by rinsing in millipore water before SAM formation. The monolayers were prepared by keeping the Au wire electrode in neat thiol (in the case of TP and o-ATP) and 20mM thiol solution in ethanol (in the case of p-ATP) for about 1 hour. We have found from our earlier work that good surface coverage is obtained in view of the high concentration of thiols

used for the monolayer preparation [97]. After the adsorption of thiol, the electrode was rinsed with ethanol, distilled water and finally with millipore water and immediately used for the analysis. We have used two different thiols for mixed SAM formation with aromatic thiols namely, 1-Octanethiol (neat thiol) and 1,6-Hexanedithiol (neat thiol), which have comparable chain lengths to that of aromatic thiols used for the monolayer formation on Au surface. In the case of mixed SAM formation, initially the gold wire electrode was dipped in aromatic thiols for about 1 hour. After the adsorption of thiol, the electrode was rinsed with ethanol followed by cleaning in distilled water and immediately kept in neat thiol of either 1-Octanethiol or 1,6-Hexanedithiol for about 1 hour. On completion of mixed SAM formation, the monolayer-coated electrode was rinsed with ethanol; cleaned in distilled water and finally rinsed with millipore water and used for the analysis immediately. The mixed SAM formation was carried out in the following way viz., (a) 1-Octanethiol with TP or o-ATP or p-ATP on Au surface and (b) 1,6-Hexanedithiol with TP or o-ATP or p-ATP on Au surface.

4.5.4. Electrochemical characterization

Cyclic voltammetry and electrochemical impedance spectroscopy were used for the electrochemical characterization of monolayer coated and mixed SAM modified electrodes. The barrier property of the monolayer has been evaluated by studying the electron transfer reaction using two different redox probes namely, potassium ferrocyanide (negative redox probe) and hexaammineruthenium(III) chloride (positive redox probe). Cyclic voltammetry was performed in aqueous solutions of 10mM potassium ferrocyanide in 1M NaF at a potential range of –0.1V to +0.5V vs. SCE and 1mM hexaammineruthenium(III) chloride in 0.1M lithium perchlorate at a potential

range of –0.45V to +0.1V vs. SCE. The impedance measurements were carried out using an alternating current (ac) of a 10mV amplitude signal at a formal potential of the redox couple using a wide frequency range of 100kHz to 0.1Hz, in solution containing always equal concentrations of both the oxidized and reduced forms of the redox couple namely, 10mM potassium ferrocyanide and 10mM potassium ferricyanide in 1M NaF as the supporting electrolyte. The gold oxide stripping analysis was conducted in 0.1M perchloric acid in the potential range from 0.2V to 1.4V vs. SCE. The packing density and ordering of the monolayer can be understood by measuring the charge under the cathodic Au oxide stripping peak and comparing with that of the bare Au electrode. The pH of the medium was adjusted using 0.1M H_2SO_4 and 0.5M NaOH in order to maintain the respective acidic and basic conditions to study the redox reactions on the SAM modified electrodes.

In order to analyze the effect of potential cycling on the barrier property and structural organization of the monolayer on Au surface, the following experiments were carried out. Immediately after the monolayer formation, the electrode is subjected to potential cycling between 0.0V and 0.6V vs. SCE in a solution containing purely supporting electrolyte without any redox species and the same electrode is subsequently used for the cyclic voltammetry and impedance spectroscopic studies to determine the barrier property of the monolayer. From the impedance data, the charge transfer resistance (R_{ct}) was determined using the equivalent circuit fitting analysis. In addition, EIS data were used for the analysis of pinholes and defects in the cases of monolayer and mixed monolayer modified electrodes. From the R_{ct} values and pinholes and defects analysis, the surface coverage (θ) values of the monolayer and mixed monolayer on Au surface were also determined. All the experiments were performed at room temperature of 25^0C.

4.5.5. Instrumentation

Cyclic voltammetry was carried out using an EG&G potentiostat (model 263A) interfaced to a computer through a GPIB card (National Instruments). The potential ranges and scan rates used are shown in the respective diagrams. For electrochemical impedance spectroscopy measurements the potentiostat was used along with an EG&G 5210 lock-in-amplifier controlled by Power Sine software. The impedance spectroscopy data were used for the equivalent circuit fitting analysis using Zsimpwin software (EG&G) developed on the basis of Boukamp's model. Based on this procedure, the charge transfer resistance values (R_{ct}) of SAM modified electrodes were calculated, from which the surface coverage values of the monolayers on Au surface were also determined.

4.6. Results and discussion

4.6.1. Using aromatic SAM modified electrodes

4.6.1.1. Cyclic voltammetry

Cyclic voltammetry is an important tool to assess the quality of the monolayer and its blocking ability by studying the electron transfer reaction on the SAM modified surfaces using diffusion controlled redox couple as probe molecule. The SAMs of TP, o-ATP and p-ATP were formed on the polycrystalline Au surface by dipping the Au wire electrode in the respective thiol solutions. Figure 14 shows the cyclic voltammograms of bare Au electrode and SAM modified electrodes in 10mM potassium ferrocyanide with 1M NaF as the supporting electrolyte at a potential scan rate of 50mV/s. It can be seen from inset of the figure that the bare Au electrode shows a perfect reversible voltammogram for the redox couple indicating that the electron transfer reaction is completely under diffusion control process. Figures 14(a), (b) and (c)

show the respective cyclic voltammograms of SAMs of TP, o-ATP and p-ATP in the same solution. In contrast to the bare Au electrode, the SAM modified electrodes in the cases of TP and o-ATP do not show any peak formation implying that the redox reaction is inhibited. It can be seen from figure 14(a) that the SAM of TP on Au electrode shows 's' shaped curve with a large current separation between the forward and reverse direction indicating the moderate blocking behaviour of the monolayer with a large number of pinholes and defects. This observation is at variance with the results reported by Rubinstein et al. [84]. These authors reported that the monolayer of TP on Au is hardly blocking the electron transfer reaction. The difference in the blocking ability of the SAM of TP in the present case is attributed to the longer time of adsorption (1 hour) and the use of neat thiol for monolayer formation, in contrast to 15 minutes adsorption in 1mM aqueous solution of TP in the other case [84]. In the case of o-ATP (Fig. 14(b)) the CV shows a complete blocking to the electron transfer reaction implying the formation of highly compact and ordered monolayer on Au surface. On the other hand, SAM of p-ATP shows a quasi-reversible behaviour for the redox reaction exhibiting a rather imperfect blocking ability. This implies the formation of a highly disorganized and disordered poor monolayer film in the case of p-ATP on Au surface.

Figure 15 shows the comparison of cyclic voltammograms of bare Au electrode and SAM modified electrodes in 1mM hexaammineruthenium(III) chloride with 0.1M $LiClO_4$ as the supporting electrolyte at a potential scan rate of 50mV/s. It can be seen from inset of the figure that the bare Au electrode shows a reversible voltammogram implying the diffusion-controlled process for the redox reaction. Figures 15(a), (b) and (c) show the cyclic voltammograms of SAMs of TP, o-ATP and p-ATP in the same solution respectively. It can be noted from the figures that the redox reaction of ruthenium complex is not

inhibited significantly in all the cases although the SAM of TP on Au exhibits a very poor blocking behaviour. The results obtained in the case of SAM of p-ATP on Au surface is similar to the report of Crooks et al. [85], where they found that the redox reaction of ruthenium complex is quite facile for p-ATP modified Au electrode. These experiments lead to an interesting observation that the aromatic SAM is selective to ruthenium redox reaction and not to ferrocyanide redox reaction.

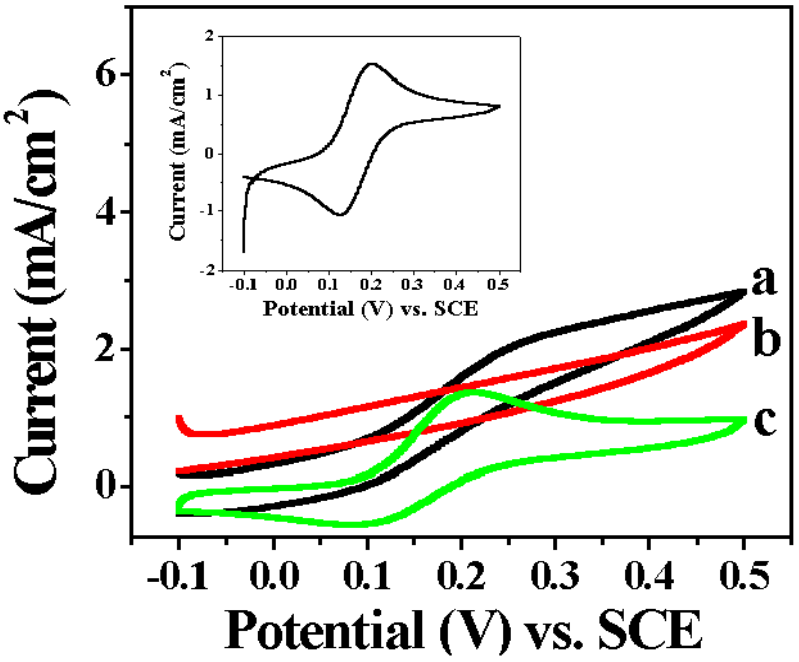

Figure 14: Cyclic voltammograms of SAMs of (a) Thiophenol (TP), (b) o-Aminothiophenol (o-ATP) and (c) p-Aminothiophenol (p-ATP) on Au surface in 10mM potassium ferrocyanide with 1M NaF as a supporting electrolyte at a potential scan rate of 50mV/s. Inset shows the cyclic voltammogram of a bare Au electrode in the same solution for comparison.

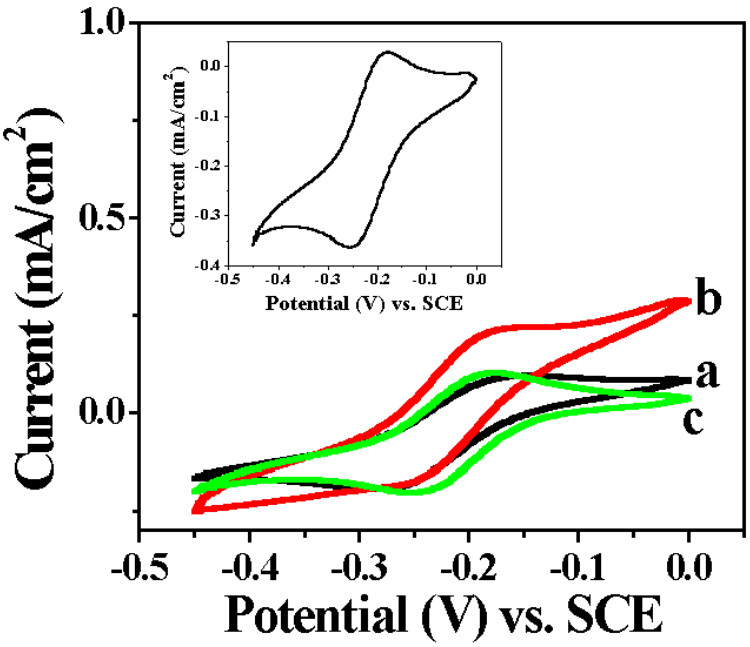

Figure 15: Cyclic voltammograms in 1mM hexaammineruthenium(III) chloride with 0.1M $LiClO_4$ as a supporting electrolyte at a potential scan rate of 50mV/s for the SAMs of (a) Thiophenol (TP), (b) o-Aminothiophenol (o-ATP) and (c) p-Aminothiophenol (p-ATP) on Au electrode. For comparison the cyclic voltammogram of bare Au electrode in the same solution is shown in the inset of the figure.

4.6.1.2. Electrochemical impedance spectroscopy

Electrochemical impedance spectroscopy is a powerful technique to evaluate the structural integrity of the monolayer and to determine the charge transfer resistance of the SAM modified electrodes against the diffusion of the redox probe in a quantitative manner. In addition, the impedance data are useful in the determination of the surface coverage and other kinetic parameters of the

monolayer coated electrodes. Figure 16A shows the impedance plot (Nyquist plot) of the bare Au electrode in equal concentrations of potassium ferro/ferri cyanide solution with NaF as the supporting electrolyte. Figure 16B shows the same plot for the SAM modified electrodes. It can be seen from the figure 16A that the bare Au electrode shows a low frequency straight line with a very small semicircle at high frequency region indicating that the electron transfer process is essentially diffusion controlled. On the other hand, SAM modified electrodes in the cases of TP (Fig. 16B(a)) and o-ATP (Fig. 16B(b)) show the formation of semicircle implying a good blocking behaviour and charge transfer control for the electron transfer reaction. It can be noted from figure 16B(a) that the impedance values are almost constant at lower frequencies in the case of SAM of TP on Au indicating the diffusion of probe molecules through the pores and pinholes. In contrast, SAM of p-ATP on Au (Fig. 16B (c)) shows a straight line at low frequency and a very small semicircle at high frequency region similar to that of bare Au implying the poor blocking ability of the SAM towards the redox reaction.

Figures 17A and B show the respective Nyquist plots of bare Au electrode and SAM modified electrodes in 1mM hexaammineruthenium(III) chloride solution with 0.1M $LiClO_4$ as the supporting electrolyte. The impedance plot of bare Au electrode (Fig. 17A) exhibits a low frequency straight line with a very small semicircle formation at high frequency indicating the diffusion-controlled process for the electron transfer reaction of ruthenium complex.

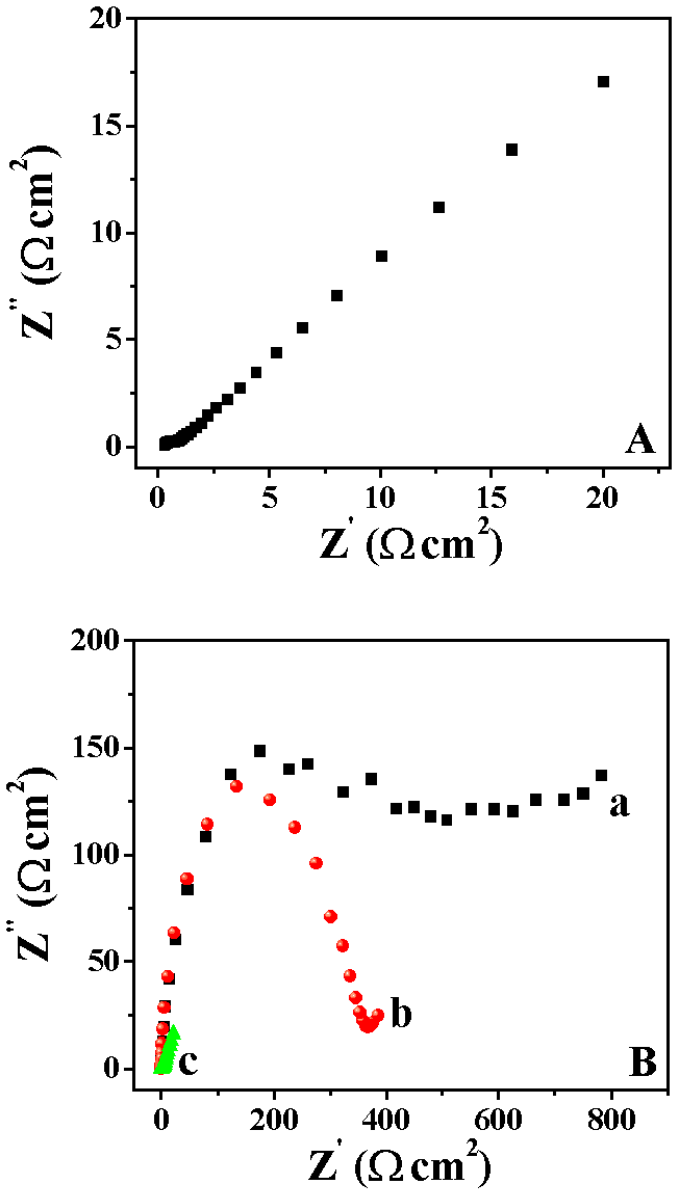

Figure 16: Impedance plots in 10mM potassium ferrocyanide and 10mM potassium ferricyanide with 1M NaF as supporting electrolyte for, (A) Bare Au electrode and (B) SAMs of TP (a), o-ATP (b) and p-ATP (c) on Au surface.

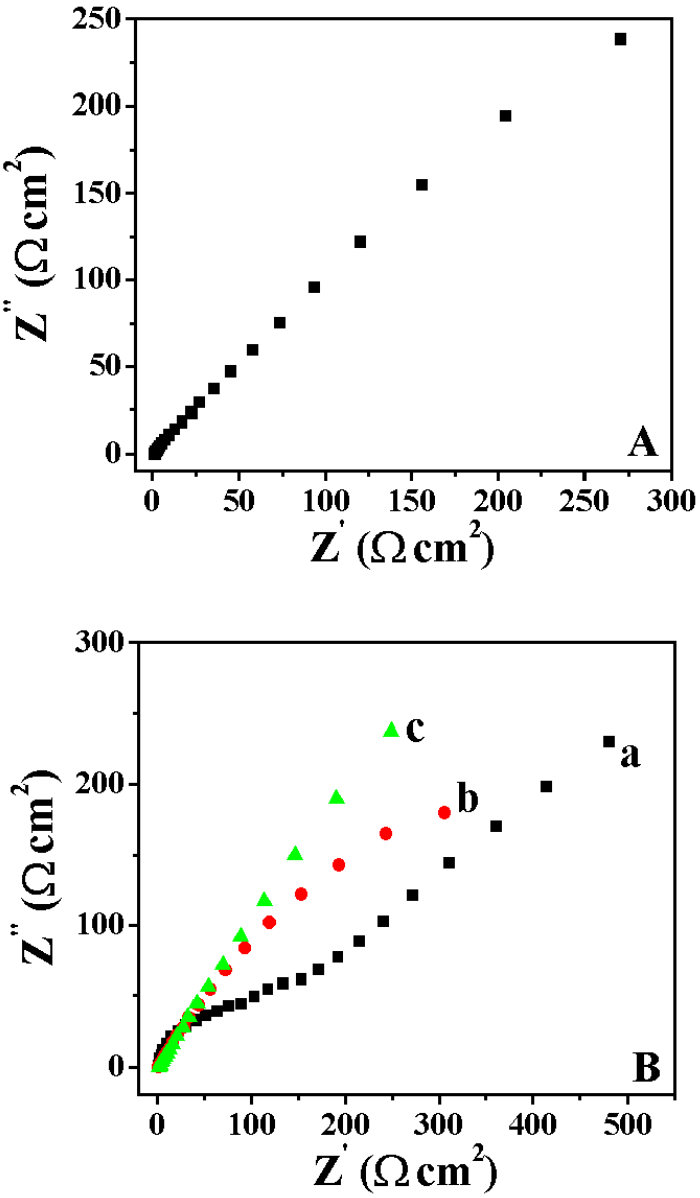

Figure 17: Impedance plots in 1mM hexaammineruthenium(III) chloride with 0.1M $LiClO_4$ as supporting electrolyte for, (A) Bare Au electrode and (B) SAMs of TP (a), o-ATP (b) and p-ATP (c) on Au electrode.

Similarly, the SAM modified electrodes in the cases of o-ATP (Fig. 17B(b)) and p-ATP (Fig. 17B(c)) show the facile nature of the Ru(III) electron transfer reaction indicating a very poor blocking ability of the monolayer. It can be seen from figure 17B(a) that the SAM of TP on Au shows a formation of semicircle at high frequency region and a straight line at low frequency with small increase in the charge transfer resistance implying the quasi-reversible behaviour for the redox reaction showing the poor blocking ability of the monolayer. These results are in conformity with our observations using cyclic voltammetric studies discussed earlier.

4.6.1.3. Gold oxide stripping analysis

The qualitative analysis of surface coverage of the monolayer can be carried out using oxide-stripping method. The cyclic voltammogram of bare Au electrode in 0.1M $HClO_4$ shows the usual features of gold oxide formation during the positive potential scanning and oxide stripping upon reversing the scan direction. The quantity of electric charges passed during its removal of oxide is proportional to the effective electrode area. By comparing the charge of a SAM modified electrode with the respective charge of the bare gold electrode, the surface coverage of the monolayer can be determined qualitatively.

Figure 18 shows the cyclic voltammograms of different electrodes in 0.1M $HClO_4$ for the gold oxide stripping analysis. For comparison the cyclic voltammogram of bare Au electrode was also given in figure 18(a) and it shows the gold oxide formation and stripping peaks. Figures 18(b), (c) and (d) show the respective cyclic voltammograms of SAMs of TP, o-ATP and p-ATP on Au surface in 0.1M $HClO_4$ solution. Compared with the bare Au electrode, the measured charges of the SAM modified electrodes are significantly less, as expected. The area fraction of the coverage is calculated using the formula (1–

$Q_{SAM}/Q_{Bare\ Au}$), where Q_{SAM} and $Q_{Bare\ Au}$ are the charges measured for the SAM modified electrodes and the bare Au electrode respectively.

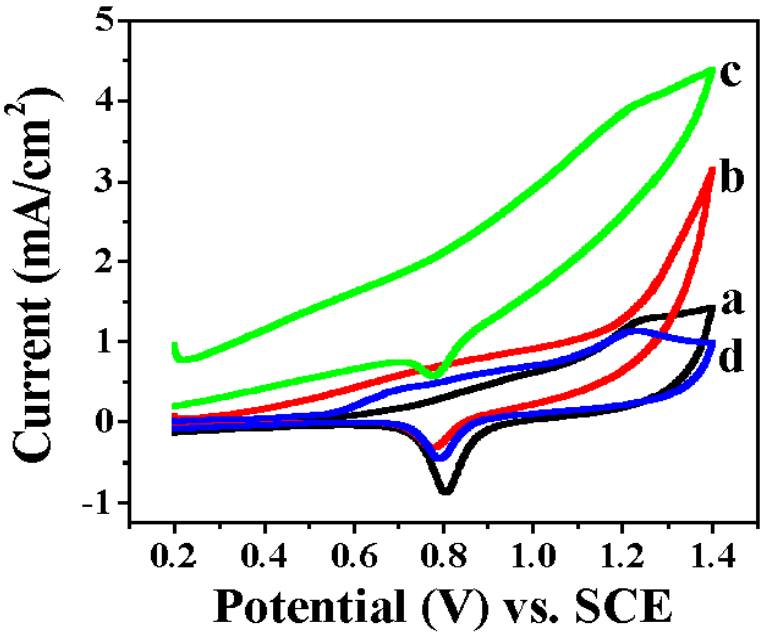

Figure 18: Cyclic voltammograms of gold oxide stripping analysis in 0.1M $HClO_4$ for, (a) bare Au electrode, (b) SAM of TP on Au electrode, (c) SAM of o-ATP on Au surface and (d) SAM of p-ATP on Au electrode.

It can be seen from the figures 18(b) and (c) that the charge values measured from the cathodic stripping peaks for the SAMs of TP and o-ATP are almost the same (~350 nC/cm^2) and a surface coverage value of 80% has been obtained, which is higher than the surface coverage value of 31% reported for TP on gold surface [84]. In the case of SAM of p-ATP (Fig. 18(d)), the calculated charge value is quite high, which results in a very low surface coverage value of 55%. The fact that the surface coverage values determined

using gold oxide stripping analysis are lower can be attributed to the smaller size of OH^- ion which acts as a probe in the present study that can have an easy access to the electrode surface through the pinholes and defects when compared to that of bulkier ions. However, after repeated cycles in perchloric acid, the SAM modified electrodes show the cyclic voltammogram similar to that of bare Au electrode indicating the complete removal of the monolayer. This confirms the fact that the monolayer is not electrochemically stable when cycled to high positive potentials.

4.6.1.4. Effect of pH on the blocking property of aromatic SAMs on Au

We have investigated the effect of pH on the blocking ability of SAMs of o-ATP and p-ATP on Au surface. Due to the presence of amino group in these molecules, depending upon the pH of the medium (acidic or basic), the surface modification of SAMs to hydrophilic or hydrophobic nature can be obtained. We have performed the study of electron transfer reaction of redox probe molecules on the SAM modified surfaces in acidic (pH = 3.2 to 3.5) and basic (pH = 11.0 to 11.2) conditions. The pH of the medium was adjusted using 0.1M H_2SO_4 and 0.5M NaOH aqueous solutions.

Cyclic voltammetry

(a). Acidic condition

Figure 19A shows the cyclic voltammograms of SAM modified surfaces in 10mM potassium ferrocyanide with 1M NaF as a supporting electrolyte at a potential scan rate of 50mV/s under the acidic condition. It can be seen from the figure that both the SAMs of o-ATP (Fig. 19A (a)) and p-ATP (Fig. 19A (b)) on Au surface show the facile kinetics of the electron transfer reaction, implying a very poor blocking ability of the monolayer. Figure 19B

shows the cyclic voltammograms of the monolayer-coated electrodes in 1mM hexaammineruthenium(III) chloride with 0.1M $LiClO_4$ as a supporting electrolyte at a potential scan rate of 50mV/s under the acidic condition. Figures 19B (a) and (b) show the respective cyclic voltammograms of SAMs of o-ATP and p-ATP on Au surface for the redox reaction of ruthenium complex. Surprisingly, the electron transfer reaction is allowed in both the cases showing the facile nature of Ru(III) reaction on the SAM modified surfaces indicating the poor blocking behaviour of the monolayer. The results obtained are similar to the report of Crooks et al. [85], where they found that the redox reaction of ruthenium complex is completely allowed in the case of SAM of p-ATP on Au surface under the acidic condition and no mechanism for this unusual behaviour of the monolayer is proposed.

(b). Basic condition

Figure 20A shows the cyclic voltammograms of monolayer-coated surfaces in 10mM potassium ferrocyanide with 1M NaF as a supporting electrolyte at a potential scan rate of 50mV/s under the basic condition. It can be seen from the figure 20A (a) that the SAM of o-ATP on Au shows the good blocking ability to the redox reaction indicating the formation of a highly dense and ordered hydrophobic SAM of o-ATP. In contrast, the SAM of p-ATP on Au (Fig. 20A (b)) does not inhibit the electron transfer reaction implying the formation of a poorly ordered SAM under the basic condition. Figure 20B shows the cyclic voltammograms of SAM modified surfaces in 1mM hexaammineruthenium(III) chloride with 0.1M $LiClO_4$ as a supporting electrolyte at a potential scan rate of 50mV/s under the basic condition. It can be seen from the figure that both the SAMs of o-ATP (Fig. 20B (a)) and p-ATP

(Fig. 20B (b)) on Au surface show a facile kinetics for the ruthenium redox reaction, indicating the poor blocking ability of SAMs.

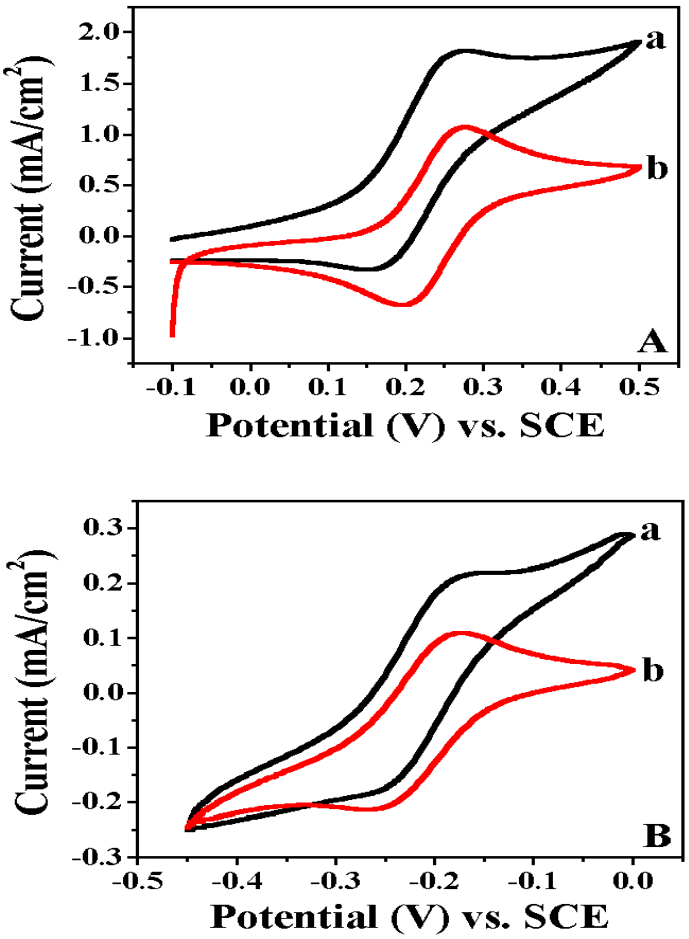

Figure 19: (A) Cyclic voltammograms in 10mM potassium ferrocyanide with 1M NaF as a supporting electrolyte at a potential scan rate of 50mV/s under the acidic condition (pH = 3.2 – 3.5) for, (a) SAM of o-ATP on Au surface and (b) SAM of p-ATP on Au surface. (B) Cyclic voltammograms in 1mM hexaammineruthenium(III) chloride with 0.1M $LiClO_4$ as a supporting electrolyte at a potential scan rate of 50mV/s under the acidic condition (pH = 3.2 – 3.5) for, (a) SAM of o-ATP on Au electrode and (b) SAM of p-ATP on Au electrode.

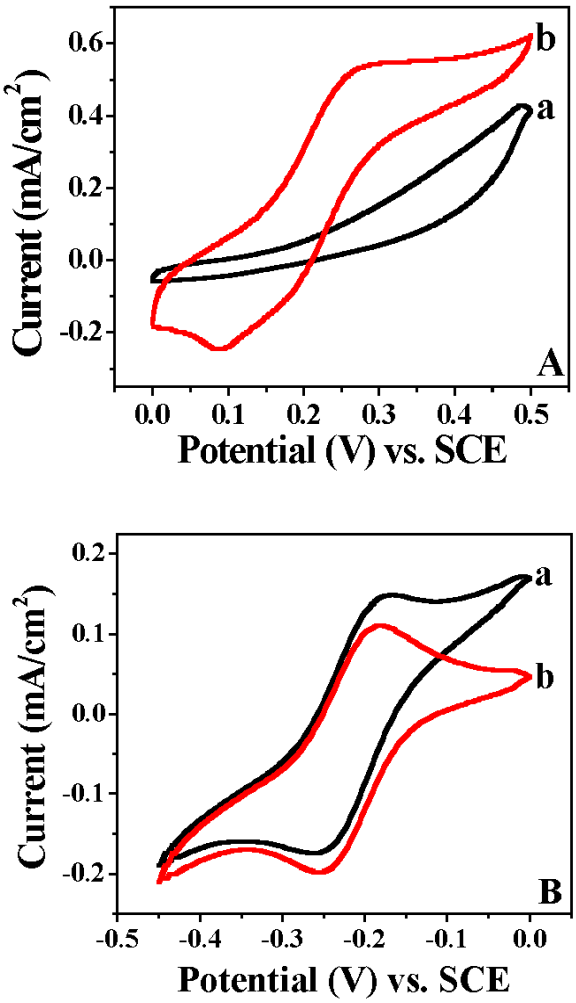

Figure 20: Cyclic voltammograms in 10mM potassium ferrocyanide with 1M NaF as a supporting electrolyte at a potential scan rate of 50mV/s under the basic condition (pH = 11.0 – 11.2) for, (a) SAM of o-ATP on Au surface and (b) SAM of p-ATP on Au surface. (B) Cyclic voltammograms in 1mM hexaammineruthenium(III) chloride with 0.1M $LiClO_4$ as a supporting electrolyte at a potential scan rate of 50mV/s under the basic condition (pH = 11.0 – 11.2) for, (a) SAM of o-ATP on Au electrode and (b) SAM of p-ATP on Au electrode.

Electrochemical impedance spectroscopy

(a). Acidic condition

Figure 21A shows the impedance (Nyquist) plots of SAM modified surfaces in 10mM potassium ferrocyanide and 10mM potassium ferricyanide with 1M NaF as a supporting electrolyte under the acidic condition. It can be seen from the figure that the SAM of o-ATP on Au (Fig. 21A (a)) shows the formation of a small semicircle at high frequency region and a straight line at low frequency indicating the poor blocking ability of the monolayer. Similarly, the SAM p-ATP on Au (Fig. 21A (b)) shows the formation of straight line in the entire range of frequency used for the study implying the diffusion-controlled process for the electron transfer reaction. Figure 21B shows the Nyquist plots of the monolayer coated electrodes in 1mM hexaammineruthenium(III) chloride with 0.1M $LiClO_4$ as a supporting electrolyte under the acidic condition. It can be noted from the figure that both the SAMs of o-ATP (Fig. 21B (a)) and p-ATP (Fig. 21B (b)) on Au surface show the facile kinetics for the ruthenium electron transfer reaction implying the poor blocking ability of the monolayer under the acidic condition.

(b). Basic condition

Figure 22A shows the typical impedance plots of SAM modified electrodes in 10mM potassium ferrocyanide and 10mM potassium ferricyanide with 1M NaF as a supporting electrolyte under the basic condition. It can be seen from the figure 22A (a) that the SAM of o-ATP on Au exhibits a semicircle indicating the good blocking behaviour of SAM to the redox reaction, while the SAM of p-ATP on Au (Fig. 22A (b)) shows a smaller semicircle and a diffusion controlled straight line at low frequency implying a less blocking behaviour of the SAM under the basic condition.

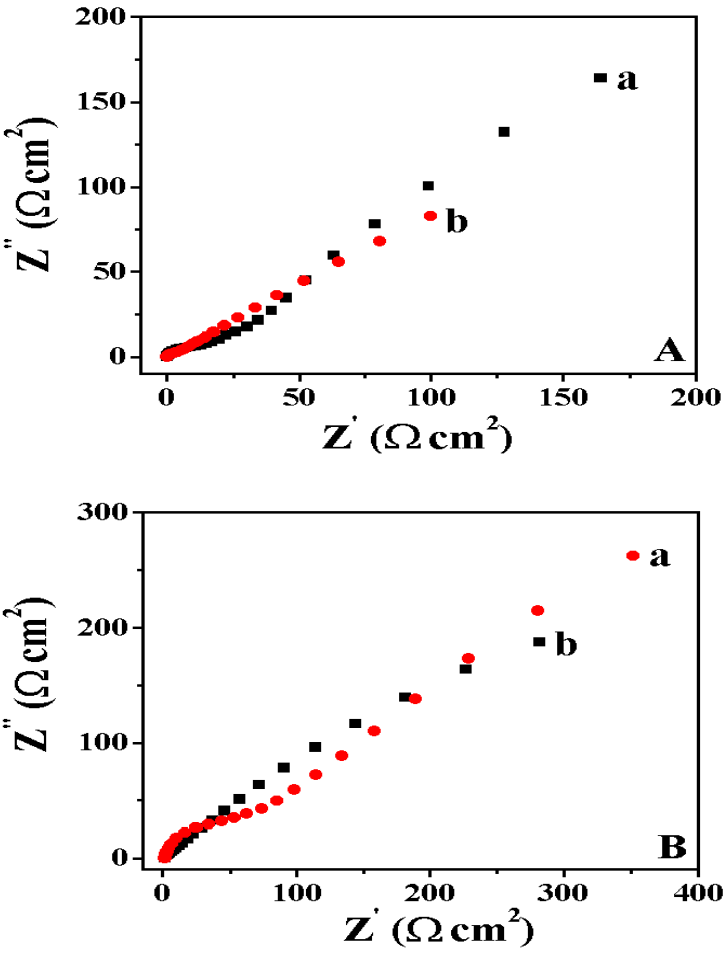

Figure 21: Impedance plots in equal concentrations of both potassium ferrocyanide and potassium ferricyanide with NaF as a supporting electrolyte under the acidic condition (pH = 3.2 – 3.5) for, (a) SAM of o-ATP on Au electrode and (b) SAM of p-ATP on Au electrode. (B) Impedance plots in 1mM hexaammineruthenium(III) chloride with 0.1M $LiClO_4$ as a supporting electrolyte under the acidic condition (pH = 3.2 – 3.5) for, (a) SAM of o-ATP on Au surface and (b) SAM of p-ATP on Au surface.

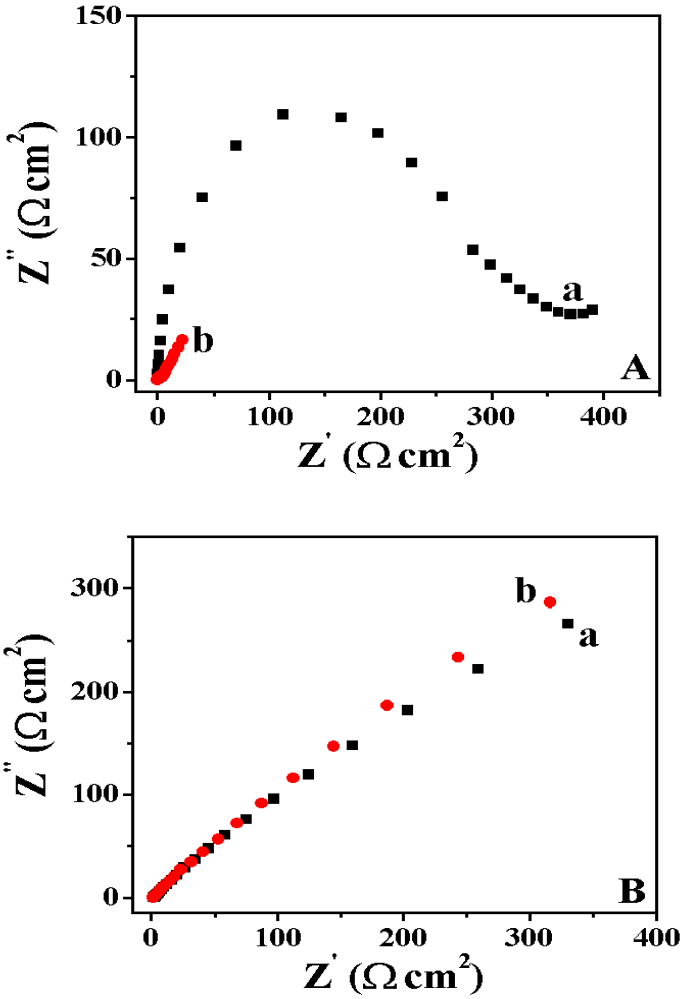

Figure 22: Impedance plots in equal concentrations of both potassium ferrocyanide and potassium ferricyanide with NaF as a supporting electrolyte under the basic condition (pH = 11.0 – 11.2) for, (a) SAM of o-ATP on Au electrode and (b) SAM of p-ATP on Au electrode. (B) Impedance plots in 1mM hexaammineruthenium(III) chloride with 0.1M $LiClO_4$ as a supporting electrolyte under the basic condition (pH = 11.0 – 11.2) for, (a) SAM of o-ATP on Au surface and (b) SAM of p-ATP on Au surface.

Figure 22B shows the Nyquist plots of the monolayer coated electrodes in 1mM hexaammineruthenium(III) chloride with 0.1M $LiClO_4$ as a supporting electrolyte under the basic condition. It can be seen from the figure 22B (a) that the SAM o-ATP on Au shows a very small semicircle at high frequency region and a straight line at low frequency region indicating a very poor blocking ability of SAM towards the redox reaction of ruthenium complex. Similarly, SAM of p-ATP on Au (Fig. 22B (b)) shows a straight-line formation in the entire range of frequency implying the facile kinetics of ruthenium redox reaction on the SAM modified surface under the basic condition. These results are in conformity with our CV results under the similar acidic and basic conditions. From the experiments we have observed that the SAMs are selective to ruthenium redox reaction even under the acidic condition, an aspect that will be discussed later.

4.6.2. Effect of potential cycling

We find from the cyclic voltammetry and electrochemical impedance spectroscopic studies discussed earlier that the self-assembled monolayers of thiophenol (TP), o-aminothiophenol (o-ATP) and p-aminothiophenol (p-ATP) on gold surface form stable and reproducible but moderately blocking monolayers. From the experimental results, we concluded that these monolayers have a large number of pinholes and defects, which accounts for the poor blocking ability of these monolayers. We have tried to improve the blocking behaviour of these monolayer-modified electrodes by two different processes, namely by subjecting the freshly formed SAM electrodes to (i) potential cycling in a pure supporting electrolyte without any redox species and (ii) mixed SAM formation with either 1-Octanethiol or 1,6-Hexanedithiol. Immediately after the SAM formation of respective aromatic thiols on Au surface, the monolayer-

coated electrodes are potential cycled in the positive potential range from 0.0V to 0.6V vs. SCE in 1M NaF aqueous solution without any redox species. After the potential cycling, the same electrode is used for the cyclic voltammetric and electrochemical impedance spectroscopic studies to evaluate the barrier property of the monolayers.

4.6.2.1. Cyclic voltammetry

Figure 23 shows the cyclic voltammograms of bare Au electrode, SAM modified electrodes and potential cycled electrodes (after the SAM formation) in 10mM potassium ferrocyanide with 1M NaF as the supporting electrolyte at a potential scan rate of 50mV/s. It can be seen from figure 23A that the bare Au electrode shows a perfect reversible voltammogram for the redox couple indicating that the electron transfer reaction is completely under diffusion control process. Figure 23B shows the cyclic voltammograms of (a) SAM of TP on Au surface and (b) potential cycled SAM modified electrode in the same solution. In contrast to bare Au electrode, the SAM modified and potential cycled electrodes do not show any peak formation implying that the redox reaction is inhibited. It can be noted from figure 23B (b) that the potential cycled electrode shows a significantly less current when compared to SAM modified electrode indicating a possible structural reorganization of monolayer, which causes a reduction in the number of pinholes and defects. The CVs show ‘s’ shaped curve with a large current separation between the forward and reverse scans implying a microelectrode array type behaviour [98-100] in which the pinholes are distributed randomly over the surface. Figure 23C shows the comparison of cyclic voltammograms of SAM of o-ATP on Au surface (a) and potential cycled monolayer-coated electrode (b). It can be seen from figure 23C that the SAM of o-ATP on Au surface shows a good blocking behaviour to the

electron transfer reaction. The potential cycled electrode (after SAM formation) (Fig. 23C (b)) shows a significant decrease in the current value when compared to the SAM modified electrode (Fig. 23C (a)) indicating that the blocking ability of the monolayer is improved to a large extent after the potential cycling. Figure 23D shows the CVs of SAM of p-ATP on Au electrode (a) and the potential cycled electrode (b). It can be seen from Fig. 23D (a) that the SAM of p-ATP on Au surface shows a quasi-reversible behaviour for the redox reaction implying a poor blocking ability of the monolayer. Although there is a small decrease in the current after the potential cycling, the monolayer exhibits a rather imperfect blocking behaviour. It can be observed that in all these cases of SAMs of aromatic thiols on Au surface, the blocking ability of the monolayer has improved significantly after the potential cycling. This can only be attributed to structural modification and more compact organization of the monolayer leading to a large reduction in the number of pinholes and defects.

Figure 24 shows the cyclic voltammograms of bare Au electrode, monolayer-coated electrodes and potential cycled electrodes in 1mM hexaammineruthenium(III) chloride with 0.1M $LiClO_4$ as the supporting electrolyte at a potential scan rate of 50mV/s. It can be seen from figure 24A that the bare Au electrode shows a reversible behaviour for the redox reaction indicating that the electron transfer process is under diffusion control. Figures 24B (a) and (b) show the CVs of the SAM of TP on Au surface and the potential cycled electrode after the SAM formation respectively. It can be seen from the figure that the redox reaction of ruthenium complex is not inhibited significantly in the case of SAM of TP even after potential cycling, implying a rather poor blocking property of the monolayer. Figures 24C (a) and (b) show the comparison of cyclic voltammograms of the SAM of o-ATP on Au surface and the corresponding potential cycled electrode. It can be noted from the figure

that the SAM of o-ATP on Au shows a considerable blocking to the ruthenium redox reaction after the potential cycling, though it is not totally inhibited.

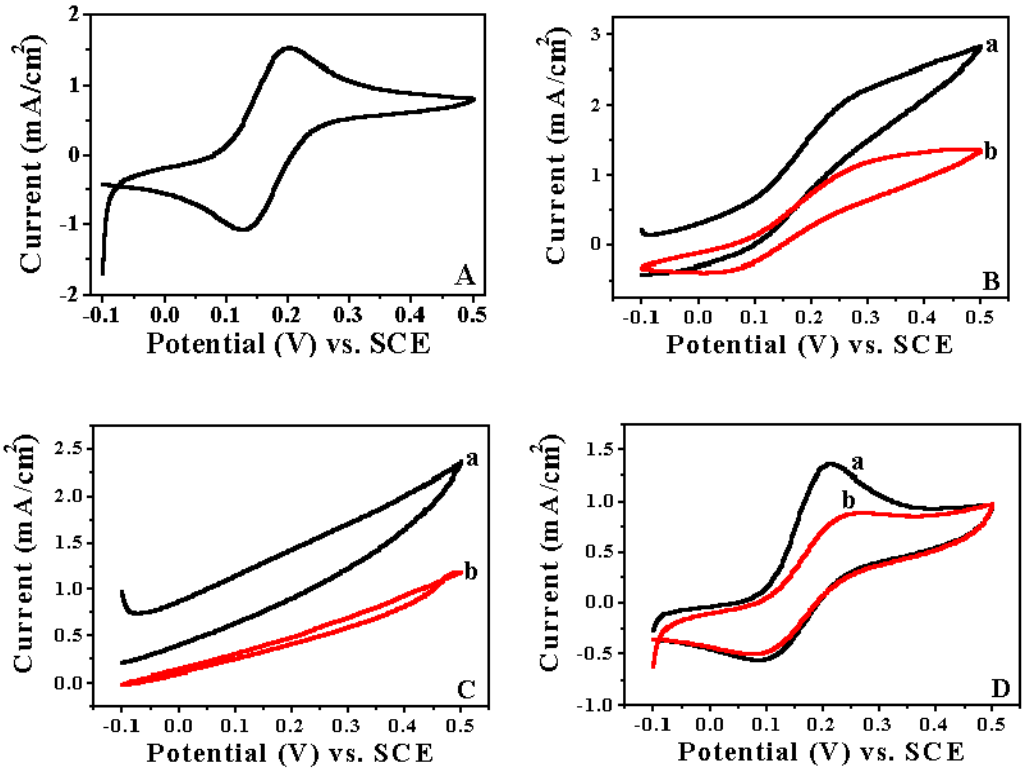

Figure 23: Cyclic voltammograms in 10mM potassium ferrocyanide with 1M NaF as a supporting electrolyte at a potential scan rate of 50mV/s for, (A) Bare Au electrode. (B) SAM of thiophenol (TP) on Au electrode (a), a potential cycled electrode after the SAM formation of TP on Au (b). (C) SAM of o-aminothiophenol (o-ATP) on Au electrode (a), a potential cycled electrode after the SAM formation of o-ATP on Au (b). (D) SAM of p-aminothiophenol (p-ATP) on Au electrode (a), a potential cycled electrode after the SAM formation of p-ATP on Au (b).

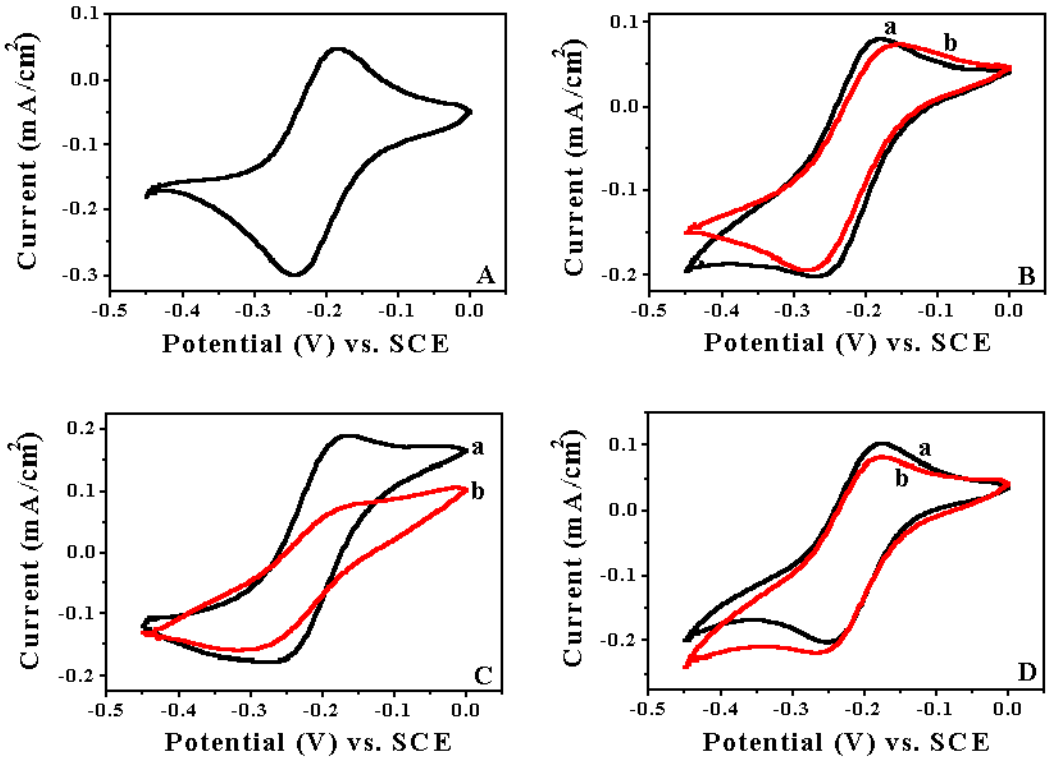

Figure 24: Cyclic voltammograms in 1mM hexaammineruthenium(III) chloride with 0.1M $LiClO_4$ as a supporting electrolyte at a potential scan rate of 50mV/s for, (A) Bare gold electrode. (B) SAM of thiophenol (TP) on Au electrode (a), a potential cycled electrode after the SAM formation of TP on Au (b). (C) SAM of o-aminothiophenol (o-ATP) on Au electrode (a), a potential cycled electrode after the SAM formation of o-ATP on Au (b). (D) SAM of p-aminothiophenol (p-ATP) on Au electrode (a), a potential cycled electrode after the SAM formation of p-ATP on Au (b).

Figures 24D (a) and (b) show the CVs of the SAM of p-ATP on Au surface and the corresponding potential cycled electrode (after the SAM formation). It can be observed that the redox reaction of ruthenium complex is not at all inhibited as indicated by the reversible nature of the cyclic voltammograms. Thus shows the facile nature of the electron transfer process with the redox reaction under diffusion control. Even after the potential cycling, the SAM modified electrode does not show any improvement in the blocking behaviour. It can be noticed from the figures that the SAM modified electrodes and the corresponding potential cycled electrodes hardly block the redox reaction of ruthenium complex, which is very much in contrast to the behaviour of ferrocyanide | ferricyanide redox couple.

4.6.2.2. Electrochemical impedance spectroscopy

Figure 25 shows the impedance plots (Nyquist plots) of the bare gold electrode, SAM modified electrodes and the potential cycled electrodes (after the SAM formation) in equal concentrations of potassium ferrocyanide and potassium ferricyanide aqueous solution with 1M NaF as the supporting electrolyte. Figure 25A shows a straight line at low frequency and a very small semicircle at high frequency region indicating that the electron transfer process is essentially under diffusion control for the redox couple on the bare Au electrode. Figures 25B (a) and (b) show the respective impedance plots of SAM of TP on Au surface and the corresponding potential cycled electrode. In contrast to bare Au electrode, SAM of TP on Au and the corresponding potential cycled electrode show a good blocking behaviour of the monolayer with a well-defined semicircle at higher frequency region. It is well known that the charge transfer resistance (R_{ct}) can be determined from the intercept of semicircle on the Z' axis. It can be seen from the figure that the R_{ct} value of

potential cycled electrode (Fig. 25B (b)) is significantly increased when compared to the monolayer-coated electrode (Fig. 25B (a)). This confirms an improvement in blocking ability of the monolayer after the potential cycling. Similar behaviour was observed for the SAM of o-ATP on Au surface (Fig. 25C (a)) and the corresponding potential cycled electrode (Fig. 25C (b)). The better blocking property of the monolayer of o-ATP on Au after the potential cycling is manifested by the increase in the charge transfer resistance, R_{ct} value. On the other hand, it can be seen from the Nyquist plots of figure 25D that the monolayer of p-ATP on Au surface and the corresponding potential cycled electrodes do not significantly block the redox reaction. In this case the Nyquist plot shows a straight line at low frequency region implying that the electron transfer process is under diffusion control. In other words the SAM of p-ATP on Au surface shows a poor blocking behaviour although there is a marginal increase in the R_{ct} value after the potential cycling.

Figure 26 shows the impedance plots (Nyquist plots) of the bare Au electrode, SAM modified electrodes and the potential cycled electrodes in 1mM hexaammineruthenium(III) chloride with 0.1M $LiClO_4$ as the supporting electrolyte. It can be seen from the figure 26A that the bare Au electrode exhibits a low frequency straight line with a very small semicircle at high frequency region indicating the diffusion-controlled process for the redox reaction of ruthenium complex. Figures 26B,C and D show the respective impedance plots of SAM of TP, o-ATP and p-ATP on Au surface and their corresponding potential cycled electrodes in the same solution. It can be noticed from the figures of the SAM modified electrodes and their corresponding potential cycled electrodes that the Ru(III) electron transfer reaction is facile though there is a marginal increase in R_{ct} value in the latter case. It is worth recalling that these SAM modified electrodes and their corresponding potential

cycled electrodes show a very good blocking ability to ferrocyanide | ferricyanide redox reaction, an aspect which will be discussed later. It is worth pointing out that these results are in conformity with our observations using cyclic voltammetric studies described earlier.

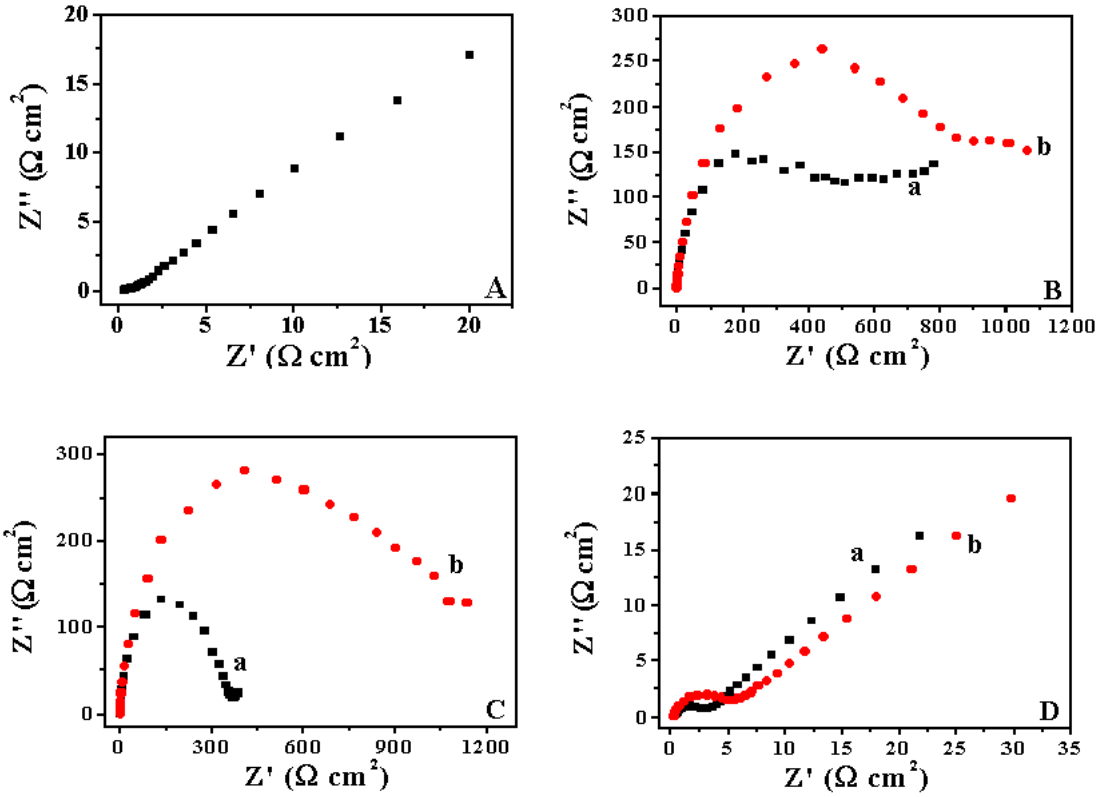

Figure 25: Impedance plots in an aqueous solution of 10mM potassium ferrocyanide and 10mM potassium ferricyanide with 1M NaF as a supporting electrolyte for, (A) Bare Au electrode. (B) SAM of thiophenol (TP) on Au electrode (a), a potential cycled electrode after the SAM formation of TP on Au (b). (C) SAM of o-aminothiophenol (o-ATP) on Au electrode (a), a potential cycled electrode after the SAM formation of o-ATP on Au (b). (D) SAM of p-aminothiophenol (p-ATP) on Au electrode (a), a potential cycled electrode after the SAM formation of p-ATP on Au (b).

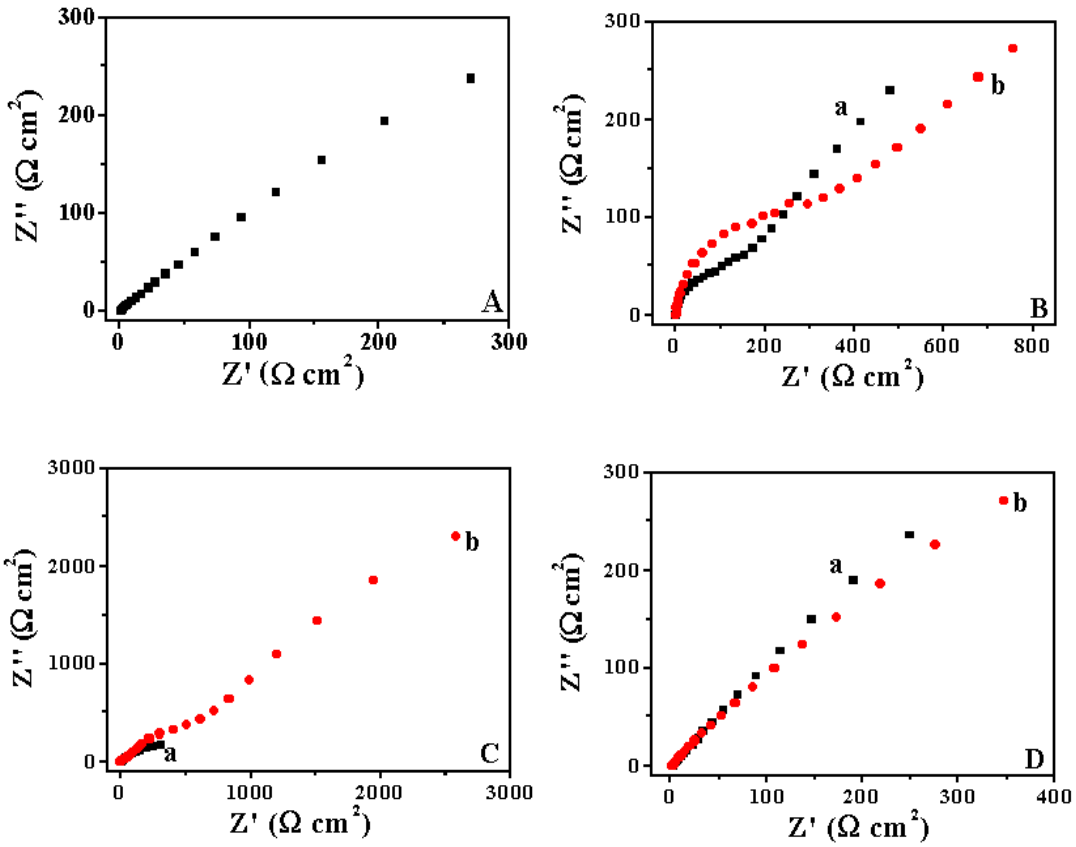

Figure 26: Impedance plots in 1mM hexaammineruthenium(III) chloride with 0.1M $LiClO_4$ as a supporting electrolyte for, (A) Bare Au electrode. (B) SAM of thiophenol (TP) on Au electrode (a), a potential cycled electrode after the SAM formation of TP on Au (b). (C) SAM of o-aminothiophenol (o-ATP) on Au electrode (a), a potential cycled electrode after the SAM formation of o-ATP on Au (b). (D) SAM of p-aminothiophenol (p-ATP) on Au electrode (a), a potential cycled electrode after the SAM formation of p-ATP on Au (b).

4.6.2.3. Gold oxide stripping analysis

The surface coverage of these monolayers on Au surface can be determined qualitatively using gold oxide stripping method. The cyclic voltammogram of bare gold electrode in 0.1M $HClO_4$ shows the usual features of gold oxide formation during the positive potential scanning and oxide stripping upon reversal of the scan direction. The quantity of electric charges passed during the removal of oxide is proportional to the effective electrode area. By comparing the charge of a SAM modified electrode and its corresponding potential cycled electrode with the respective charge of the bare gold electrode, the surface coverage of the monolayer can be determined in a qualitative manner.

Figure 27 shows the cyclic voltammograms of gold oxide formation and stripping for the SAM modified electrodes and the potential cycled electrodes in 0.1M $HClO_4$ aqueous solution. For comparison the cyclic voltammogram of bare Au electrode was also shown in Fig. 27A and it shows the respective gold oxide formation and stripping peaks. Figures 27B, C and D show the cyclic voltammograms of SAMs of TP, o-ATP and p-ATP on Au surface and their corresponding potential cycled electrodes in 0.1M $HClO_4$ aqueous solution respectively. It can be seen from the figures that the measured charges of the monolayer-coated electrodes are significantly less when compared to the charge of bare Au electrode, which is as expected. In the cases of SAMs of TP (Fig. 27B) and o-ATP (Fig. 27C) on Au surface, the charge values are not significantly affected even after the potential cycling. However, the more horizontal base line in the cases of potential cycled electrodes indicates that the ionic permeability of the monolayer is uniform throughout the scanned potential range. This implies that potential cycling has incorporated the structural changes of the monolayer film. This is not further affected by the

subsequent potential scans. In contrast, there is a significant reduction in the measured charge value in the case of SAM of p-ATP on Au surface after the potential cycling as can be seen from the Fig. 27D. This indicates the fact that the monolayer of p-ATP on Au surface undergoes a large structural organization and also decreased ionic permeability during the process of potential cycling. This ultimately leads to the formation of a compact and well-ordered SAM with less number of pinholes and defects.

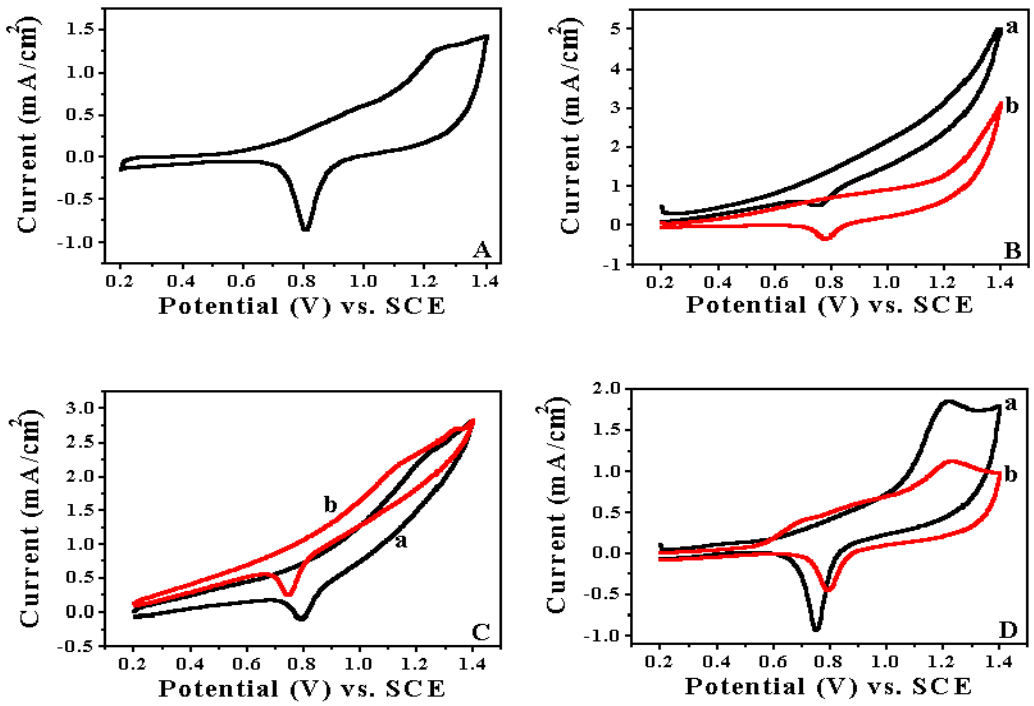

Figure 27: Cyclic voltammograms of gold oxide stripping analysis in 0.1M $HClO_4$ for, (A) Bare gold electrode. (B) SAM of thiophenol (TP) on Au electrode (a), a potential cycled electrode after the SAM formation of TP on Au (b). (C) SAM of o-aminothiophenol (o-ATP) on Au electrode (a), a potential cycled electrode after the SAM formation of o-ATP on Au (b). (D) SAM of p-aminothiophenol (p-ATP) on Au electrode (a), a potential cycled electrode after the SAM formation of p-ATP on Au (b).

We have obtained a surface coverage value of 90% (after potential cycling) in the cases of SAMs of TP and o-ATP on Au surface and 80% in the case of p-ATP on Au surface. The surface coverage values calculated from the gold oxide stripping method are lower than the values obtained using the redox probes, which can be attributed to the fact that the probe ion in this case is OH^- ions that is very much smaller in size and can have easy access to the electrode surface through the pinholes and defects when compared to that of other bulkier ions. In addition to this, it is always possible that potential cycling to large positive potentials of 1.4V vs. SCE induces some structural damage to the film which can show low surface coverage determined from the charge values obtained from the cathodic stripping peak. Infact after repeated cycles in perchloric acid, the CV is almost similar to that of bare Au electrode, indicating the complete removal of the monolayer. This confirms that the monolayer is not electrochemically stable when cycled to high positive potentials.

4.6.3. Formation of mixed SAM with 1-Octanethiol

We have tried to improve the blocking ability of the monolayers of aromatic thiols on Au surface by forming a mixed SAM with 1-Octanethiol. Immediately after the adsorption of corresponding aromatic thiols, the monolayer-coated electrodes were rinsed in ethanol and distilled water and dipped in neat thiol of 1-Octanethiol for the formation of mixed SAM. After this procedure, the electrode was rinsed with ethanol, which is followed by cleaning in distilled water and millipore water for subsequent use in electrochemical studies.

4.6.3.1. Cyclic voltammetry

Figure 28A shows the cyclic voltammograms of mixed SAM modified electrodes in 10mM potassium ferrocyanide with 1M NaF as a supporting electrolyte at a potential scan rate of 50mV/s. The mixed SAM modified electrodes show a good blocking behaviour to the electron transfer reaction. Figures 28A (a), (b) and (c) show the respective cyclic voltammograms of mixed SAM coated electrodes using 1-Octanethiol with the monolayers of TP, o-ATP and p-ATP respectively on Au surface. It can be seen from the figures that the mixed SAM modified electrodes in the cases of TP and p-ATP show a better blocking behaviour. But in the case of o-ATP, the mixed SAM coated electrode exhibits a quasi-reversible behaviour for the redox reaction implying a poor blocking ability of the monolayer film. This anomalous behaviour will be discussed later. Interestingly, the blocking property of p-ATP has been improved to a very large extent after the mixed SAM formation.

Figure 28B shows the comparison of cyclic voltammograms of mixed SAM coated electrodes in 1mM hexaammineruthenium(III) chloride with 0.1M $LiClO_4$ as a supporting electrolyte at a potential scan rate of 50mV/s. Figures 28B (a), (b) and (c) show the respective cyclic voltammograms of mixed SAM modified electrodes using 1-Octanethiol with the monolayers of TP, o-ATP and p-ATP on Au surface. It can be seen from the figures that the mixed SAMs in the cases of TP and o-ATP on Au surface do not inhibit the redox reaction of ruthenium complex, while the mixed SAM in the case of p-ATP on Au surface exhibits a quasi-reversible behaviour for the electron transfer reaction implying a rather poor blocking property.

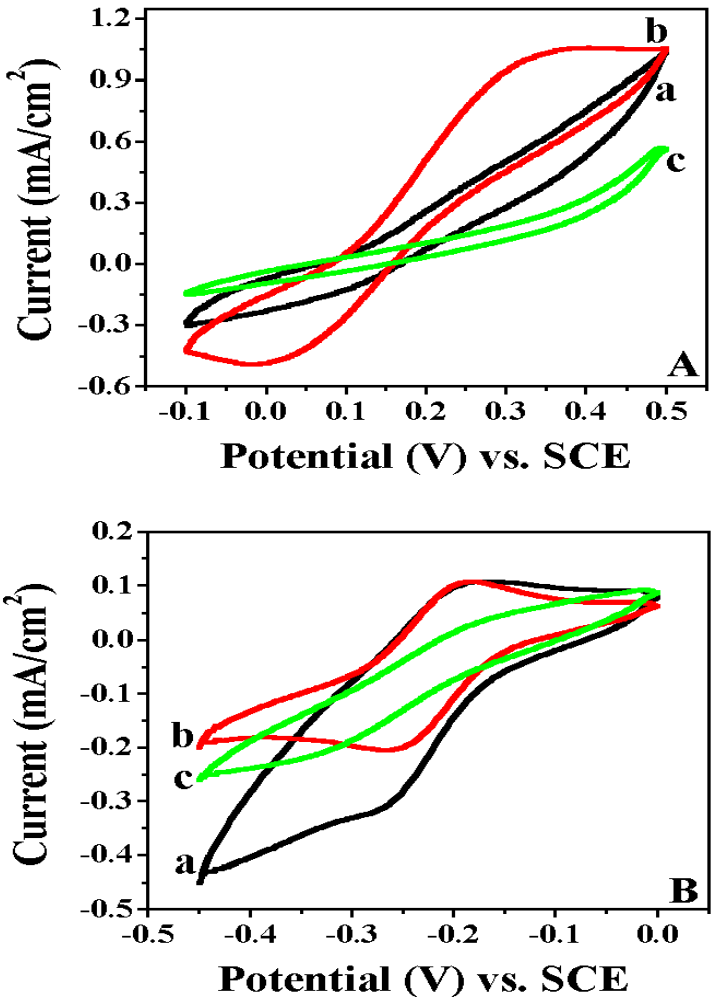

Figure 28: (A) Cyclic voltammograms in 10mM potassium ferrocyanide with 1M NaF as a supporting electrolyte at a potential scan rate of 50mV/s of mixed SAM modified electrodes with 1-Octanethiol for, (a) SAM of TP on Au electrode, (b) SAM of o-ATP on Au surface and (c) SAM of p-ATP on Au electrode. (B) Cyclic voltammograms in 1mM hexaammineruthenium(III) chloride with 0.1M $LiClO_4$ as a supporting electrolyte at a potential scan rate of 50mV/s of mixed SAM coated electrodes with 1-Octanethiol for, (a) SAM of TP on Au surface, (b) SAM of o-ATP on Au electrode and (c) SAM of p-ATP on Au surface.

4.6.3.2. Electrochemical impedance spectroscopy

Figure 29A shows the impedance plots (Nyquist plots) of mixed SAM coated electrodes using 1-Octanethiol with the corresponding monolayers of TP, o-ATP and p-ATP on Au surface in 10mM potassium ferrocyanide and 10mM potassium ferricyanide with 1M NaF as a supporting electrolyte. Figures 29A (a) and (b) show the respective Nyquist plots of mixed SAM for the cases of TP and p-ATP on Au surface and the inset shows the corresponding plot for o-ATP on Au surface. It can be seen from the figure that the mixed SAMs of TP and p-ATP show that the electron transfer reaction is under charge transfer control. The R_{ct} value is highest in the case of p-ATP among the three mixed SAM modified electrodes studied in this work. It can be noted from the inset of figure that the mixed SAM of o-ATP shows a semicircle at higher frequency region and a straight line at lower frequency indicating a quasi-reversible behaviour for the electron transfer reaction, which implies a poor blocking ability of the monolayer.

Figure 29B shows the Nyquist plots of mixed SAM of different aromatic thiols and 1-Octanethiol on gold surface in 1mM hexaammineruthenium(III) chloride with 0.1M $LiClO_4$ as a supporting electrolyte. It can be seen from the inset of the figure that the mixed SAM coated electrodes in the cases of TP (Fig. 29B (a)) and o-ATP (Fig. 29B (b)) on Au surface show a straight line almost in the entire frequency range used for the study implying a diffusion control process for the electron transfer reaction. The mixed SAM of 1-Octanethiol with p-ATP on Au surface (Fig. 29B) shows a semicircle at higher frequencies and a straight line at low frequency indicating the quasi-reversible behaviour for the redox reaction of ruthenium complex. The charge transfer resistance (R_{ct}) value is higher in the case of p-ATP when

compared to other mixed SAM coated electrodes. These results are largely in conformity with our CV results described in the previous section.

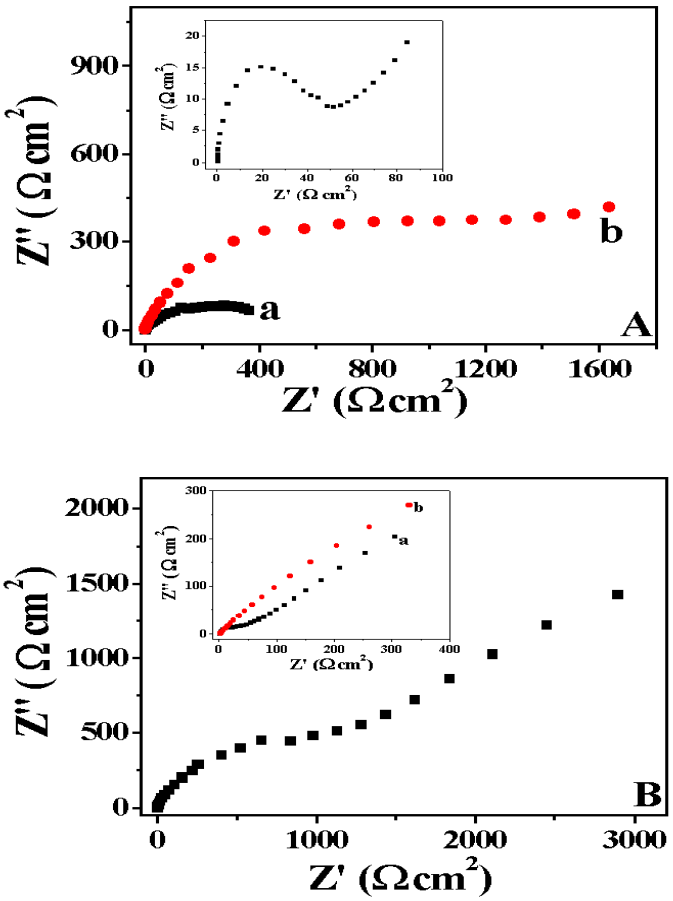

Figure 29: (A) Typical impedance plots in 10mM potassium ferrocyanide and 10mM potassium ferricyanide with 1M NaF as a supporting electrolyte of mixed SAM modified electrodes with 1-Octanethiol for, (a) SAM of TP on Au electrode and (b) SAM of p-ATP on Au surface. Inset shows the same plot for SAM of o-ATP on Au electrode. (B) Impedance plots in 1mM hexaammineruthenium(III) chloride with 0.1M $LiClO_4$ as a supporting electrolyte of mixed SAM coated electrodes with 1-Octanethiol for the SAM of p-ATP on Au electrode. Inset shows the similar plots for, (a) SAM of TP on Au surface and (b) SAM of o-ATP on Au electrode.

4.6.4. Formation of mixed SAM with 1,6-Hexanedithiol

We have carried out experiments to improve the blocking property of the monolayers of aromatic thiols by forming a mixed SAM with an aliphatic dithiol namely, 1,6-Hexanedithiol. Immediately after the adsorption of the corresponding aromatic thiols, the monolayer-modified electrodes were rinsed in ethanol and distilled water and dipped in neat thiol of 1,6-Hexanedithiol for mixed SAM formation. After this procedure, the electrode was rinsed again with ethanol followed by cleaning in distilled water and millipore water and immediately used for the analysis using electrochemical techniques.

4.6.4.1. Cyclic voltammetry

Figure 30A shows the comparison of cyclic voltammograms of mixed SAM modified electrodes using 1,6-Hexanedithiol in 10mM potassium ferrocyanide with 1M NaF as a supporting electrolyte at a potential scan rate of 50mV/s. It can be seen from the figures that the mixed SAM modified electrodes in all the cases of monolayers of TP (Fig. 30A (a)), o-ATP (Fig. 30A (b)) and p-ATP (Fig. 30A (c)) on Au surface show a good blocking behaviour to the electron transfer reaction indicating the formation of highly ordered, well-organized and compact monolayer with less number of pinholes and defects. Figure 30B shows the CVs of mixed SAM coated electrodes using 1,6-Hexanedithiol with the corresponding monolayers of TP, o-ATP and p-ATP on Au surface in 1mM hexaammineruthenium(III) chloride with 0.1M $LiClO_4$ as a supporting electrolyte at a potential scan rate of 50mV/s. It can be noted from the figures that the mixed SAM modified electrodes in all the cases of the monolayers of TP (Fig. 30B (a)), o-ATP (Fig. 30B (b)) and p-ATP (Fig. 30B (c)) on Au surface show a quasi-reversible behaviour for the redox reaction of ruthenium complex implying the poor blocking ability of these monolayers.

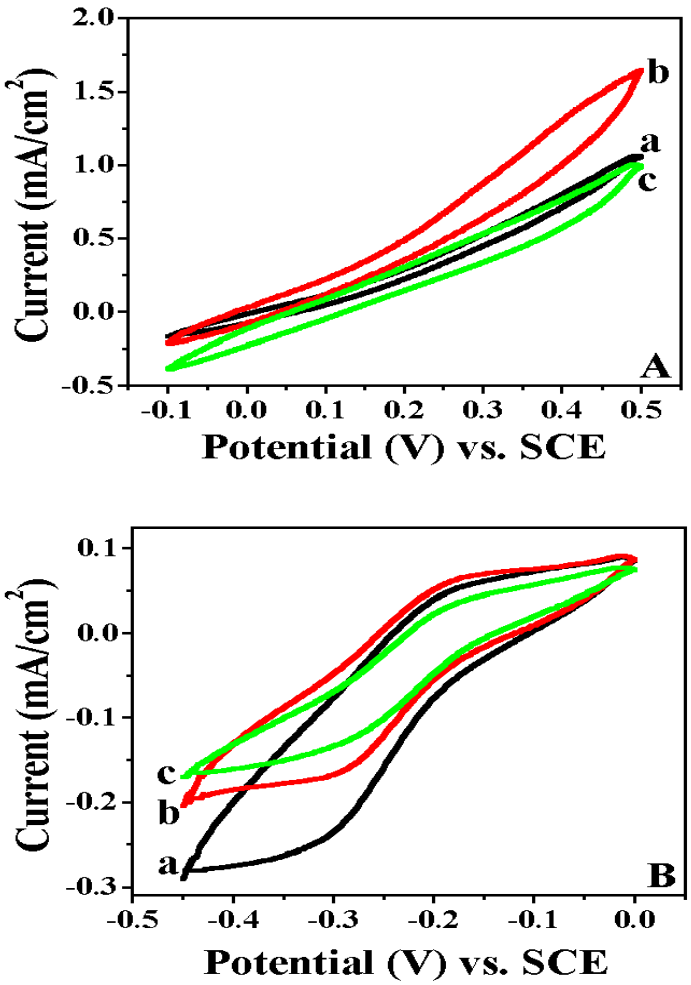

Figure 30: (A) Cyclic voltammograms of mixed SAM modified electrodes with 1,6-Hexanedithiol in 10mM potassium ferrocyanide with 1M NaF as a supporting electrolyte at a potential scan rate of 50mV/s for, (a) SAM of TP on Au electrode, (b) SAM of o-ATP on Au electrode and (c) SAM of p-ATP on Au electrode. (B) Cyclic voltammograms of mixed SAM coated electrodes with 1,6-Hexanedithiol in 1mM hexaammineruthenium(III) chloride with 0.1M $LiClO_4$ as a supporting electrolyte at a potential scan rate of 50mV/s for, (a) SAM of TP on Au surface, (b) SAM of o-ATP on Au electrode and (c) SAM of p-ATP on Au surface.

4.6.4.2. Electrochemical impedance spectroscopy

Figure 31A shows the impedance (Nyquist) plots of mixed SAM modified electrodes using 1,6-Hexanedithiol in 10mM potassium ferrocyanide and 10mM potassium ferricyanide with 1M NaF as a supporting electrolyte. It can be noted from the figures that the mixed SAM coated electrodes in all the cases of the monolayers of TP (Fig. 31A (a)), o-ATP (Fig. 31A (b)) and p-ATP (Fig. 31A (c)) on Au surface show a semicircle formation almost in the entire range of frequency used for the study implying the charge transfer control process for the electron transfer reaction. The mixed SAM modified electrodes show a good blocking ability to the redox reaction and the charge transfer resistance (R_{ct}) value increases from TP to o-ATP to p-ATP on Au surface. Figure 31B shows the Nyquist plots of mixed SAM coated electrodes using 1,6-Hexanedithiol in 1mM hexaammineruthenium(III) chloride with 0.1M $LiClO_4$ as a supporting electrolyte. It can be seen from the figures that the mixed SAM modified electrodes in all the cases of the monolayers of TP (Fig. 31B (a)), o-ATP (Fig. 31B (b)) and p-ATP (Fig. 31B (c)) on Au surface show a depressed semicircle at higher frequencies and a straight line at lower frequency indicating a quasi-reversible behaviour for the electron transfer reaction. It can also be noted that the charge transfer resistance (R_{ct}) value increases in the order p-ATP>o-ATP>TP SAMs on Au surface. Overall, the blocking ability of these monolayers has been significantly improved due to the mixed SAM formation. These results are in conformity with our cyclic voltammetry studies discussed in the previous section.

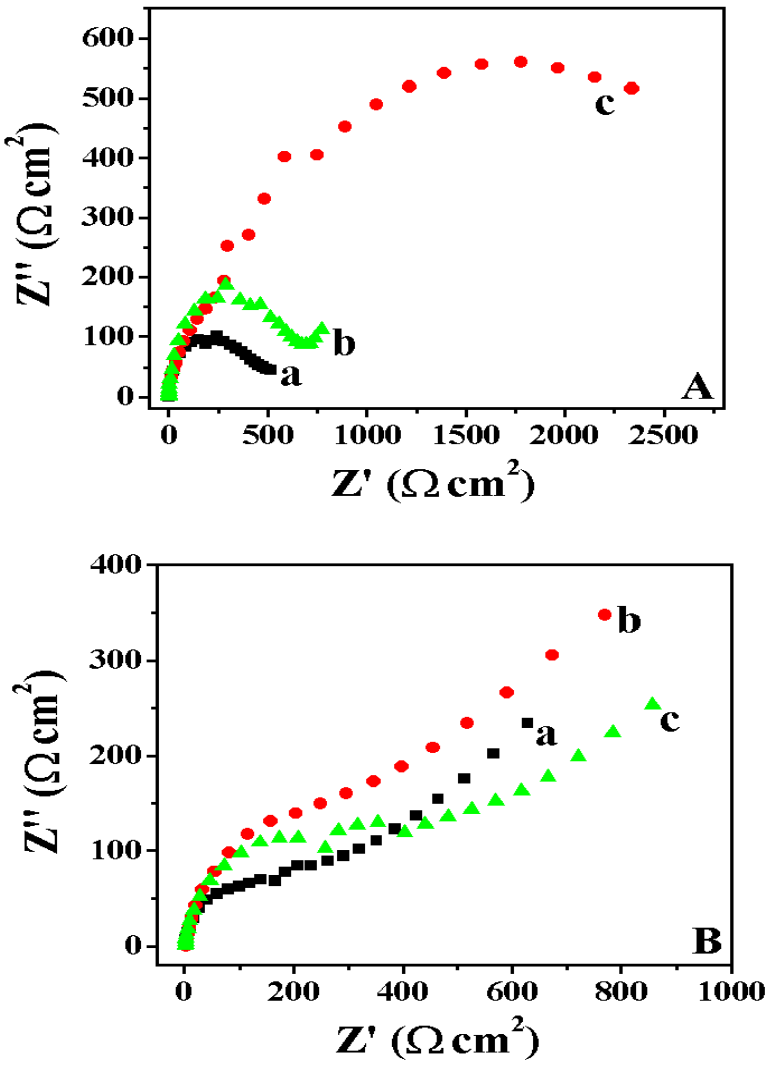

Figure 31: (A) Impedance plots of mixed SAM modified electrodes with 1,6-Hexanedithiol in 10mM potassium ferrocyanide and 10mM potassium ferricyanide with 1M NaF as a supporting electrolyte for, (a) SAM of TP on Au electrode, (b) SAM of o-ATP on Au surface and (c) SAM of p-ATP on Au electrode. (B) Typical impedance plots of mixed SAM coated electrodes with 1,6-Hexanedithiol in 1mM hexaammineruthenium(III) chloride with 0.1M $LiClO_4$ as a supporting electrolyte for, (a) SAM of TP on Au electrode, (b) SAM of o-ATP on Au surface and (c) SAM of p-ATP on Au electrode.

4.6.5. Analysis of impedance data

The impedance data obtained for bare Au electrode, SAM modified electrodes, potential cycled electrodes (after the SAM formation) and the mixed SAM coated electrodes were fitted to a suitable equivalent circuit in order to determine the charge transfer resistance (R_{ct}) value, which is the measure of blocking ability of the monolayer against the diffusion of redox probes through the film. The measured charge transfer resistance (R_{ct}) values of SAM coated electrodes are higher than the corresponding R_{ct} value of the bare Au electrode due to the inhibition of electron transfer rate by the monolayer film. The impedance values are fitted to a standard Randle's equivalent circuit model comprising of a parallel combination of a constant phase element (CPE) represented by Q and a faradaic impedance Z_f in series with the uncompensated solution resistance, R_u. The faradaic impedance Z_f is a series combination of charge transfer resistance, R_{ct} and the Warburg impedance, W for the cases of bare Au electrode, SAM of p-ATP on Au, potential cycled electrodes (after the SAM formation) and some of the mixed SAM modified electrodes, especially for the redox reaction of ruthenium complex. For the other cases of monolayer-coated electrodes, the faradaic impedance Z_f consists only of the charge transfer resistance, R_{ct}. We have determined the R_{ct} values by equivalent circuit fitting procedure using the impedance plots of the respective bare Au electrode and the SAM modified electrodes. Table 2 shows the charge transfer resistance (R_{ct}) values of bare Au electrode and SAM modified electrodes (based on aromatic thiols) obtained by fitting their corresponding impedance data to a suitable equivalent circuit. Similarly, table 3 shows the charge transfer resistance values obtained from the equivalent circuit fitting analysis using impedance plots of SAMs of o-ATP and p-ATP on Au surface under the acidic and basic conditions.

Table-2

The charge transfer resistance (R_{ct}) values obtained from the impedance plots of bare Au electrode and various SAM modified electrodes using two different redox couples as probe molecules.

Sample	$[Fe(CN)_6]^{3-\|4-}$ R_{ct} (Ω cm^2)	$[Ru(NH_3)_6]^{2+\|3+}$ R_{ct} (Ω cm^2)
Bare Au	**0.4488**	**0.216**
TP/Au	**360.0**	**137.02**
o-ATP/Au	**330.8**	**0.632**
p-ATP/Au	**2.756**	**0.707**

Table-3

The charge transfer resistance (R_{ct}) values obtained from the impedance plots of SAMs of o-ATP and p-ATP on Au surface under the acidic and basic conditions using two different redox couples as probe molecules.

Redox probe	o-ATP/Au [R_{ct} (Ω cm^2)]		p-ATP/Au [R_{ct} (Ω cm^2)]	
	Acidic	Basic	Acidic	Basic
$[Fe(CN)_6]^{3-\|4-}$	12.438	287.8	3.79	3.432
$[Ru(NH_3)_6]^{2+\|3+}$	52.56	2.914	4.044	1.1264

It can be seen from the table 2 that the R_{ct} values of SAM modified electrodes are higher as expected when compared to that of bare Au electrode. The parameter R_{ct} is a measure of blocking ability of the monolayer to the electron transfer reactions. Higher the R_{ct} value, better the blocking behaviour of the SAM towards the redox reactions. It can also be noted from the table 3 that the R_{ct} values of SAMs of o-ATP and p-ATP on Au surface are very much lower under the acidic and basic conditions implying the poor blocking ability of SAM towards the redox reaction of ruthenium complex. From the calculated R_{ct} values, it is clear that the blocking ability of the SAMs follows the order TP > o-ATP > p-ATP, which is in conformity with our results of cyclic voltammetry and impedance spectroscopy studies. Table 4 shows the R_{ct} values of potential cycled electrodes (after SAM formation) obtained from their corresponding impedance plots. It can be seen from the tables 2 & 4 that the R_{ct} values of the potential cycled electrodes are very much higher when compared to the bare Au electrode and the respective SAM modified electrodes. As can be noted from table 4 that the R_{ct} values are significantly increased after the potential cycling implying the improvement in the blocking behaviour of the SAMs of TP and o-ATP on Au surface. Though there is a small increase in the R_{ct} values in the case of p-ATP on Au surface, the overall blocking ability of this monolayer film has not improved significantly by potential cycling. As described earlier, we have carried out the CV and EIS studies on mixed SAMs of aromatic and aliphatic thiols viz., 1-Octanethiol and 1,6-Hexanedithiol. The calculated R_{ct} values obtained from the impedance plots are shown in table 5. It can be seen from the table 5 that the R_{ct} values of both the mixed SAMs of p-ATP on Au surface are increased to a very large extent indicating the significant improvement in the blocking behaviour. But in the case of TP SAM coated electrodes, the electron transfer reaction is not inhibited significantly. Very

surprisingly, in the case of o-ATP, the charge transfer resistance (R_{ct}) is very much decreased implying much poorer blocking property of the monolayer.

Table-4

The charge transfer resistance (R_{ct}) values determined from the impedance plots of bare Au electrode and various potential cycled electrodes (after the SAM formation) by equivalent circuit fitting analysis using two different redox couples as probe molecules.

Sample	**Charge transfer resistance values R_{ct} (Ω cm^2)**	
	$[Fe(CN)_6]^{3-\|4-}$	**$[Ru(NH_3)_6]^{2+\|3+}$**
Bare Au	**0.4488**	**0.216**
TP/Au	**770.4**	**345.2**
o-ATP/Au	**812.4**	**907.4**
p-ATP/Au	**5.164**	**0.780**

Table-5

The charge transfer resistance (R_{ct}) values obtained from the impedance plots of mixed SAM modified electrodes by the equivalent circuit fitting analysis using two different redox couples as probe molecules.

Sample	**Charge transfer resistance (R_{ct}) values (Ω cm^2)**			
	Mixed SAM with 1-Octanethiol		**Mixed SAM with 1,6-Hexanedithiol**	
	$[Fe(CN)_6]^{3-\|4-}$	**$[Ru(NH_3)_6]^{2+\|3+}$**	**$[Fe(CN)_6]^{3-\|4-}$**	**$[Ru(NH_3)_6]^{2+\|3+}$**
TP/Au	**321.2**	**332.8**	**415.4**	**252.2**
o-ATP/Au	**46.5**	**50.94**	**565.4**	**336.6**
p-ATP/Au	**1414.2**	**1097.4**	**2214.0**	**392.8**

From the charge transfer resistance (R_{ct}) values, we have calculated the surface coverage (θ) of the monolayer on the gold surface using equation (6), by assuming that the current is due to the presence of pinholes and defects within the monolayer.

$$\theta = 1 - (R_{ct}/R'_{ct}) \quad (6)$$

where R_{ct} is the charge transfer resistance of bare Au electrode and R'_{ct} is the charge transfer resistance of the corresponding SAM modified electrodes. We have determined a surface coverage value of ~99.9% for the SAMs of TP and o-ATP on Au surface. In the case of SAM of p-ATP on Au, the surface coverage value is found to be 84%, which is very low implying the existence of large number of pinholes and defects in the monolayer. Table 6 shows the surface coverage values of different potential cycled electrodes and mixed SAM modified electrodes of aromatic thiols on Au surface obtained from the respective R_{ct} values. It can be seen from the table 6 that the surface coverage value is >99.9% in almost all the cases of the monolayer coated electrodes. In the case of p-ATP on Au surface, the surface coverage value increases significantly from 91% after the potential cycling to >99.9% after the mixed SAM formation. This clearly establishes that after potential cycling the monolayer is structurally organized to form a well-ordered and compact film. In the case of mixed SAM, the added thiol occupies the pinholes and defects within the monolayer, thereby increasing the blocking ability of the film with much less number of pinholes and defects except in the case of SAM of o-ATP on Au. From these experiments we conclude that both the processes of potential cycling and the mixed SAM formation significantly increase the blocking property of the monolayers of TP, o-ATP and p-ATP on Au surface.

Table-6

The surface coverage (θ) values obtained for the different potential cycled electrodes and mixed SAM modified electrodes from the corresponding R_{ct} values determined using $[Fe(CN)_6]^{3-|4-}$ redox couple as a probe molecule.

Sample	Surface coverage (θ) values		
	Potential cycled electrodes	Mixed SAM modified electrodes	
		1-Octanethiol	1,6-Hexanedithiol
TP/Au	**0.9994**	**0.9986**	**0.9990**
o-ATP/Au	**0.9995**	**0.9904**	**0.9992**
p-ATP/Au	**0.9131**	**0.9997**	**0.9998**

4.6.6. Pinhole analysis of SAM modified surfaces

Electrochemical impedance spectroscopic studies on the monolayer-coated electrodes, potential cycled electrodes (after the SAM formation) and mixed SAM modified electrodes can provide valuable information on the distribution of pinholes and defects in the monolayer. Finklea et al. [60] developed a model for the impedance response of a monolayer-coated electrode, which behaves as an array of microelectrodes. Fawcett and his co-workers have extensively studied the structural integrity and organization of the monolayer by pore size analysis using the electrochemical impedance spectroscopy data [61-63]. Based on the work of Matsuda [64] and Amatore [65], a model has been developed to fit the faradaic impedance data obtained for the electron transfer reactions at the SAM modified electrode to understand the distribution of pinholes and defects within the monolayer. The impedance

expressions have been derived by assuming that the total pinhole area fraction, (1-θ) is less than 0.1, where θ is the surface coverage of the monolayer on Au surface. Both the real and imaginary parts of the faradaic impedance values are plotted as a function of $\omega^{-1/2}$. There are two limiting cases for this model to be applied. At higher frequencies, the diffusion profiles of each individual microelectrode constituent of the array are separated, in contrast to the situation at lower frequencies where there is an overlap of diffusion profiles.

In the case of SAMs of TP, o-ATP and p-ATP on Au surface, the distribution of pinholes and defects are analyzed using the above-described model. Figures 32 (a-d) show the real part of the faradaic impedance of different SAM modified electrodes plotted as a function of $\omega^{-1/2}$. For comparison, the plot of bare gold electrode is also shown in figure 32 (a). Figures 32 (b-d) show the plots of real component of faradaic impedance, Z'_f vs. $\omega^{-1/2}$, for the SAMs of TP, o-ATP and p-ATP on Au surface respectively. Figures 33 (a-c) show the plots of imaginary component of faradaic impedance, Z''_f vs. $\omega^{-1/2}$ for the above-mentioned electrodes. The faradaic impedance plots show the features similar to that of an array of microelectrodes. Analysis of figures 32 and 33 shows that there are two linear domains at high and low frequencies for the Z'_f vs. $\omega^{-1/2}$ plots and a peak formation in the Z''_f vs. $\omega^{-1/2}$ plots corresponding to the frequency of transition between the two linear domains. According to the model described earlier, this frequency separates the two time-dependent diffusion profiles for the microelectrodes.

As discussed before, we tried to improve the surface coverage of these monolayers by subjecting the SAM coated electrodes to potential cycling and mixed SAM formation with 1-Octanethiol and 1,6-Hexanedithiol. We have analyzed these results using the above-mentioned model. Both the real (Z'_f) and

imaginary (Z''_f) components of the faradaic impedance were calculated and plotted as a function of $\omega^{-1/2}$ (Figures not shown). The faradaic impedance plots show the features similar to that of an array of microelectrodes. As an example, we have shown the plots of Z'_f vs. $\omega^{-1/2}$ and Z''_f vs. $\omega^{-1/2}$ for the mixed SAM modified electrodes in the case of SAM of p-ATP on Au surface in the figures 34A and B respectively. We have obtained similar plots for the other cases of monolayer-coated electrodes (Figures not shown), from which the distribution of pinholes and defects within the corresponding monolayer are analyzed.

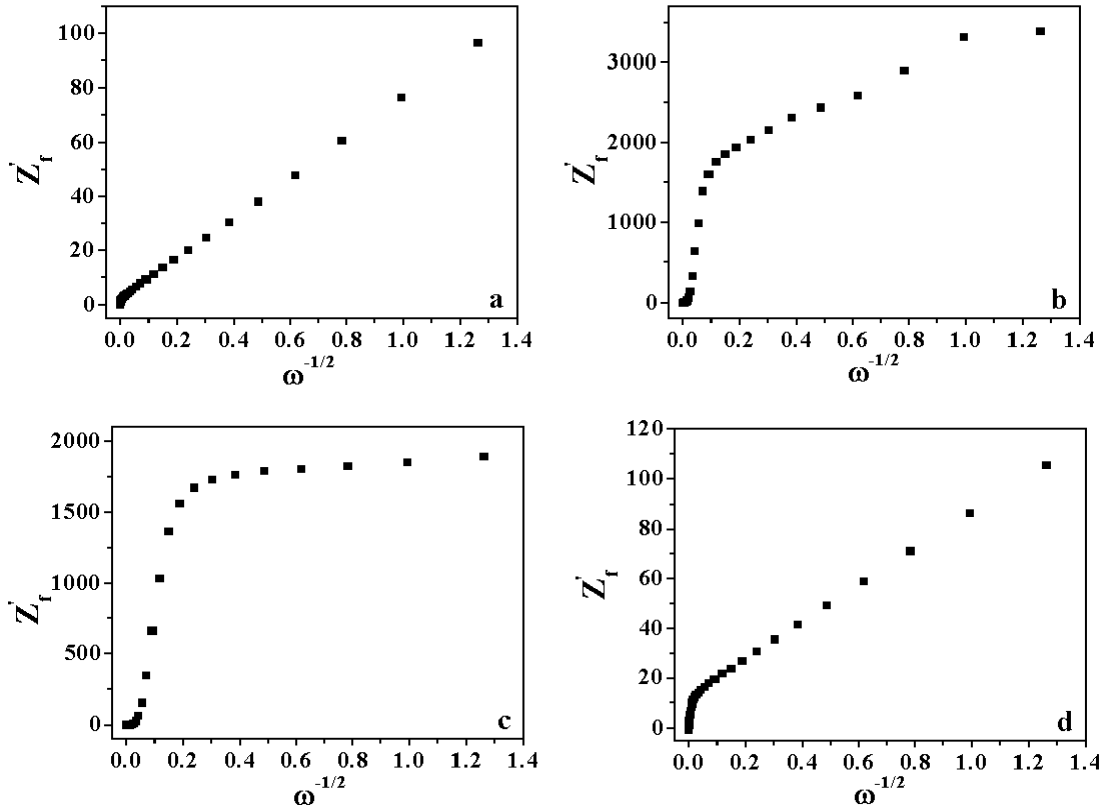

Figure 32: Plots of real part of faradaic impedance (Z'_f) vs. $\omega^{-1/2}$ for, (a) Bare Au electrode, (b) SAM of TP on Au surface, (c) SAM of o-ATP on Au electrode and (d) SAM of p-ATP on Au surface.

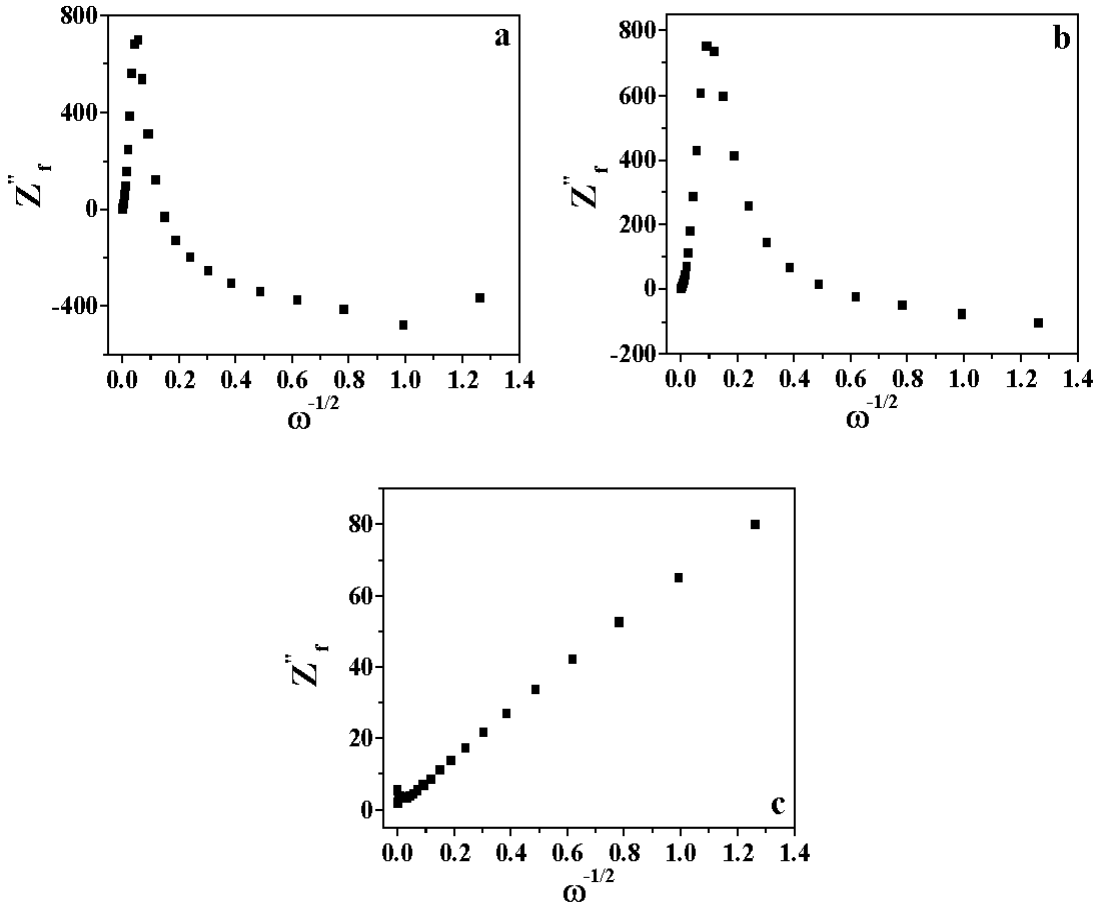

Figure 33: Plots of imaginary part of faradaic impedance (Z''_f) as a function of $\omega^{-1/2}$ for, (a) SAM of TP on Au electrode, (b) SAM of o-ATP on Au surface and (c) SAM of p-ATP on Au electrode.

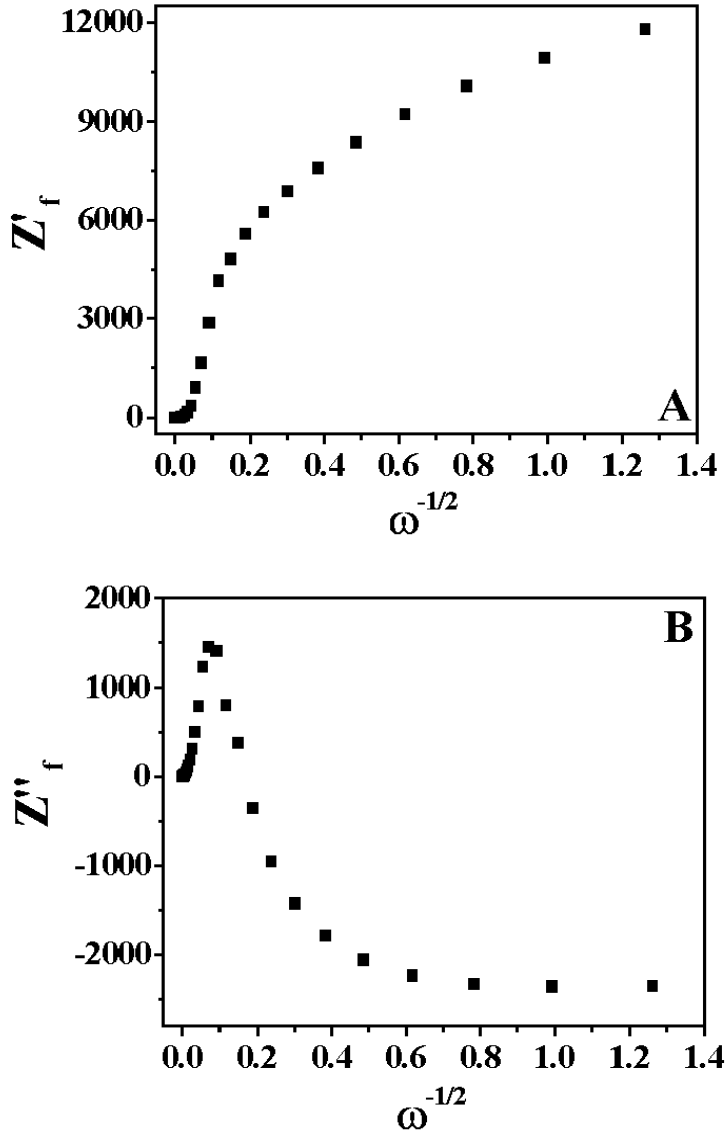

Figure 34: The faradaic impedance plots of mixed SAM modified electrode for the monolayer of p-ATP on Au surface with 1,6-Hexanedithiol. (A) Plot of real part of faradaic impedance (Z'_f) as a function of $\omega^{-1/2}$. (B) Plot of imaginary part of faradaic impedance (Z''_f) vs. $\omega^{-1/2}$.

The surface coverage of the monolayer can be determined from the slope of the Z'_f vs. $\omega^{-1/2}$ plot at a higher frequency region, which is given by [61-63],

$$m = \sigma + \sigma/(1-\theta) \quad (5)$$

and $$\theta = 1 - [\sigma / (m-\sigma)] \quad (7)$$

where m is the slope obtained from the faradaic impedance plots, θ is the surface coverage of the monolayer and σ the Warburg coefficient, which can be obtained from the unmodified bare Au electrode.

From the plots, we observed that at lower frequencies the slope of the curve decreases with increase in $\omega^{-1/2}$. We also find that the Warburg coefficient (slope m) calculated for the SAM modified electrodes is always higher than that of the corresponding value of the bare Au electrode. The increase in the apparent value of the Warburg coefficient of the monolayer-coated electrodes suggests that the pinholes are distributed in patches over the surface. Using eqn. (7) we have calculated the surface coverage values of 0.9974, 0.9950, and 0.9200 for the SAMs of TP, o-ATP and p-ATP on Au respectively. The surface coverage values are very much less compared to the SAMs of aliphatic thiols, which implies that the aromatic thiols studied in this work do not form a highly dense, well-organized and compact monolayer when compared to that of long chain aliphatic thiols. Among the different aromatic thiols studied in this work, we find that the SAM of p-ATP on Au surface possesses comparatively a poorer blocking behaviour. The pinholes and defects analysis of SAMs indicates the existence of a large number of pinholes and defects in the case of aromatic thiols. We have also calculated the surface coverage values of different potential cycled electrodes and mixed SAM modified electrodes of the monolayers of TP, o-ATP and p-ATP on Au surface using eqn. (7) and the

corresponding values are given in table 7. It can be seen from the table 7 that the surface coverage values of these aromatic thiols on Au surface are significantly increased after the potential cycling and mixed SAM formation, especially in the case of p-ATP on Au surface. By comparing the tables 6 and 7 it can be noted that these surface coverage values are largely in agreement with the corresponding surface coverage values determined from the R_{ct} values.

Table-7

The surface coverage (θ) values determined for various potential cycled electrodes and mixed SAM modified electrodes from the pinholes and defects analysis using the impedance data obtained for $[Fe(CN)_6]^{3-|4-}$ redox couple as a probe molecule.

Sample	Surface coverage (θ) values		
	Potential cycled electrodes	Mixed SAM modified electrodes	
		1-Octanethiol	1,6-Hexanedithiol
TP/Au	**0.9984**	**0.9975**	**0.9973**
o-ATP/Au	**0.9989**	**0.9887**	**0.9986**
p-ATP/Au	**0.9240**	**0.9989**	**0.9994**

Based on the analysis of cyclic voltammetry and electrochemical impedance spectroscopic studies on SAMs of aromatic thiols on Au surface, we find that the molecules of TP, o-ATP and p-ATP form a moderately good blocking monolayer film with pinholes and defects. These monolayers block the redox reaction of potassium ferro/ferri cyanide redox couple indicating fairly good blocking behaviour of the SAM. In contrast, the redox reaction of ruthenium complex is quite facile in all the SAM modified electrodes. Under

the acidic conditions, where the SAMs of o-ATP and p-ATP acquire a positive charge at the electrode surface owing to protonation of –OH group, the redox reaction of potassium ferro/ferri cyanide complex is facile due to the electrostatic attraction between the SAM and the redox couple. Surprisingly, the SAM modified electrodes allow the redox reaction of ruthenium complex under the acidic condition, where it is expected to show the blocking behaviour due to the repulsive interactions. This aspect has been explained below. Under the basic conditions, the SAM modified electrodes show a facile kinetics for ruthenium redox reaction and somewhat good blocking ability for the potassium ferro/ferri cyanide reaction. These observations are confirmed quantitatively by the determination of R_{ct} values, which are shown in the table 2 and 3. From the studies of electron transfer reactions on the SAM modified electrodes, it is clear that the monolayers are selective to redox reaction of ruthenium complex.

Similarly, in the case of potential cycled electrodes (after the SAM formation), the redox reaction of $[Fe(CN)_6]^{3-|4-}$ redox couple is inhibited and the extent of blocking is more after the potential cycling when compared to as prepared SAM electrodes (Fig. 23 and 25). In contrast, the redox reaction of ruthenium complex is quite facile even after the potential cycling, although there is a very small increase in the R_{ct} values (Fig. 24 and 26).

We have carried out experiments in order to evaluate the structural integrity of the monolayer and to rule out the possibility of any reaction product blocking the redox reactions of the probe molecules. The experiment involves carrying out the cyclic voltammetric studies of SAM modified electrodes in the potential range of –0.1V to 0.5V vs. SCE in 1M NaF aqueous solution. We find that the CVs do not show any peak formation for the SAMs of aromatic thiols on Au surface implying that the monolayer is structurally rigid and it does not undergo any reaction in this potential range where the electron transfer

reactions of redox probe molecules are studied. These experiments prove the fact that the monolayer does not undergo any structural disorganization within the potential range used for the study.

Usually, the electron transfer reactions on the SAM modified electrodes usually occur either through the pinholes and defects or by a tunneling process. In the case of aromatic thiols, the electron transfer can be further facilitated by the delocalized π-electrons present in the aromatic phenyl ring because of extended conjugation. It may be pointed out that the sizes of ferrocyanide (6Å) and ruthenium (6.4Å) complexes are almost comparable [19] and if ruthenium redox reaction is assumed to occur by access to the electrode surface through the pinholes and defects present in the monolayer, then the redox reaction of ferrocyanide is also expected to show facile kinetics. Obviously, it is not so and therefore it is felt that the Ru(III) redox reaction may take place by a tunneling process through the monolayer. It is well known that the redox reaction of hexaammineruthenium(III) chloride follows an outer sphere electron transfer reaction [35], where the physical access to the electrode surface is not a pre-requisite for the electron transfer to occur since the process is facilitated by a tunneling mechanism. This is in contrast to ferrocyanide redox reaction, which is an inner sphere electron transfer reaction, where the access of redox species to the electrode surface is necessary for the reaction to occur [36]. These results are in conformity with our studies on SAMs of 2-naphathelenethiol on Au surface (discussed in the previous section), in which the aromatic ring with highly delocalized π-electrons mediate the electron transfer between the SAM and the redox species. We believe a similar process can occur in the cases of SAMs of TP, o-ATP and p-ATP on Au surface.

The process of potential cycling has introduced significant structural organization on the monolayers, resulting in the formation of highly compact,

well-ordered monolayers with less number of pinholes and defects. It can also be seen from our experiments that although the potential cycling has generally improved the blocking ability of the monolayers of aromatic thiols on Au surface, we do not find significant improvement in the case of p-ATP SAM. We have studied mixed SAM formation with 1-Octanethiol and 1,6-Hexanedithiol (we have chosen these thiols because of comparable chain lengths to that of the aromatic thiols) essentially to improve the blocking behaviour of the monolayer of p-ATP on Au electrode. The adsorption energy of aliphatic thiols to the gold surface is lower in comparison to the energy required for the replacement of existing aromatic thiols. The added aliphatic thiol and dithiol molecules therefore fill up the pinholes, defects and domain boundaries present within the monolayers, resulting in the formation of highly organized, well ordered, compact monolayer leading to a significant improvement in the blocking efficiency of these SAMs. It can be noted from the cyclic voltammetry and impedance spectroscopic studies that the mixed SAM coated electrodes show significant improvement in the blocking behaviour when compared to simple SAM modified electrodes, especially in the case of p-ATP on Au surface. Even in the cases of mixed SAM modified electrodes, the redox reaction of ruthenium complex shows the quasi-reversible behaviour indicating a tunneling mechanism for the electron transfer process. On the other hand, the redox reaction of potassium ferrocyanide is fully inhibited. It can be noted that the mixed SAM of o-ATP with 1-Octanethiol show a quasi-reversible behaviour for the redox reaction implying a rather poor blocking ability of the monolayer. In the case of SAM of o-ATP on Au surface, the nitrogen atom from the amino group is also known to bind with the gold surface through the lone pair of electrons [88]. The intercalation of alkanethiol molecules within the space is inhibited by the amino group of o-ATP and not in the case of p-ATP, as it is

vertically oriented. The blocking ability of the monolayer of p-ATP on Au surface is significantly improved after the mixed SAM formation, which is evidenced by the large increase in the R_{ct} values and the surface coverage (θ) values, as can be seen from the tables 5, 6 and 7. On the whole, the blocking ability of the monolayers of TP and p-ATP on Au surface is improved to a large extent by the process of potential cycling and mixed SAM formation. In the case of o-ATP, only the process of potential cycling improves the blocking ability of the monolayer and not the mixed SAM formation.

Based on the experimental results, it is proposed that the redox reaction of $[Fe(CN)_6]^{3-|4-}$ occurs mainly through the pinholes and defects present in the monolayers. On the other hand, the redox reaction of $[Ru(NH_3)_6]^{2+|3+}$ occurs by a tunneling through bond mechanism where the SAMs act as a mediator for the electron transfer between Au surface and the redox couple. In these cases, the process of tunneling is facilitated not only by the presence of highly delocalized π-electrons in the aromatic phenyl ring but also by the smaller length of the aromatic molecules used for the monolayer formation and its characterization. We think that our results on the study of electron transfer reactions are important in biological systems involving proteins and DNA, where the structural units contain mainly aromatic core that play a vital role in the electron transfer mechanisms. The SAM modified electrodes are the ideal candidates to mimic the biological systems in order to understand the various physiological and chemical processes occurring in these systems.

III. SAMs OF ALKOXYCYANOBIPHEYL THIOLS ON Au SURFACE

4.7. Introduction

Similar to aromatic thiols, we have also studied the monolayer formation and characterization of alkoxycyanobiphenyl thiols having different alkyl chain lengths on gold surface using dichloromethane as a solvent. The special feature of these alkoxycyanobiphenyl thiols is that it contains both the aliphatic and aromatic parts in its structure. These molecules show a nematic liquid crystalline phase in the bulk sample. The fundamental studies on interfacial electron transfer and electrochemical processes at the SAM modified electrode | solution interface are attaining a great deal of interest and widely reported in literature [37,41,101]. The blocking ability of the monolayer-coated electrode to the electron transfer process is usually evaluated by studying the redox reactions using potassium ferro/ferri cyanide and hexaammineruthenium(III) chloride complexes as redox probes [61-63,76]. Some ruthenium complexes in solutions have also been used as redox probes in many chemical, biological and photochemical sensors [102-107].

Apart from commonly studied SAMs of aliphatic thiols, there is also a great deal of interest on the monolayers of aromatic thiols [79,81,84,86] in recent times. SAMs of aromatic thiols are of interest owing to their higher rigidity and the presence of delocalized π-electrons in the aromatic ring. Among several aromatic thiols reported in literature, there are some scattered reports on SAM of biphenyl thiol [108-110]. Cyganik et al. reported the scanning tunneling microscopic observation of the influence of spacer chain on the molecular packing of SAMs of ω-biphenylalkanethiols on Au (111) [108]. Long et al. studied the effect of odd-even number of alkyl chains on SAMs of biphenyl-based thiols using cyclic voltammetry [109].

Reports on self-assembled monolayer of molecules, which show the liquid crystalline phase behaviour in bulk are also very rare. In literature, both discotic and calamitic (types of liquid crystalline phases) molecules have been shown to form highly ordered SAMs on gold leading to many interesting properties and phenomena [111-117]. A number of terminally substituted alkoxycyanobiphenyl compounds such as bromo-, hydroxy-, amino-, carboxy-, epoxy- and olefine- terminated cyanobiphenyls are already known. However, we find that the terminal thiol functionalized cyanobiphenyls have not yet been explored. Recently, Kumar et al. reported the synthesis of a number of terminal thiol-substituted alkoxycyanobiphenyls [118] that have been used for the monolayer preparation and characterization in the present work.

In this section, we report our studies on self-assembled monolayer films of some alkoxycyanobiphenyl molecules functionalized with thiols. The liquid crystalline phase behaviour of these molecules is confirmed by polarizing light microscopy. Electrochemical techniques such as cyclic voltammetry (CV) and electrochemical impedance spectroscopy (EIS) were used for the evaluation of barrier property of the SAM-modified electrodes using potassium ferrocyanide and hexaammineruthenium(III) chloride complexes as redox probes. Impedance spectroscopy data were used for the calculation of surface coverage and other kinetic parameters for the SAM modified electrodes.

4.8. Experimental section

4.8.1. Chemicals

Dichloromethane (Spectrochem), potassium ferrocyanide (Loba), potassium ferricyanide (Qualigens), hexaammineruthenium(III) chloride (Alfa Aesar), sodium fluoride (Qualigens) and lithium perchlorate (Acros Organics) were used in this study as received. Alkoxycyanobiphenyl thiol compounds of

different chain lengths (C_5(a), C_8(b) and C_{10}(c)) were synthesized by Kumar et al. [118] and the synthetic scheme is described elsewhere [119]. All the chemical reagents used in this work were analytical grade (AR) reagents. Millipore water having a resistivity of 18 MΩ cm was used to prepare the aqueous solutions. The structure of the alkoxycyanobiphenyl thiol compounds studied in this work is shown in the following figure.

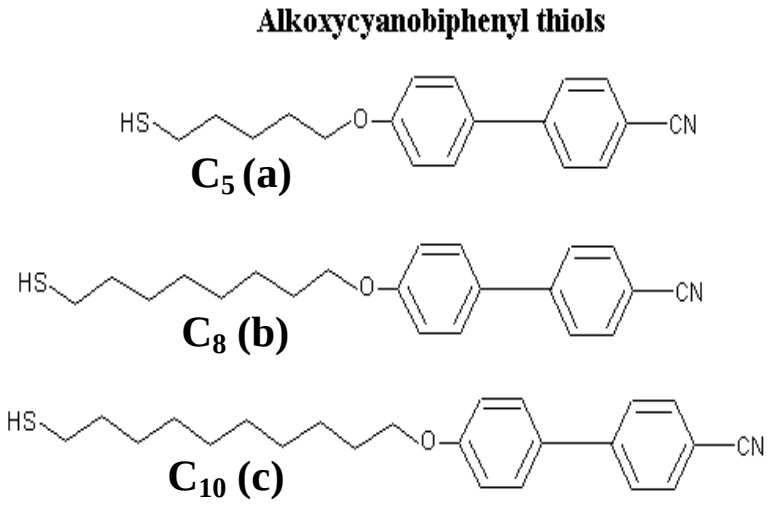

4.8.2. Sample preparation

Gold sample of purity 99.99% was obtained from Arora Mathey, India. Evaporated gold (~100 nm thickness) on glass with chromium underlayers (~2-5 nm thickness) was used for the monolayer formation and its characterization using electrochemical techniques. The substrate was heated to 350^0C during gold evaporation under a vacuum pressure of 2 X 10^{-5} mbar, a process that normally yields a very smooth gold substrate with predominantly Au (111) orientation. The evaporated gold samples were used as strips for SAM formation and its analysis.

4.8.3. Preparation of SAMs of alkoxycyanobiphenyl thiols on Au

Self-assembled monolayers (SAMs) of the above-mentioned alkoxycyanobiphenyl thiols of different chain length (C_5(a), C_8(b) and C_{10}(c)), have been formed on gold and characterized using electrochemical techniques. The evaporated Au samples were used as strips for the monolayer preparation and its characterization. Before SAM formation, the gold strips were pretreated with "piranha" solution, which is a mixture of 30% H_2O_2 and conc. H_2SO_4 in 1:3 ratio. The monolayers were prepared by keeping the Au strips in 1mM thiol solution in dichloromethane for about 1 hour and 15 hours. After the adsorption of thiol, the Au coated electrode was rinsed with dichloromethane; thoroughly cleaned using distilled water and finally with millipore water and used for the analysis immediately. For comparison the self-assembled monolayers of decanethiol and hexadecanethiol on Au were also prepared using a similar procedure.

4.8.4. Electrochemical characterization of SAMs on Au surface

A conventional three-electrode electrochemical cell with large surface area Pt foil as a counter electrode, saturated calomel electrode (SCE) as a reference electrode and SAM modified Au strips as working electrode was used for the electrochemical characterization of SAMs. The barrier property of the monolayer has been evaluated by studying the electron transfer reaction on the modified surfaces using two different redox probes namely potassium ferrocyanide (negative redox probe) and hexaammineruthenium(III) chloride (positive redox probe). Cyclic voltammetric measurements were carried out in 10mM potassium ferrocyanide in 1M NaF at a potential range of –100mV to 500mV vs. SCE and 1mM hexaammineruthenium(III) chloride in 0.1M $LiClO_4$ at a potential range of –400mV to 100mV vs. SCE. The impedance

measurements were carried out using an ac signal of 10mV amplitude at a formal potential of the redox couple at a wide frequency range of 100kHz to 0.1Hz. The electrolytic solution contained equal concentrations of both the oxidized and reduced forms of the redox couple namely, 10mM potassium ferrocyanide and 10mM potassium ferricyanide in 1M NaF. From the impedance data, the charge transfer resistance (R_{ct}) was determined using the equivalent circuit fitting analysis. From the R_{ct} values, the surface coverage (θ) of the monolayer on Au surface and the rate constant of the electron transfer reaction on the SAM modified electrodes were calculated.

4.8.5. Instrumentation

The cyclic voltammetric studies were performed using an EG&G potentiostat (model 263A) interfaced to a PC through a GPIB card (National Instruments). For electrochemical impedance spectroscopy studies the potentiostat is used along with an EG&G 5210 lock-in-amplifier controlled by Power Sine software (EG&G). The equivalent circuit fitting of the impedance data has been carried out using Zsimpwin software (EG&G) developed on the basis of Boukamp's model.

4.9. Results and discussion

4.9.1. Cyclic voltammetry

Cyclic voltammetry is an important technique to evaluate the blocking property of the monolayer-coated electrodes using diffusion controlled redox couples as probes. Figure 35A shows the cyclic voltammograms of bare Au and SAM modified Au electrodes in 10mM potassium ferrocyanide with 1M NaF as the supporting electrolyte at a potential scan rate of 50mV/s. It can be seen from the figure that the bare Au electrode (Fig. 35A (a)) shows a reversible

voltammogram for the redox couple indicating that the electron transfer reaction is completely diffusion controlled. In contrast, the absence of any peak formation in the CVs of the monolayer modified electrodes shows that the redox reaction is inhibited. It can also be seen that in the case of C_5 thiol (Fig. 35A (b)), the CV exhibits a rather imperfect blocking behaviour. In the case of C_8 and C_{10} thiols (Fig. 35A (c) and 35A (d)) the CVs indicate a good blocking behaviour for the electron transfer reaction, which means that a highly ordered, compact monolayer of alkoxycyanobiphenyl thiol is formed on the Au surface. The CVs also exhibit the microelectrode array characteristics [98-100]. The microelectrode array behaviour obtained in the case of C_8 and C_{10} thiols arises due to the access of ions through the pinholes and pores present in the SAM, which facilitates the radial diffusion of the redox species in contrast to the linear diffusion, observed in the case of bare Au surface.

Figure 35B shows the cyclic voltammograms of bare Au and monolayer-modified electrodes in 1mM hexaammineruthenium(III) chloride with 0.1M $LiClO_4$ as the supporting electrolyte at a potential scan rate of 50mV/s. It can be seen from the figure that the bare Au electrode (Fig. 35B (a)) shows a reversible behaviour implying that the redox reaction is under diffusion control. In contrast, the SAM modified electrodes in the case of C_8 (Fig. 35B (c)) and C_{10} thiols (Fig. 35B (d)) show a good blocking behaviour. The CVs exhibit characteristics that are typical of an array of microelectrodes [98-100]. On the other hand, the ruthenium redox reaction through the SAM of C_5 thiol (Fig. 35B (b)) shows a quasi-reversible behaviour with peak current values close to that of the bare Au electrode. It is worth recalling that the redox reaction of $[Fe(CN)_6]^{3-|4-}$ is blocked in the case of C_5 thiol.

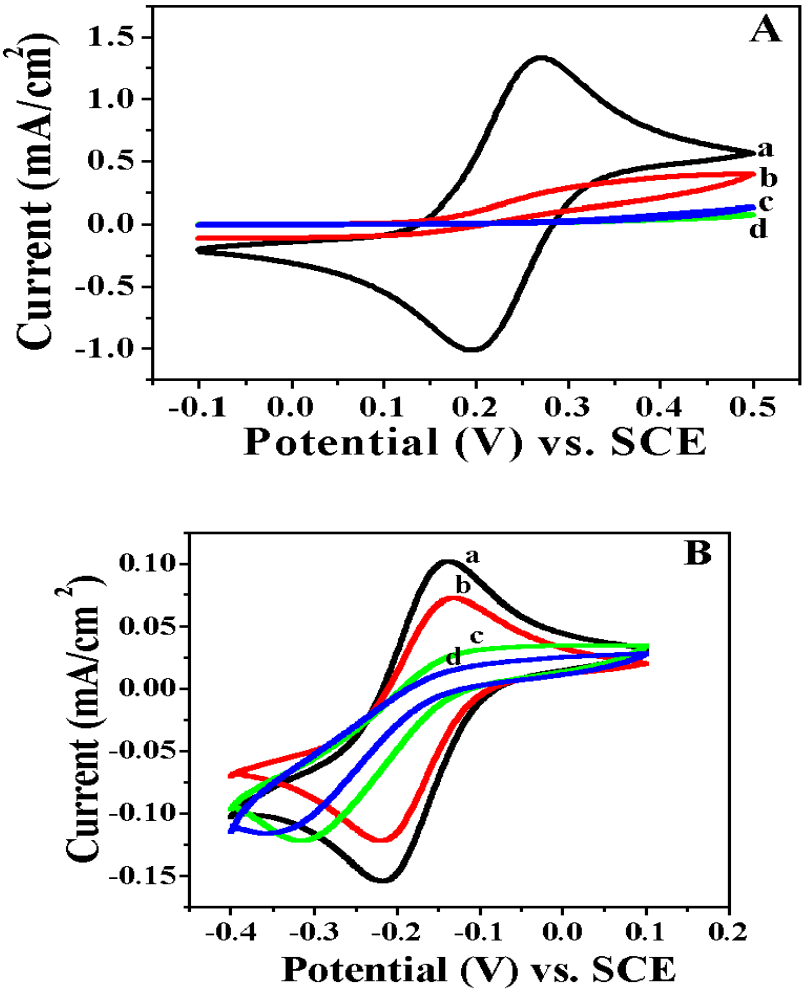

Figure 35: (A) Cyclic voltammograms in 10mM potassium ferrocyanide with 1M NaF as supporting electrolyte at a potential scan rate of 50mV/s for (a) bare Au electrode, (b), (c) and (d) are SAMs of alkoxycyanobiphenyl thiols with different alkyl chain lengths of C_5, C_8 and C_{10} on Au surface respectively. (B) Cyclic voltammograms in 1mM hexaammineruthenium(III) chloride with 0.1M $LiClO_4$ as supporting electrolyte at a potential scan rate of 50mV/s for (a) bare Au electrode, (b), (c) and (d) are SAMs of alkoxycyanobiphenyl thiols with various alkyl chain lengths of C_5, C_8 and C_{10} on Au surface respectively.

In order to understand the mechanism of electron transfer process of hexaammineruthenium(III) chloride through the SAM of C_5 thiol on Au electrode, we have carried out similar studies using aliphatic thiols with methyl group at the terminal position namely decanethiol and hexadecanethiol, which have chain lengths comparable to that of C_5 and C_8 alkoxycyanobiphenyl thiols. Though we have carried out the experiments for both the aliphatic thiols, we discuss the results obtained on the SAM of decanethiol on Au, which has a shorter chain length and comparable to C_5 thiol. The monolayer was prepared by keeping the Au strips in 1mM decanethiol solution in dichloromethane for about 15 hours and the results are compared with the monolayer of C_5 thiol on Au obtained using a similar procedure. After the adsorption of thiol, the SAM coated Au electrodes were rinsed with dichloromethane, thoroughly cleaned using distilled water and finally with millipore water and used for the analysis immediately.

Figure 36A shows the cyclic voltammograms of bare Au and SAM modified Au electrodes in 10mM potassium ferrocyanide with 1M NaF as the supporting electrolyte at a potential scan rate of 50mV/s. It can be seen from the figure that the bare Au electrode (Fig. 36A (a)) shows a reversible voltammogram for the redox couple indicating the diffusion-controlled process for the electron transfer reaction on the bare Au surface. On the other hand, CVs of SAM modified electrodes show that the redox reaction is completely inhibited. Figures 36A (b) and 36A (c) show the CVs of SAMs of C_5 thiol and decanethiol on Au coated electrodes. It can be noted that the CVs show the characteristics of microelectrode array behaviour, indicating the formation of a highly ordered, compact monolayer on the Au surface.

Figure 36B shows the comparison of cyclic voltammograms of bare Au and SAM modified electrodes in 1mM hexaammineruthenium(III) chloride

with 0.1M $LiClO_4$ as the supporting electrolyte at a potential scan rate of 50mV/s. It can be seen from the figure that the bare Au electrode (Fig. 36B (a)) shows a reversible behaviour for the electron transfer reaction implying the process is under diffusion control. In contrast, the CV of SAM of decanethiol on Au (Fig. 36B (c)) shows a very good blocking behaviour indicating the characteristics of an array of microelectrodes. On the other hand, the CV of SAM of C_5 thiol on Au (Fig. 36B (b)) shows a quasi-reversible behaviour with a large peak-to-peak separation value and the peak current values are close to that of bare Au electrode. It can be noted that the Ru(III) redox reaction is almost completely inhibited in the case of decanethiol in contrast to that of SAM of C_5 thiol although the chain lengths of these two thiols are comparable.

4.9.2. Electrochemical impedance spectroscopy

Electrochemical impedance spectroscopy is a powerful tool to determine the kinetic parameters and the surface coverage with the structural integrity of the monolayer on Au surface by evaluating the presence of pores and pinholes using redox couple as the probe molecule.

4.9.2.1. Potassium Ferrocyanide – Ferricyanide redox reaction

Figure 37A shows the impedance plots (Nyquist plots) of the SAM modified electrodes based on C_8 and C_{10} (Fig. 37A (a) and (b)) thiols in equal concentrations of potassium ferro/ferri cyanide with NaF as the supporting electrolyte. Figure 37B shows the same plot for SAM of C_5 thiol-modified electrode and the inset shows for bare Au electrode. It can be seen from the inset of figure 37B that the bare Au shows a low frequency straight line with a very small semicircle at high frequency region indicating a diffusion-controlled process for the redox couple on bare Au surface.

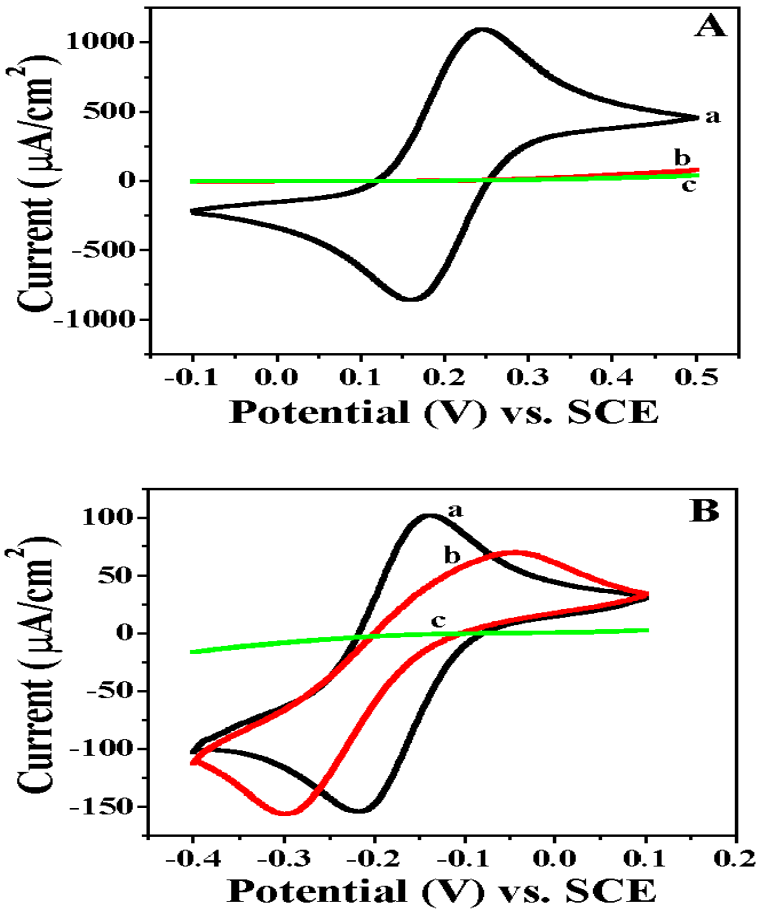

Figure 36: (A) Cyclic voltammograms in 10mM potassium ferrocyanide with 1M NaF as supporting electrolyte at a potential scan rate of 50mV/s for (a) bare Au electrode, (b) and (c) are the respective SAMs of C_5 alkoxycyanobiphenyl thiol and decanethiol on Au obtained by keeping the Au strips in 1mM thiol solution for about 15 hours. (B) Cyclic voltammograms in 1mM hexaammineruthenium(III) chloride with 0.1M $LiClO_4$ as supporting electrolyte at a potential scan rate of 50mV/s for (a) bare Au electrode, (b) and (c) are the respective SAMs of C_5 thiol and decanethiol on Au obtained by keeping the Au strips in 1mM thiol solution for about 15 hours.

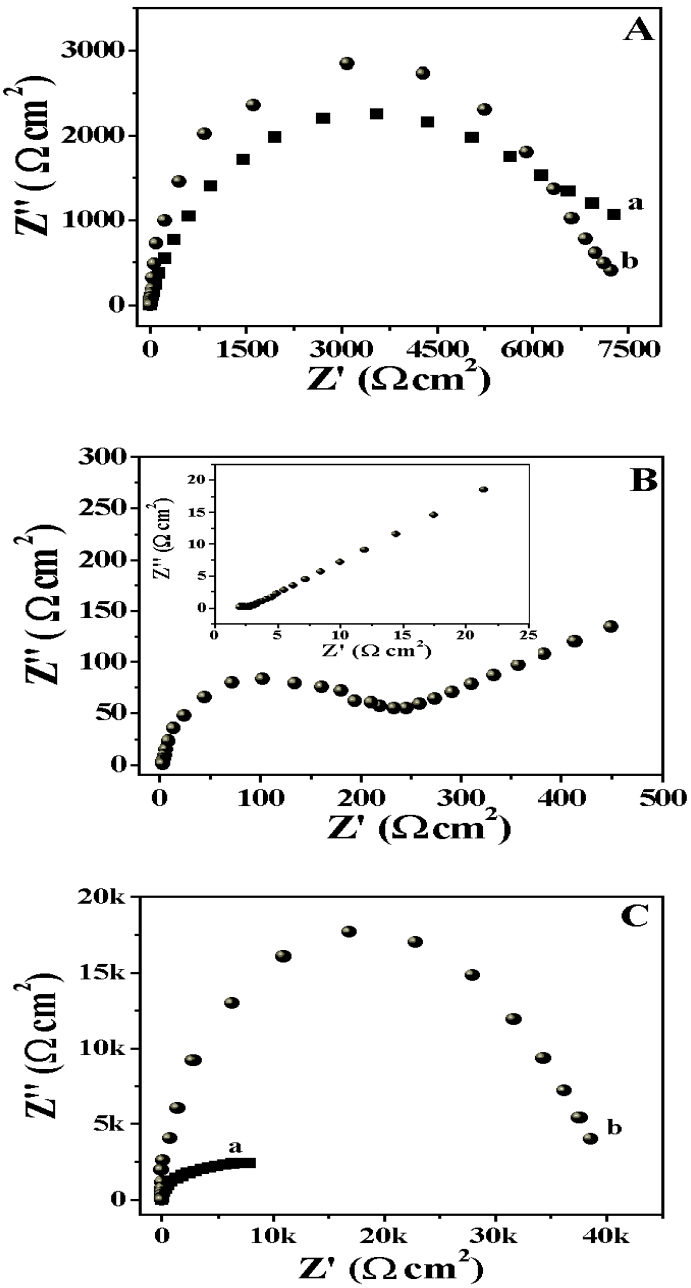

Figure 37: Impedance plots in equal concentrations of both potassium ferrocyanide and potassium ferricyanide solution with NaF as the supporting electrolyte for, (A) SAMs of C_8 (a) and C_{10} (b) alkoxycyanobiphenyl thiols on Au surface. (B) SAM of C_5 alkoxycyanobiphenyl thiol on Au electrode. (C) SAMs of C_5 thiol (a) and decanethiol (b) on Au surface (15 hours). Inset shows the same plot for the bare Au electrode.

In the case of C_5, there is a semicircle at high frequency region and a straight line at low frequency region, again indicating a diffusion controlled process implying that the SAM of C_5 thiol has a somewhat poor blocking ability. However the impedance plots of C_8 and C_{10} thiols (Figures 37A (a) and (b)) show large semicircles in the entire range of frequency, characteristic of complete charge transfer control implying a perfect blocking behaviour.

Figure 37C shows the Nyquist plots of SAM modified gold electrodes obtained by keeping the Au strips in thiol solution for about 15 hours to improve the monolayer characteristics. Figures 37C (a) and 37C (b) show the respective Nyquist plots of SAM of C_5 thiol and decanethiol on Au in equal concentrations of potassium ferro/ferri cyanide with NaF as the supporting electrolyte. It can be seen from the figure that the SAM of decanethiol on Au (Fig. 37C (b)) shows a large semicircle formation in the entire range of frequency indicating the complete charge transfer control for the redox reaction. In the case of C_5 thiol, the formation of depressed semicircle implies that the electron transfer process is under charge transfer control with a poor blocking ability of the monolayer.

4.9.2.2. Hexaammineruthenium(II) –ruthenium(III) redox reaction

Figure 38A shows the Nyquist plots of the SAM modified electrodes based on C_8 and C_{10} (Fig. 38A (a) and (b)) thiol molecules in 1mM hexaammineruthenium(III) chloride with 0.1M $LiClO_4$ as the supporting electrolyte. Figure 38B shows a similar plot for the SAM of C_5 thiol-modified electrode and the inset shows the same plot for bare Au electrode. The impedance plot of bare Au electrode (Inset of Fig. 38B) exhibits a low frequency straight line with a very small semicircle formation at high frequency region implying the diffusion controlled process for the Ru(III) electron transfer

reaction. Similarly, the SAM of C_5 thiol on Au (Fig. 38B) shows that the Ru(III) reaction is quite facile. The small semicircle at high frequency region implies that the electron transfer reaction is quasi-reversible. Such a behaviour indicates that the SAM shows a very poor blocking ability. In contrast, the SAMs based on C_8 and C_{10} (Fig. 38A (a) and (b)) thiol molecules show the formation of larger semicircles (almost in the entire range of frequency) with a straight line at very low frequency implying that they form a better blocking monolayer film.

Figure 38C shows the Nyquist plots of monolayer modified electrodes on Au obtained by keeping Au strips in thiol solution for about 15 hours. Figure 38C shows the Nyquist plot of SAM of decanethiol on Au in 1mM hexaammineruthenium(III) chloride with 0.1M $LiClO_4$ as the supporting electrolyte. Inset shows a similar plot for the SAM of C_5 thiol on Au surface. It can be seen from the inset of figure that the SAM of C_5 thiol shows a semicircle at high frequency region and a straight line at low frequency region, indicating the facile nature of the ruthenium redox reaction. The plot obtained is typical characteristics of a quasi-reversible redox reaction implying the poor blocking ability of the monolayer. The formation of a large semicircle in the entire range of frequency in the case of SAM of decanethiol on Au surface indicates the complete charge transfer control for the redox reaction with a very good blocking behaviour. These results are in conformity with our observations using cyclic voltammetric studies discussed earlier.

4.9.3. Analysis of impedance data

The impedance values are fitted to a standard Randle's equivalent circuit comprising of a parallel combination of a constant phase element (CPE) represented by Q and a faradaic impedance Z_f in series with the uncompensated

solution resistance, R_u for the cases of bare Au surface and SAM of C_5 thiol modified electrode.

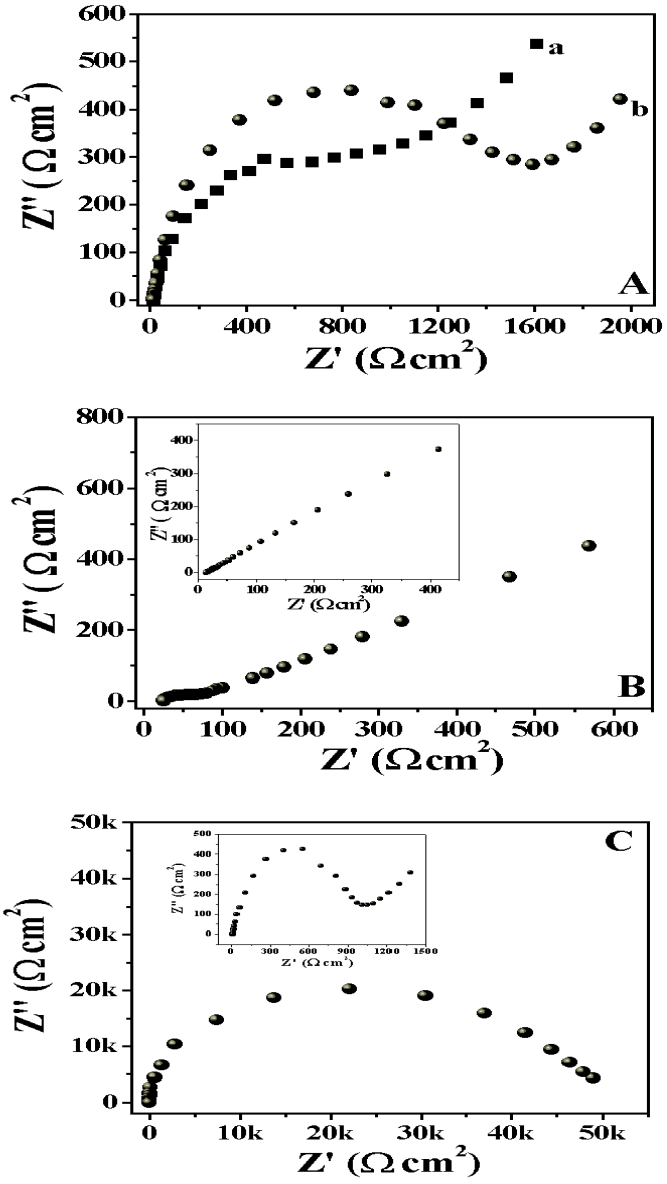

Figure 38: Impedance plots in 1mM hexaammineruthenium(III) chloride with 0.1M $LiClO_4$ as supporting electrolyte for, (A) SAMs of C_8 (a) and C_{10} (b) alkoxycyanobiphenyl thiols on Au surface. (B) SAM of C_5 thiol on Au electrode. Inset shows the same impedance plot for the bare Au electrode. (C) SAM of decanethiol on Au surface (15 hours). Inset shows the same impedance plot for the SAM of C_5 thiol on Au electrode (15 hours).

The faradaic impedance, Z_f is a series combination of charge transfer resistance, R_{ct} and the Warburg impedance, W. For C_8 and C_{10} thiols modified Au electrodes, the Z_f consists only of charge transfer resistance, R_{ct}. Table 8 shows the charge transfer resistance values (R_{ct}) of bare gold and SAM modified electrodes obtained from the impedance plots. It can be seen from the table that the R_{ct} values of SAM modified electrodes, as expected are very much higher when compared to bare Au electrode due to the inhibition of electron transfer rate by the presence of monolayer on the electrode surface. From the R_{ct} values, we can calculate the surface coverage (θ) of the monolayer on the gold electrode using equation (6), by assuming that the current is due to the presence of defects within the monolayer.

$$\theta = 1 - (R_{ct}/R'_{ct}) \qquad (6)$$

where R_{ct} is the charge transfer resistance of bare Au electrode and R'_{ct} is the charge transfer resistance of the corresponding SAM modified electrodes.

Table-8

The charge transfer resistance (R_{ct}) values obtained from the impedance plots of the different electrodes using two different redox couples as probe molecules.

Sample	**Charge transfer resistance (R_{ct}) values (Ω cm^2)**	
	$[Fe(CN)_6]^{3-\|4-}$	**$[Ru(NH_3)_6]^{2+\|3+}$**
Bare Au	**0.5535**	**1.26**
C_5 thiol/Au	**220.6**	**65.5**
C_8 thiol/Au	**6636.6**	**952.8**
C_{10} thiol/Au	**6953.75**	**1362**

The surface coverage values determined from the R_{ct} for all the alkoxycyanobiphenyl thiols used in this work are presented in table 9. From the calculated R_{ct} values it is clear that the higher alkyl chain containing alkoxycyanobiphenyl thiols form a better blocking monolayer and the extent of blocking follows the order $C_{10} > C_8 > C_5$, which is in conformity with our CV studies.

Using the R_{ct} values obtained from the impedance plots, we have determined the rate constant value of $[Fe(CN)_6]^{3-|4-}$ for the SAM modified electrodes. The monolayer, acting as an array of microelectrodes, provides a barrier for electron transfer reaction leading to an expected decrease in rate constant values. The R_{ct} can be expressed as follows,

$$R_{ct} = RT/nFI_o \quad (8)$$

and $$I_o = nFAkC \quad (9)$$

Substituting eqn. (9) in (8), we get,

$$R_{ct} = RT/n^2F^2AkC \quad (10)$$

From eqn. (10), for a one electron first order reaction with $C_0=C_r=C$ and for unit geometric area, the apparent rate constant can be given as follows,

$$k_{app} = RT/F^2R_{ct}C \quad (11)$$

The real rate constant k_o can be expressed as,

$$k_o = k_{app}/(1-\theta) \quad (12)$$

where R is the gas constant, T the temperature, F the Faraday's constant, n the number of electrons, I_o the exchange current density, A the area of electrode, C the concentration of the redox couple, R_{ct} the charge transfer resistance, θ the surface coverage, k_{app} and k_o the apparent and the real rate constants respectively.

Using equations (11) and (12), we have calculated the real and apparent rate constants for bare Au and SAM modified electrodes. It was found

that the apparent rate constant values of monolayer coated electrodes are almost four orders of magnitude lower when compared to the rate constant of bare Au electrode. The surface coverage and rate constants obtained from R_{ct} values of monolayer modified electrodes and the bare Au electrode using $[Fe(CN)_6]^{3-|4-}$ redox couple as probe are shown in table 9.

Table-9

The surface coverage, the apparent and real rate constant values calculated for $[Fe(CN)_6]^{3-|4-}$ redox couple using R_{ct} values obtained from the impedance plots of different SAM modified electrodes.

Sample	Surface coverage (θ)	Apparent rate constant k_{app} (cm/s)	Real rate constant k_o (cm/s)
Bare Au	**----**	**------**	**0.4824**
C_5 thiol/Au	**0.9975**	**1.206×10^{-3}**	**0.4807**
C_8 thiol/Au	**0.9999**	**0.400×10^{-4}**	**0.4000**
C_{10} thiol/Au	**0.9999**	**0.383×10^{-4}**	**0.3830**

It may be pointed out that the sizes of ferrocyanide (6Å) and ruthenium (6.4Å) complexes are almost comparable and if ruthenium redox reaction is assumed to occur by access of the redox species to the electrode surface through the pinholes and defects present in the monolayer, then the reaction of ferrocyanide should also exhibit a facile kinetics. Since it is not so, it is felt that the Ru(III) redox reaction does not take place by access of the redox species to the electrode surface but by a tunneling process through the bond. The C_5 molecule with a relatively short alkyl chain length of 7.7Å of the methylene

units (as shown in Fig. 41) and the delocalized π-electrons of the aromatic ring in series can bridge the redox species and the gold surface effectively to facilitate the electron transfer process. It is well known that the redox reaction of hexaammineruthenium(III) chloride follows the outer sphere electron transfer reaction. In this case physical access to the electrode surface is not a pre-requisite for the electron transfer to occur since the process is facilitated by tunneling mechanism. This is in contrast to ferrocyanide redox reaction, which is an inner sphere electron transfer reaction where the access of redox species to the electrode surface is necessary for the electron transfer reaction to occur [36]. However in the case of C_8 (11.6Å) and C_{10} (14.1Å) thiols, with longer chain lengths, the reaction rate decays exponentially with distance with a decay length β of 0.8 per Å units [119-121]. In this case the access of redox species to the electrode surface is controlled mainly through the pinholes and pores present in the monolayer.

From the impedance plots of Fig. 37C, we have obtained the surface coverage values of 0.9997 and 0.9999 for the SAMs of C_5 thiol and decanethiol on Au surface. Obviously, forming the SAM for longer time of about 15 hours has the effect of reducing the pinholes and defects significantly. It can be seen from the Fig. 36B that the ruthenium redox reaction is quite facile in the case of SAM of C_5 thiol in contrast to the SAM of decanethiol on Au, although their chain lengths and surface coverage values are comparable. It can also be recalled that both these thiols are equally blocking the ferrocyanide redox reaction. The facile nature of Ru(III) redox reaction therefore suggests that in the case of C_5 thiol the tunneling through the delocalized π-electrons of the aromatic ring is a dominating mechanism for the electron transfer process. The

very low density of pinholes and defects cannot account for the fast electron transfer kinetics in the case of ruthenium complex.

4.9.4. Pinhole analysis

The study of electrochemical impedance spectroscopy on SAM modified electrodes provides a valuable information on the distribution of pinholes and defects in the monolayer. Finklea et al. [60] developed a model for the impedance response of a SAM modified electrode, which behaves as an array of microelectrodes. Based on the work of Matsuda [64] and Amatore [65], a model has been developed to fit the faradaic impedance data obtained for the electron transfer reactions at the monolayer-modified electrode, to understand the distribution of pinholes in the monolayer. The impedance expressions have been derived by assuming that the total pinhole area fraction, $(1-\theta)$ is less than 0.1, where θ is the surface coverage of the monolayer. Both the real and imaginary parts of the faradaic impedance values are plotted as a function of $\omega^{-1/2}$. At higher frequencies the diffusion profiles of each individual microelectrode constituent of the array is separated in contrast to the situation at lower frequencies where there is an overlap.

In the case of SAM of alkoxycyanobiphenyl thiols on Au surface, the presence of pinholes and defects are analyzed using the above described model. Figures 39 (a-d) show the real part of the faradaic impedance of different SAM modified electrodes plotted as a function of $\omega^{-1/2}$. For comparison the plot of bare gold electrode is also shown in Fig. 39(a). Figures 39 (b-d) show the plots of real component of faradaic impedance Z'_f vs. $\omega^{-1/2}$ for the monolayer coated electrodes of alkoxycyanobiphenyl thiols with different alkyl chain lengths of C_5, C_8 and C_{10} respectively. Figures 40 (a-c) show the plots of imaginary

component of the faradaic impedance Z''_f vs. $\omega^{-1/2}$ for the above-mentioned electrodes. The faradaic impedance plots have features similar to that of an array of microelectrodes. Analysis of figures 39 and 40 shows that there are two linear domains at high and low frequencies for the Z'_f vs. $\omega^{-1/2}$ plots and a peak formation in the Z''_f vs. $\omega^{-1/2}$ plots corresponding to the frequency of transition between the two linear domains. According to the model described earlier, this frequency separates the two time dependent diffusion profiles for the microelectrodes.

The surface coverage of the monolayer can be determined from the slope of the Z'_f vs. $\omega^{-1/2}$ plot at high frequency region and it is given by,

$$\theta = 1 - [\sigma/(m-\sigma)] \qquad (7)$$

where m is the slope obtained from the faradaic impedance plots, θ the surface coverage of the monolayer and σ the Warburg coefficient, which can be obtained from the unmodified bare gold electrode.

It can be seen from Fig. 39 that at lower frequency the slope of the curve is decreased as $\omega^{-1/2}$ is increased. We also find the Warburg coefficient (slope m) calculated for the SAM modified electrodes is always greater than that obtained from the bare gold electrode. The increase in the apparent value of the Warburg coefficient for monolayer-coated electrodes suggests that the pinholes are distributed in patches over the surface. Using eqn. (7) we have calculated the surface coverage values of 0.9978, 0.9994 and 0.9996 for the SAMs of C_5, C_8 and C_{10} thiols on Au respectively and these values are in good agreement with the surface coverage values determined from the R_{ct} values shown in table 9.

From the studies of cyclic voltammetry and electrochemical impedance spectroscopy on SAMs of alkoxycyanobiphenyl thiols on Au surface, we find

that these liquid crystalline molecules form a highly dense and well-packed compact monolayer. These monolayers block the redox reaction of potassium ferro/ferri cyanide couple indicating the good barrier property of the SAMs on Au surface. In contrast, the redox reaction $[Ru(NH_3)_6]^{2+|3+}$ is quite facile when the alkyl chain length is shorter (C_5) whereas it is inhibited when the alkyl chain length is longer (C_8 & C_{10}).

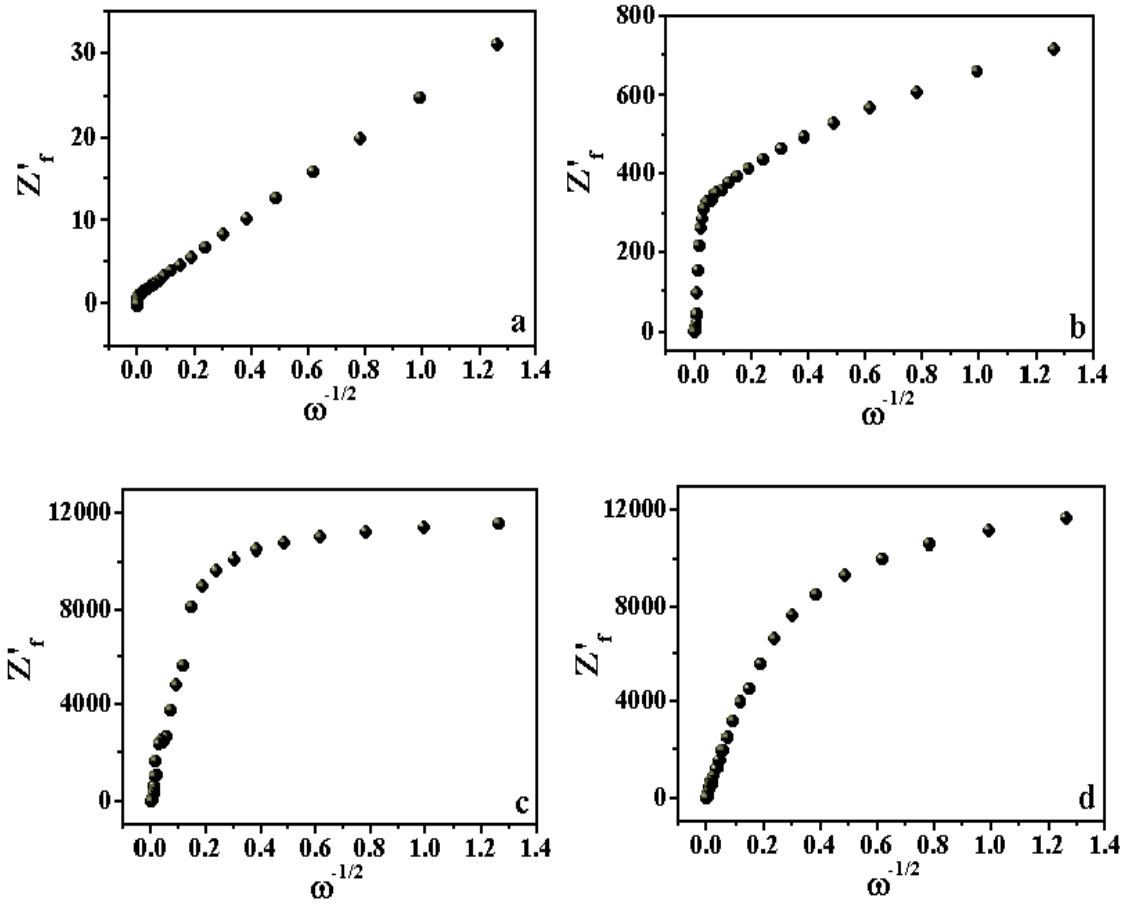

Figure 39: Plots of real part of faradaic impedance (Z'_f) vs. $\omega^{-1/2}$ for, (a) Bare Au electrode, (b) SAM of C_5 thiol on Au electrode, (c) SAM of C_8 thiol on Au surface and (d) SAM of C_{10} thiol on Au electrode.

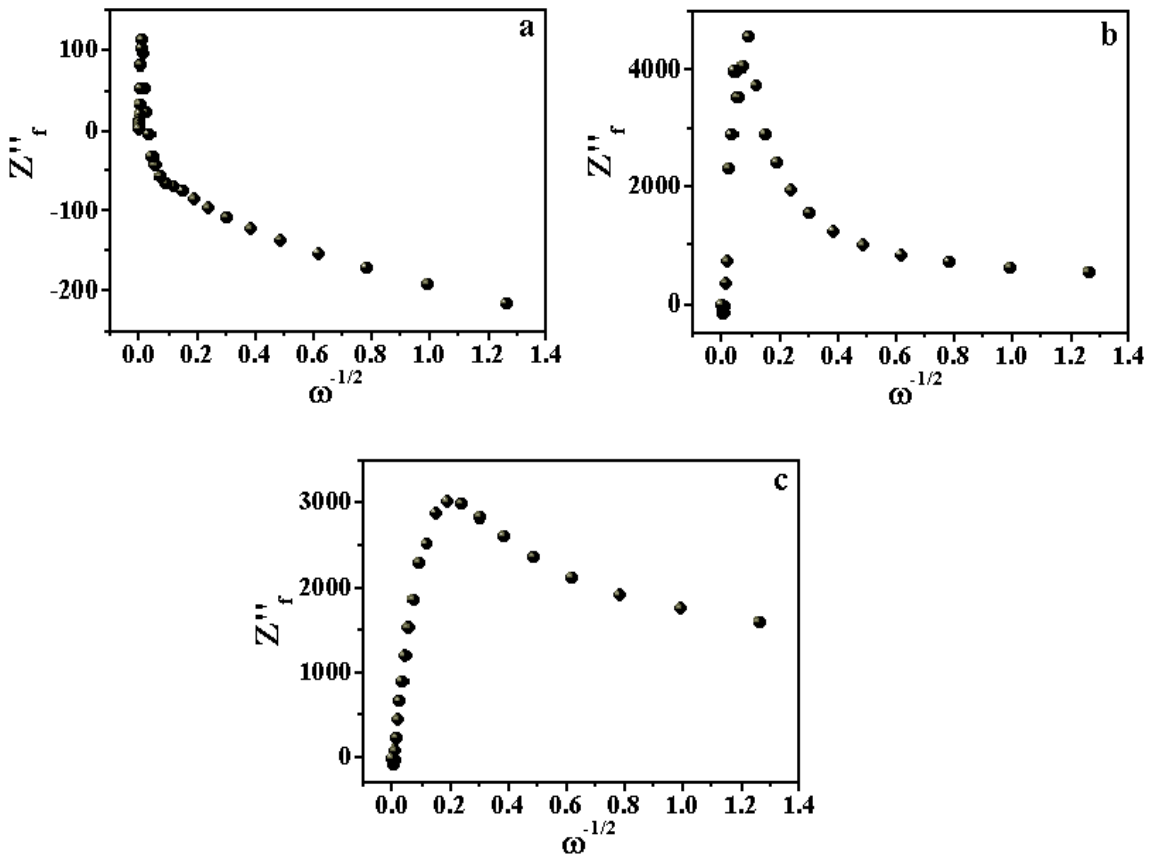

Figure 40: Plots of imaginary part of faradaic impedance (Z''_f) as a function of $\omega^{-1/2}$ for, (a) SAM of C_5 thiol on Au electrode, (b) SAM of C_8 thiol on Au surface and (c) SAM of C_{10} thiol on Au electrode.

Figure 41 shows the proposed mechanism for the Ru(III) electron transfer reaction on the SAM modified electrodes. In the case of C_5 thiol, the SAM provides tunneling pathway for Ru(III) redox reaction by mediating the electron transfer between Au surface and the redox couple. Our results are significant in studies involving electron transfer through molecules containing aromatic core and aliphatic chains in their structure. In these cases the aromatic core with delocalized electrons facilitates the charge transfer while the short methylene (aliphatic) chains provide through bond tunneling pathway. Such systems have interesting applications in the study of bridge mediated electron transfer reactions and in the study of biological sensors and molecular electronics.

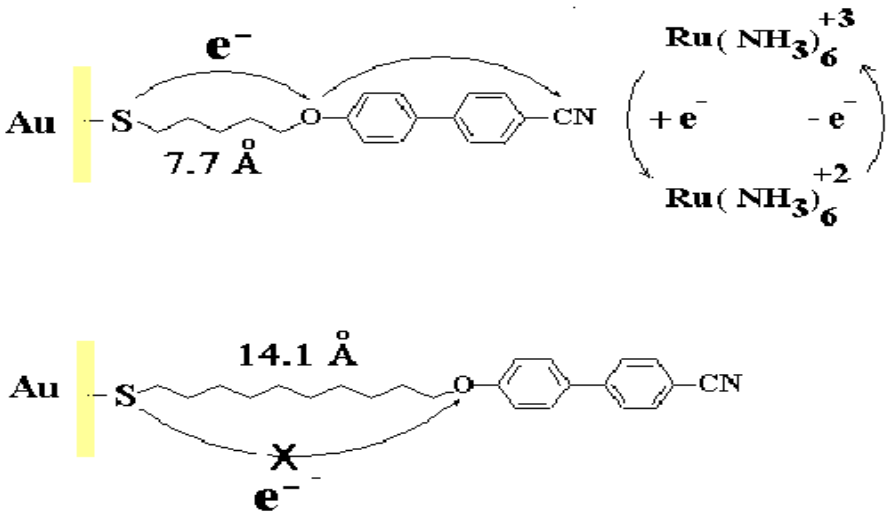

Figure 41: Schematic representation of proposed mechanism for electron transfer reaction on SAM modified electrodes using $[Ru(NH_3)_6]^{2+|3+}$ as redox probe. SAMs formed by liquid crystalline molecules of thiol terminated alkoxycyanobiphenyls mediate electron transfer between Au electrode and $[Ru(NH_3)_6]^{2+|3+}$ when the alkyl chain length is shorter (C_5) and inhibit the process when the alkyl chain length is longer (C_8 & C_{10}).

4.10. Conclusions

In this chapter, we have described the monolayer formation and its characterization of some aromatic thiols and alkoxycyanobiphenyl thiols on Au surface obtained using organic solvents as an adsorbing medium. We have studied the monolayer formation of 2-naphthalenethiol, thiophenol, o-aminothiophenol, p-aminothiophenol and alkoxycyanobiphenyl thiols having different alkyl chain lengths of C_5, C_8 and C_{10} on Au surface. The barrier property, insulating property and blocking ability of these monolayers were evaluated using electrochemical techniques such as cyclic voltammetry, electrochemical impedance spectroscopy and gold oxide stripping analysis. We have used two important redox couples namely, $[Fe(CN)_6]^{3-|4-}$ and $[Ru(NH_3)_6]^{2+|3+}$ as redox probe to study the electron transfer reactions on the SAM modified electrodes. The charge transfer resistance (R_{ct}), which is a measure of the blocking ability of the monolayer, was determined from their impedance values by equivalent circuit fitting procedure. In addition, EIS data were used for the pinholes and defects analysis, from which the surface coverage of the monolayer on Au surface was determined.

In the case of self assembled monolayer of 2-naphthalenethiol on Au surface, the structure, adsorption kinetics and barrier properties of the monolayer were studied using electrochemical techniques, grazing angle FTIR spectroscopy and scanning tunneling microscopy (STM). The results of cyclic voltammetric and impedance measurements using redox probes show that 2-naphthalenethiol on Au forms a stable, reproducible but moderately blocking monolayer. Annealing of the SAM modified surface at $72^0 \pm 2^0$C remarkably improves the blocking property of the monolayer of 2-naphthalenethiol on Au. From the study of kinetics of SAM formation we find that the self-assembly follows Langmuir adsorption isotherm. Our STM and FTIR results show that

the molecules are adsorbed with the naphthalene ring tilted from the surface normal by forming a $\sqrt{3}$ X 3 $R30^0$ overlayer structure. From our studies we conclude that the electron transfer reaction of ferro/ferri cyanide in the freshly formed monolayer occurs predominantly through the pinholes and defects present in the monolayer. However, in the case of thermally annealed specimen, while the ferro/ferri cyanide reaction is almost completely blocked, the electron transfer reaction of hexaammineruthenium(III) chloride is completely allowed. It is proposed that the electron transfer reaction in the case of ruthenium redox couple takes place by tunneling mechanism through the high electron density aromatic naphthalene ring acting as a bridge between the monolayer-modified electrode and ruthenium complex.

We have studied the structural integrity and barrier properties of self-assembled monolayers (SAMs) of thiophenol (TP), o-aminothiophenol (o-ATP) and p-aminothiophenol (p-ATP) on Au surface using electrochemical techniques such as cyclic voltammetry (CV), electrochemical impedance spectroscopy (EIS) and gold oxide stripping analysis. The results of cyclic voltammetry and impedance spectroscopy measurements show that these aromatic thiols form stable and reproducible but moderately blocking monolayers. We have tried to improve the blocking ability of these monolayers by potential cycling and mixed SAM formation with 1-Octanethiol and 1,6-Hexanedithiol. From the results of cyclic voltammetry and impedance spectroscopic studies, we have shown that the blocking ability of these monolayers is significantly improved by potential cycling and by mixed SAM formation, especially in the case of p-ATP on Au surface. It is found that the electron transfer reaction of potassium ferrocyanide occurs mainly through the pinholes and defects present in these SAMs. In contrast, the redox reaction of ruthenium complex takes place through a tunneling mechanism mediated by a

π-electron bridge arising from the aromatic core of these molecules. From the impedance data, a surface coverage value of 99.9% has been determined for these SAMs on Au surface.

Similarly, we have also studied the self-assembled monolayers (SAMs) of liquid crystalline thiol-terminated alkoxycyanobiphenyl molecules with different alkyl chain lengths on Au surface for the first time using electrochemical techniques such as cyclic voltammetry (CV) and electrochemical impedance spectroscopy (EIS). It was found that for short length alkyl chain thiol (C_5) the electron transfer reaction of hexaammineruthenium(III) chloride takes place through tunneling mechanism. In contrast, redox reaction of potassium ferro/ferri cyanide is almost completely blocked by the SAM modified Au surface. We also find that the rate constant values of $[Fe(CN)_6]^{3-|4-}$ redox couple are decreased by almost four orders of magnitude for the SAM modified electrodes when compared to bare Au electrode. From the impedance data, a surface coverage value of >99.9% was calculated for all the thiol molecules.

References

1. H.O. Finklea, *Self-assembled monolayers on Electrodes in Encyclopedia of Analytical Chemistry*, R.A. Meyers, (Ed.), John Wiley & Sons Ltd, Chichester, U.K.
2. A. Ulman, *An Introduction to Ultrathin organic films from Langmuir-Blodgett to self-assembly*, Academic Press, San Diego, CA, (1991).
3. J.J. Hickman, D. Ofer, P.E. Laibinis, G.M. Whitesides, *Science*, 252, (1991), 688.
4. C.A. Mirkin, M.A. Ratner, *Annu. Rev. Phys. Chem.*, 43, (1992), 719.
5. C.J. Zhong, M.D. Porter, *Anal. Chem.*, 67, (1995), 709A.
6. B.A. Cornell, V.L.B. Braach-Maksvytis, L.G. King, P.D.J. Osman, B. Raguse, L. Wieczorek, R.J. Pace, *Nature*, 387, (1997), 580.
7. M.J. Tariov, D.R.F. Burgess, G. Gillen, *J. Am. Chem. Soc.*, 115, (1993), 5305.
8. J. Huang, D.A. Dahlgren, J.C. Hemminger, *Langmuir*, 10, (1994), 626.
9. E.W. Wollman, D. Kang, C.D. Frisbie, T.M. Larcovic, M.S. Wrighton, *J. Am. Chem. Soc.*, 116, (1994), 4395.
10. D. Li, M.A. Ratner, T.J. Marks, C.H. Znang, J. Yang, G.K. Wong, *J. Am. Chem. Soc.*, 112, (1990), 7389.
11. Y. Kawanishi, T. Tamaki, M. Sakuragi, T. Seki, Y. Swuzki, K. Ichimura, *Langmuir*, 8, (1992), 2601.
12. P.E. Laibinis, G.M. Whitesides, *J. Am. Chem. Soc.*, 114, (1992), 9022.
13. N. Ohno, J. Uehara, K. Aramaki, *J. Electrochem. Soc.*, 140, (1993), 2512.
14. A. Ulman, *Chem. Rev.*, 96, (1996), 1533.
15. E. Sabatani, J. Cohen-Boulakia, M. Bruening, I. Rubinstein, *Langmuir*, 9,

(1993), 2974.

16. S. Frey, V. Stadler, K. Heister, W. Eck, M. Zharnikov, M. Grunze, *Langmuir*, 17, (2001), 2408.
17. A.W. Hayes, C. Shannon, *Langmuir*, 12, (1996), 3688.
18. V. Batz, M.A. Schneeweiss, D. Kramer, H. Hagenstrom, D.M. Kolb, D. Mandler, *J. Electroanal. Chem.*, 491, (2000), 55.
19. O. Chailapakul, R.M. Crooks, *Langmuir*, 11, (1995), 1329.
20. M. Aslam, K. Bandyopadhyay, K. Vijayamohanan, V. Lakshminarayanan, *J. Colloid Interface Sci.*, 234, (2001), 410.
21. K. Bandyopadhyay, K. Vijayamohanan, *Langmuir*, 14, (1998), 625.
22. K. Bandyopadhyay, K. Vijayamohanan, M. Venkataramanan, T. Pradeep, *Langmuir*, 15, (1999), 5314.
23. M. Venkataramanan, G. Skanth, K. Bandyopadhyay, K. Vijayamohanan, T. Pradeep, *J. Colloid Interface Sci.*, 212, (1999), 553.
24. K. Bandyopadhyay, M. Sastry, V. Paul, K. Vijayamohanan, *Langmuir*, 13, (1997), 866.
25. K. Bandyopadhyay, K. Vijayamohanan, G.S. Shekhawat, R.P. Gupta, *J. Electroanal. Chem.*, 447, (1998), 11.
26. T.T. Wooster, P.R. Gamm, W.E. Geiger, *Langmuir*, 12, (1996), 6616.
27. S. Chang, I. Chao, Y. Tao, *J. Am. Chem. Soc.*, 116, (1994), 6792.
28. R. Haag, M.A. Rampi, R.E. Holmlin, G.M. Whitesides, *J. Am. Chem. Soc.*, 121, (1999), 7895.
29. R.R. Kolega, B.J. Schlenoff, *Langmuir*, 14, (1998), 5469.
30. M. Jayadevaiah, V. Lakshminarayanan, *Meas. Sci. Technol.*, 15, (2004), N35.
31. R.B. Lennox, E. Boubour, *J. Phys. Chem. B*, 104, (2000), 9004.
32. R.B. Lennox, E. Boubour, *Langmuir*, 16, (2000), 7464.

33. M.R. Anderson, M. Gatin, *Langmuir*, 10, (1994), 1638.
34. W. Paik, S. Eu, K. Lee, S. Chon, M. Kim, *Langmuir*, 16, (2000), 10198.
35. J. Blumberger, M. Sprik, *J. Phys. Chem. B*, 109, (2005), 6793.
36. M. Fleischmann, P.R. Graves, J. Robinson, *J. Electroanal. Chem.*, 182, (1985), 87.
37. C.E.D. Chidsey, *Science*, 251, (1991), 919.
38. J.F. Smalley, S.W. Feldberg, C.E.D. Chidsey, M.R. Linford, M.D. Newton, Y. Liu, *J. Phys. Chem.*, 99, (1995), 13141.
39. K. Weber, L. Hockett, S. Creager, *J. Phys. Chem. B*, 101, (1997), 8286.
40. W. Wang, T. Lee, M.A. Reed, *J. Phys. Chem. B*, 108, (2004), 18398.
41. H.D. Sikes, J.F. Smalley, S.P. Dudek, A.R. Cook, M.D. Newton, C.E.D. Chidsey, S.W. Feldberg, *Science*, 291, (2001), 1519.
42. W.B. Davis, W.A. Svec, M.A. Ratner, M.R. Wasieiewski, *Nature*, 396, (1998), 60.
43. F.D. Lewis, J. Liu, W. Weigel, W. Rettig, I.V. Kurnikov, D.N. Beratan, *Proc. Natl. Acad. Sci. U.S.A.*, 99, (2002), 12536.
44. N. Krings, H.H. Strehblow, J. Kohnert, H.D. Martin, *Electrochim. Acta*, 49, (2003), 167.
45. M.A. Rampi, G.M. Whitesides, *Chem. Phys.*, 281, (2002), 373.
46. Q. Jin, J.A. Rodriguez, C.Z. Li, Y. Darici, N.J. Tao, *Surf. Sci.*, 425, (1999), 101.
47. C. Retna Raj, J. Takeo Ohsaka, *J. Electroanal. Chem.*, 540, (2003), 69.
48. T. Sawaguchi, F. Mizutani, S. Yoshimoto, I. Taniguchi, *Electrochim. Acta*, 45, (2000), 2861.
49. Y. Yang, S.B. Khoo, *Sens. Actuators B*, 97, (2004), 221.
50. H.Z. Yu, N. Xia, J. Zhang, Z.F. Liu, *J. Electroanal. Chem.*, 448, (1998), 119.

51. L.H. Guo, J.S. Facci, G. Mclendon, *J. Phys. Chem.*, 99, (1995), 4106.
52. L.H. Guo, J.S. Facci, G. Mclendon, *J. Phys. Chem.*, 99, (1995), 8458.
53. D.S. Karpovich, G.J. Blanchard, *Langmuir*, 10, (1994), 3315.
54. O. Dannenberger, M. Buck, M. Grunze, *J. Phys. Chem. B*, 103, (1999), 2202.
55. H. Ron, I. Rubinstein, *J. Am. Chem. Soc.*, 120, (1998), 13444.
56. R. Subramanian, V. Lakshminarayanan, *Electrochim. Acta*, 45, (2000), 4501.
57. D. Yan, J.A. Saunders, G.K. Jennings, *Langmuir*, 18, (2002), 10202.
58. B.B. Damaskin, O.A. Petrii, V.V. Batrakov, *Adsorption of organic compounds on Electrodes*, Plenum Press, New York, (1971).
59. H.O. Finklea, in *Electroanalytical Chemistry, A Series of Advances*, A.J. Bard, I. Rubinstein (Eds.), Marcel Dekker, New York, Vol. 19, (1996), p. 166.
60. H.O. Finklea, D. Snider, J. Fedyk, E. Sabatani, Y. Gafni, I. Rubinstein, *Langmuir*, 9, (1993), 3660.
61. L.V. Protsailo, R. Fawcett, *Langmuir*, 18, (2002), 8933.
62. L.V. Protsailo, R. Fawcett, D. Russell, L.R. Meyer, *Langmuir*, 18, (2002), 9342.
63. R.P. Janek, R. Fawcett, A. Ulman, *Langmuir*, 14, (1998), 3011.
64. K. Tokuda, T. Gueshi, H. Matsuda, *J. Electroanal. Chem.*, 102, (1979), 41.
65. C. Amatore, J.M. Saveant, D.J. Tessler, *J. Electroanal. Chem.*, 147, (1983), 39.
66. R.G. Nuzzo, D.L. Allara, *J. Am. Chem. Soc.*, 105, (1983), 4481.
67. E. Sabatani, I. Rubinstein, *J. Electroanal. Chem.*, 219, (1987), 365.
68. Y.T. Kim, A.J. Bard, *Langmuir*, 8, (1992), 1096.
69. R.V. Duevel, R.M. Corn, *Anal. Chem.*, 64, (1992), 337.

70. G.E. Poirier, M.J. Tarlov, H.E. Rushmeier, *Langmuir*, 10, (1994), 3383.
71. A.M. Becka, C.J. Miller, *J. Phys. Chem.*, 97, (1993), 6233.
72. S.E. Creager, K. Weber, *Langmuir*, 9, (1993), 844.
73. K. Sinniah, J. Cheng, S. Terrettaz, J.E. Reutt-Robey, C.J. Miller, *J. Phys. Chem.*, 99, (1995), 14500.
74. J. Lipkowski, in *Modern aspects of Electrochemistry*, B.E. Conway, J. Bockris, R.E. White, (Eds.), Vol. 23, Plenum, New York, (1992), p.1.
75. L. Tender, M.T. Carter, R.W. Murray, *Anal. Chem.*, 66, (1994), 3173.
76. Ujjal Kumar Sur, R. Subramanian, V. Lakshminarayanan, *J. Colloid Interface Sci.*, 266, (2003), 175.
77. K.T. Carron, L.G. Hurley, *J. Phys. Chem.*, 95, (1991), 9979.
78. H.O. Finklea, D.D. Hanshew, *J. Am. Chem. Soc.*, 114, (1992), 3173.
79. M.A. Rampi, G.M. Whitesides, *Chem. Phys.*, 281, (2002), 373.
80. L.J. Wan, Y. Hara, H. Noda, M. Osawa, *J. Phys. Chem. B*, 102, (1998), 5943.
81. D.J. Wold, R. Hagg, M.A. Rampi, C.D. Frisbie, *J. Phys. Chem. B*, 106, (2002), 2813.
82. A.T. Hubbard, *Chem. Rev.*, 88, (1988), 633 and references there in.
83. M.A. Bryant, S.L. Joa, J.E. Pemberton, *Langmuir*, 8, (1992), 753.
84. E. Sabatani, J. Cohen-Boulakia, M. Bruening, I. Rubinstein, *Langmuir*, 9, (1993), 2974.
85. Li Sun, B. Johnson, I. Wade, R.M. Crooks, *J. Phys. Chem.*, 94, (1990), 8869.
86. W.A. Hayes, C. Shannon, *Langmuir*, 12, (1996), 3688.
87. J. Lukkari, K. Kleemola, M. Meretoja, T. Ollonqvist, J. Kankare, *Langmuir*, 14, (1998), 1705.
88. V. Batz, M.A. Schneeweiss, D. Kramer, H. Hagenstrom, D.M. Kolb, D.

Mandler, *J. Electroanal. Chem.*, 491, (2000), 55.
89. N. Mohri, S. Matsushita, M. Inoue, *Langmuir*, 14, (1998), 2343.
90. N. Mohri, M. Inoue, Y. Arai, *Langmuir*, 11, (1995), 1612.
91. N.L. Abbott, C.B. Gorman, G.M. Whitesides, *Langmuir*, 11, (1995), 16.
92. W. Paik, S. Eu, K. Lee, S. Chon, M. Kim, *Langmuir*, 16, (2000), 10198.
93. P.H. Lin, P. Guyot-Sionnest, *Langmuir*, 15, (1999), 6825.
94. C. Ramalechume, S. Berchmans, V. Yegnaraman, A.B. Mandal, *J. Electroanal. Chem.*, 580, (2005), 122.
95. S. Nitahara, T. Akiyama, S. Inoue, S. Yamada, *J. Phys. Chem. B*, 109, (2005), 3944.
96. A.G. Larsen, K.V. Gothelf, *Langmuir*, 21, (2005), 1015.
97. Ujjal Kumar Sur, V. Lakshminarayanan, *J. Electroanal. Chem.*, 565, (2004), 343.
98. I. Francis Cheng, L.D. Whiteley, C.R. Martin, *Anal. Chem.*, 61, (1989), 762.
99. H.O. Finklea, D.A. Snider, J. Fedyk, E. Sabatani, Y. Gafni, I. Rubinstein, *Langmuir*, 9, (1993), 3660.
100. O. Chailapakul, R.M. Crooks, *Langmuir*, 9, (1993), 884.
101. T. Felgenhauer, H.T. Rong, M. Buck, *J. Electroanal. Chem.*, 550, (2003), 309.
102. H.O. Finklea, L. Liu, M.S. Ravenscroft, S. Punturi, *J. Phys. Chem.*, 100, (1996), 18852.
103. H.O. Finklea, D.D. Hanshew, *J. Am. Chem. Soc.*, 114, (1992), 3173.
104. M.E.G. Lyons, *Sensors*, 1, (2001), 215.
105. S. Nitahara, T. Akiyama, S. Inoue, S. Yamada, *J. Phys. Chem. B*, 109, (2005), 3944.
106. M.R. Arkin, E.D.A. Stemp, C. Turro, N.J. Turro, J.K. Barton, *J. Am. Chem. Soc.*, 118, (1996), 2267.

107. D. Meisel, M.S. Matheson, J. Rabani, *J. Am. Chem. Soc.*, 100 (1978), 117.
108. P. Cyganik, M. Buck, W. Azzam, C. Woll, *J. Phys. Chem. B*, 108, (2004), 4989.
109. Y.T. Long, H.T. Rong, M. Buck, M. Grunze, *J. Electroanal. Chem.*, 524-525, (2002), 62.
110. J.F. Kang, A. Ulman, S. Liao, R. Jordan, *Langmuir*, 15, (1999), 2095.
111. H. Schonheer, F.J.B. Kremer, S. Kumar, J.A. Rego, H. Wolf, H. Ringsdorf, M. Jaschke, H. Butt, E. Bamberg, *J. Am. Chem. Soc.*, 118, (1996), 13051.
112. N. Boden, R.J. Bushby, P.S. Martin, S.D. Evans, R.W. Owens, D.A. Smith, *Langmuir*, 15, (1999), 3790.
113. R. Owens, D.A. Smith, *Mol. Cryst. Liq. Cryst.*, 329, (1999), 427.
114. H. Allinson, N. Boden, R.J. Bushby, S.D. Evans, P.S. Martin, *Mol. Cryst. Liq. Cryst.*, 303, (1997), 273.
115. Z.P. Yang, I. Engquist, J.M. Kauffmann, B. Liedberg, *Langmuir*, 12, (1996), 1704.
116. Y.T. Tao, M.T. Lee, *Thin Solid Films*, 244, (1994), 810.
117. S. Kumar, V. Lakshminarayanan, *Chem. Commun.*, (2004), 1600.
118. S.K. Pal, S. Kumar, *Liq. Cryst.*, 32, (2005), 659.
119. D.M. Adams, L. Brus, C.E.D. Chidsey, S. Creager, C. Creutz, C.R. Kagan, P.V. Kamat, M. Lieberman, S. Lindsay, R.A. Marcus, R.M. Metzger, M.E. Michel-Beyerle, J.R. Miller, M.D. Newton, D.R. Rolison, O. Sankey, K.S. Schanze, J. Yardley, X. Zhu, *J. Phys. Chem. B*, 107, (2003), 6668.
120. W. Wang, T. Lee, M.A. Reed, *J. Phys. Chem. B*, 108, (2004), 18398.
121. E.G. Petrov, V. May, *J. Phys. Chem. A*, 105, (2001), 10176.